Summer 2011

The biomechanics of the sheep cervical spine: an experimental and finite element analysis

Nicole Ann DeVries
University of Iowa

THE BIOMECHANICS OF THE SHEEP CERVICAL SPINE: AN EXPERIMENTAL AND FINITE ELEMENT ANALYSIS

by

Nicole Ann DeVries

An Abstract

Of a thesis submitted in partial fulfillment
of the requirements for the Doctor of
Philosophy degree in Biomedical Engineering
in the Graduate College of
The University of Iowa

July 2011

Thesis Supervisor: Associate Professor Nicole M. Grosland

ABSTRACT

Animal models are essential for making the transition from scientific concepts to clinical application. Such models have proven valuable for spinal research. The cervical spine of sheep is often used because there is similar geometry between sheep and human. Although anatomical similarities are important, biomechanical correspondence is imperative to understand the effects of disorders, surgical techniques, and implant designs. Therefore, the purpose of this study was to conduct a comprehensive study of the sheep cervical spine biomechanics, including experimental and finite element analysis.

To determine the flexibility of the multilevel spine, ten adult Suffolk sheep C2-C7 spines were tested, undergoing flexion-extension, lateral bending, and axial rotation. In addition to intact multilevel testing, the roles of the stabilizing structures were studied by sequentially destabilizing function spinal units. The sheep spine is highly flexible, especially in lateral bending (±65˚); motion increases with caudal progression. The sheep spine also has a large neutral zone accounting for 50-75% of the total motion. The facets and capsular ligaments play a key role in stabilization, providing the most stability at the C2-C3 level.

In addition to flexibility testing, the sheep spinal ligaments underwent tensile testing until failure to determine the material properties. The ligamentum flavum has the largest failure stress and the capsular ligaments have the largest mean failure force. The longitudinal ligaments have the largest failure strain and the lowest failure force. Overall, the C2-C3 ligaments had the highest failure forces as compared to the ligament type at different levels. This corresponds to the stability the ligaments have at the C2-C3 level during flexibility testing.

Moreover, a finite element model of the C2-C7 sheep cervical spine was developed and validated to provide additional insight in the sheep biomechanics. The model compared favorably with experimental testing for all loading cases except

extension. In general, the model matched the experimental results within one standard deviation for the multilevel motion as well as the motion at each level. Since the sheep is highly flexible and there is a large neutral zone it was difficult to capture the nonlinearity in all loading directions.

The model was used to study the effects of fusion at the C3-C4 level. As expected the motion at the fusion was less than one degree, with the non-fused levels accommodating the loss in motion. The motion increased 15-27%, with the largest increase at C6-C7. To obtain the same rotation as the intact model (±2.5 Nm), larger moments were required, increasing to over 5 Nm for flexion and lateral bending and over 3 Nm for extension and axial rotation.

The study provides insight into the sheep cervical spine biomechanics. Researchers and scientists should consider the high flexibility and large neutral zone when designing a study that is to correlate to human spines. The model provides additional details such as stresses in the bone and intervertebral disc that can help researchers determine the effects of different surgical techniques and implant designs. Overall, this study provides valuable biomechanical data that can aid designing preclinical animal studies of the sheep.

Abstract Approved: _____
Thesis Supervisor

_____
Title and Department

_____
Date

THE BIOMECHANICS OF THE SHEEP CERVICAL SPINE: AN EXPERIMENTAL AND FINITE ELEMENT ANALYSIS

by

Nicole Ann DeVries

A thesis submitted in partial fulfillment
of the requirements for the Doctor of
Philosophy degree in Biomedical Engineering
in the Graduate College of
The University of Iowa

July 2011

Thesis Supervisor: Associate Professor Nicole M. Grosland

Graduate College
The University of Iowa
Iowa City, Iowa

CERTIFICATE OF APPROVAL

PH.D. THESIS

This is to certify that the Ph.D. thesis of

Nicole Ann DeVries

has been approved by the Examining Committee
for the thesis requirement for the Doctor of Philosophy
degree in Biomedical Engineering at the July 2011 graduation.

Thesis Committee: _____
Nicole M. Grosland, Thesis Supervisor

_____
Tae-Hong Lim

_____
Vincent A. Magnotta

_____
Salam F. Rahmatalla

_____
Joseph D. Smucker

_____
David G. Wilder

To my parents

Dream as if you'll live forever. Live as if you'll die today.
James Dean

ACKNOWLEDGMENTS

First and foremost, I want thank my advisor Dr. Nicole Grosland. It was with her encouragement that I pursued my doctorate. Her knowledge and advice has guided me and helped me grow as a researcher, student, and person. Without her patience and direction this would not have been possible.

I would also like to thank my committee members for taking time out of their busy schedules. I am grateful for their input and suggestions. Their insights have led to further improvement of this research study.

A special thanks to all my fellow MIMX lab members for their assistance and advice along the way. Thank you to Dr. Kallemeyn, Dr. Shivanna, and Swathi Kode for helping with the finite element mesh development and analysis. Thank you to Anup Gandhi for his assistance with experimental testing. In addition, I want to thank Douglas Fredericks for helping obtain the sheep and providing insight into the anatomy. Also, thank you to Tony Burnes for helping prepare the ligament specimens.

I want to thank my parents and brothers for all their love and support throughout the years. Their prayers and encouragement have helped me get to where I am today. A special thanks to my grandmother, who instilled a love for learning and passion to help others at a very young age. For that I will always be grateful. Also, I want to thank Matt and his beautiful daughters for their love, support, and encouragement. I am blessed to have them in my life. I look forward to what the future brings.

TABLE OF CONTENTS

LIST OF TABLES

LIST OF FIGURES

CHAPTER 1: OBJECTIVE AND SPECIFIC AIMS

Animal models are essential for making the transition from scientific concepts to clinical application [1, 2]. Such models have proven valuable for spinal research [3, 4]. There is limited availability of human cadaveric specimens, so animal models are often utilized for *in vitro* studies of various spinal disorders and surgical techniques [5]. Animal specimens are more readily available and have more uniform geometries between specimens [5]. Sheep spines are utilized due to the similar geometry as compared to humans; the sheep and human cervical spine disc space and body widths are similar [6, 7]. Additionally, the sheep and human cervical spine have a similar lordosis [8]. Sheep are also readily available, unlike other species such as baboons or other primates. Sheep spines have often been used to study the effects of interbody cage designs and fusion techniques [9-15].

It is important to understand the similarities and differences between the human and sheep spine for constructing a valuable study and interpreting the results. Studies have identified the anatomical similarities between the sheep and human spine; however these studies have been limited to quantifying the anatomic dimensions as opposed to the biomechanical responses [4, 6, 7]. Although anatomical similarities are important, biomechanical correspondence is imperative to understand the effects of disorders, surgical techniques, and implant designs. Studies by Wilke and colleagues [3], Kandziora et al. [4], and Clarke et al. [16] have focused on experimental biomechanics of the sheep cervical functional spinal units (FSUs). Szotek and colleagues [8] studied the biomechanics of compression and impure flexion-extension for the C2-C7. However, to date, there is no comparison of the sheep spine focusing on all moments of rotation (flexion-extension, lateral bending, or axial rotation) for multilevel specimen.

Although, experimental testing can provide relative range of motion and stiffness parameters, it is difficult, if not impossible, to gather other biomechanical data such as

facet joint contact area and pressure, disc pressure, or bone stresses. Finite element modeling has often been utilized for this purpose. However, only one study has focused on the sheep cervical spine [17] and was limited to a functional spinal unit (C3-C4). A validated sheep cervical spine model provides additional biomechanical data that could offer a more in-depth comparison for the human and sheep. Additionally, once an intact sheep cervical spine finite element model is validated, it can be used to test various surgical techniques or used for a parametric study to determine which material provides the best results for a given implant design.

Therefore, the purpose of this research is to conduct a comprehensive biomechanical analysis of the sheep cervical spine. To accomplish this goal, the following specific aims were addressed:

1. To develop a geometrically accurate finite element model of the C2-C7 sheep cervical spine
2. To validate the model through kinematic experimental testing
3. To determine sheep ligament material properties utilizing soft tissue testing
4. To study the effects of fusion, using the validated finite element model

CHAPTER 2: BACKGROUND AND SIGNIFICANCE

2.1 Anatomy of the Spine

It is important to understand the anatomy of the human spine in order to understand the similarities and differences between the sheep and human cervical spine. The human spine is divided into the cervical (7), thoracic (12), lumbar (5), sacral (5 fused), and coccyx (4 fused) spine (Figure 1a). The spine vertebra are named based on region and numbered from superior to inferior, i.e. C1 is the first cervical vertebra located closest to the cranium, whereas C7 is the cervical vertebra before the first thoracic vertebra (T1). The cervical spine and lumbar spine have a lordotic curve whereas the thoracic spine and fused sacral spine have a kyphotic curve. [18]

2.1.1 Vertebra

The focus of this study is the cervical spine, specifically levels C2-C7. The C2 vertebra is called the axis, because it acts as the pivot that C1, or atlas, rotates about. The C1 and C2 vertebra have geometries that vary from C3-C7. In general the vertebra consists of two main segments: the body and the posterior region. The body is the largest part of the vertebra and bears a majority of the weight placed on the spine. The posterior region is further divided into the pedicles, laminae, transverse processes, spinous process, and articular processes (Figure 1b). The posterior region and the body connect to form the intervertebral foramina that the spinal cord passes through. The C7 vertebra has a similar structure as C3-C6; however it has a longer spinous process. [18]

2.1.2 Intervertebral Disc

The intervertebral discs (IVDs) are located between two adjacent bodies; the IVD role is to carry compressive loads as well as resist tensile and shear stresses that occur during bending and rotation. The IVD is composed of the nucleus pulposus and the annulus fibrosus (Figure 2). The nucleus pulposus is centrally located and has a high water content, thus often considered incompressible. The water content of the nucleus

decreases with age and becomes more fibrous. The annulus fibrosus is composed of many concentrically arranged fibrocartilage lamellae. Each lamella contains collagen fibers running at an approximate 25° from the vertical axis, alternating direction in adjacent lamellae as seen in Figure 2. This pattern forms a crisscross pattern, reinforcing the annulus fibrosus in all directions of loading. [18, 19]

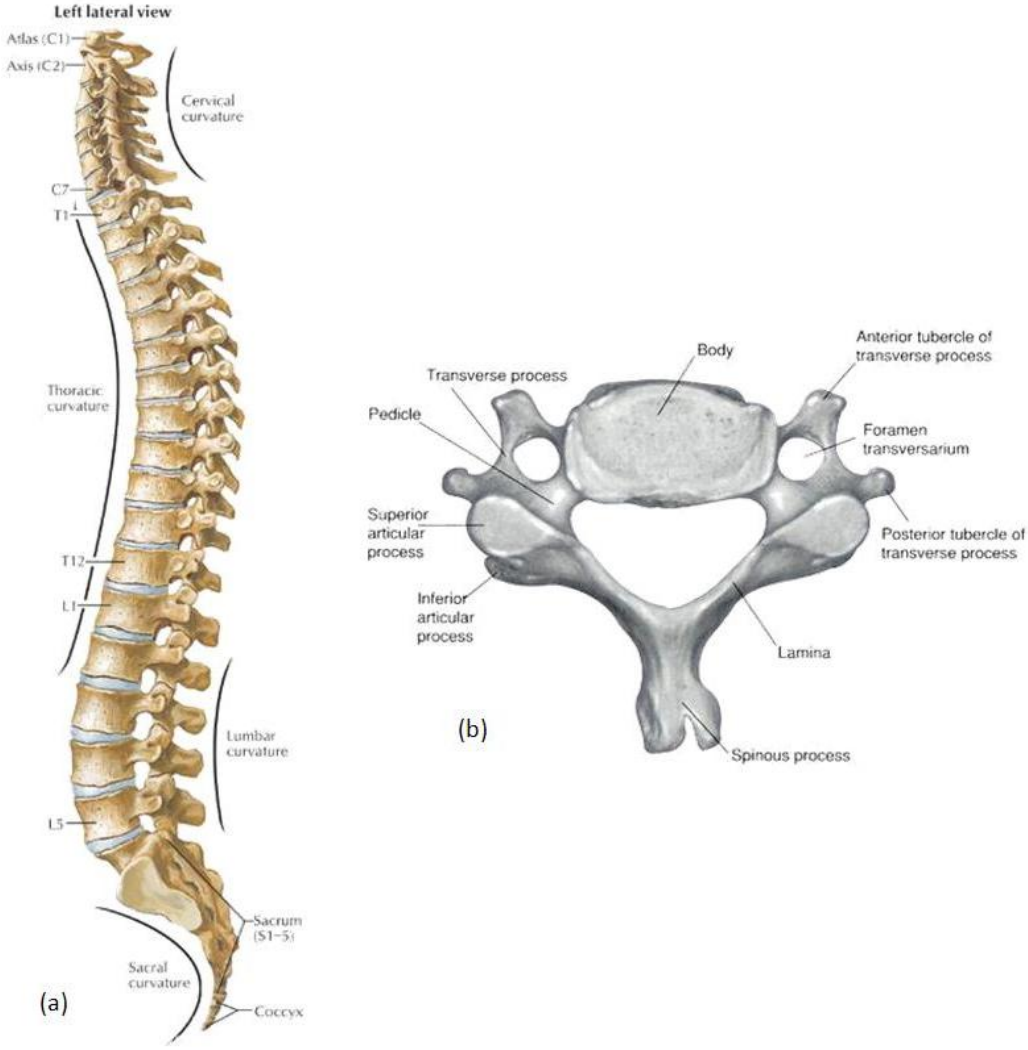

Figure 1 The anatomy of the human spine. (a) The curvature of the entire human spine [20] and (b) the detailed anatomy of the human cervical vertebra [21].

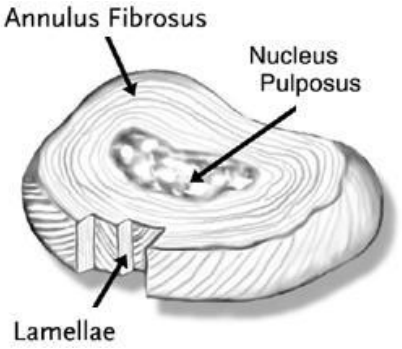

Figure 2 An example of the intervertebral disc composed of the nucleus pulposus and annulus fibrosus [22].

2.1.3 Spinal Ligaments

Other important structures in the spine that provide stability are the spinal ligaments. Ligaments are formed of collagen and elastin fibers that resist tension; they are nonlinear in nature. The major ligaments of the cervical spine (C2-C7) are the anterior longitudinal ligament (ALL), posterior longitudinal ligament (PLL), ligamentum flavum (LF), interspinous ligament (ISL), supraspinous ligament (SSL) and the capsular ligament (CL), shown in Figure 3. The ALL is a broad, strong band of fibers that extends longitudinally along the anterior surface of the bodies and intervertebral discs. The PLL extends along the posterior surface of the bodies and intervertebral discs; the PLL is denser and more compact than the ALL. Both the ALL and PLL contain long fibers that cross several vertebrae and short fibers that span a single layer or IVD. The LF is a thin broad ligament that attaches at the laminae of adjacent vertebrae, consisting of two lateral portions that join where the laminae meet to form the spinous process. The ISL is a thin ligament that adjoins adjacent spinous processes; the ISL extends the entire length of the spinal process, however it is not well defined in the cervical spine. The SSL also adjoins adjacent spinous processes, but is a fibrous membrane that is hard to decipher from the ISL. The CLs are thin and loose ligaments that attach the articular processes of the adjacent vertebra; they run perpendicular to the plane of the facet. [18, 23]

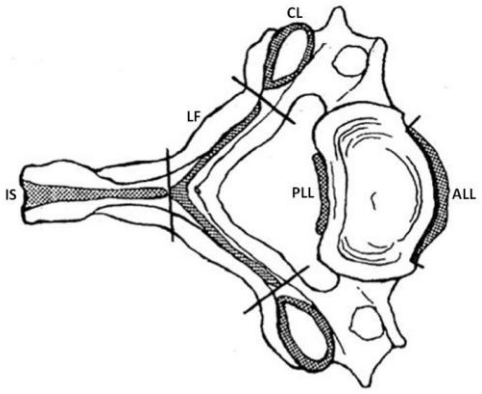

Figure 3 Superior view of the cervical vertebra illustrating the anterior longitudinal ligament (ALL), posterior longitudinal ligament (PLL), ligamentum flavum (LF), interspinous ligament (ISL), and the capsular ligaments (CL); straight lines indicate the boundaries of the various ligaments [24].

2.2 Anatomical Similarities and Differences

The sheep cervical spine has the same key bony structures as found in the human cervical spine; however they vary in shape and size (Figure 4). Figure 5 illustrates the C4 vertebra of both the sheep and human. The sheep cervical spine has a similar lordosis as found in the human cervical spine [8].

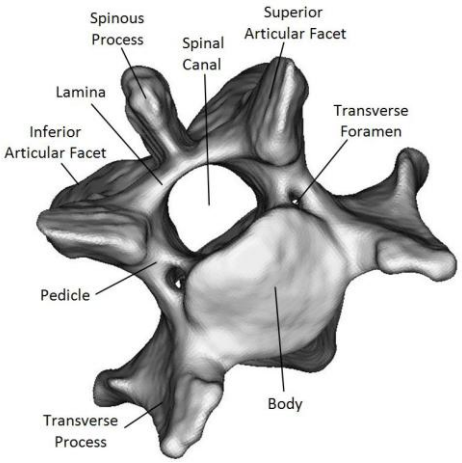

Figure 4 The bony anatomy of the C4 sheep vertebra.

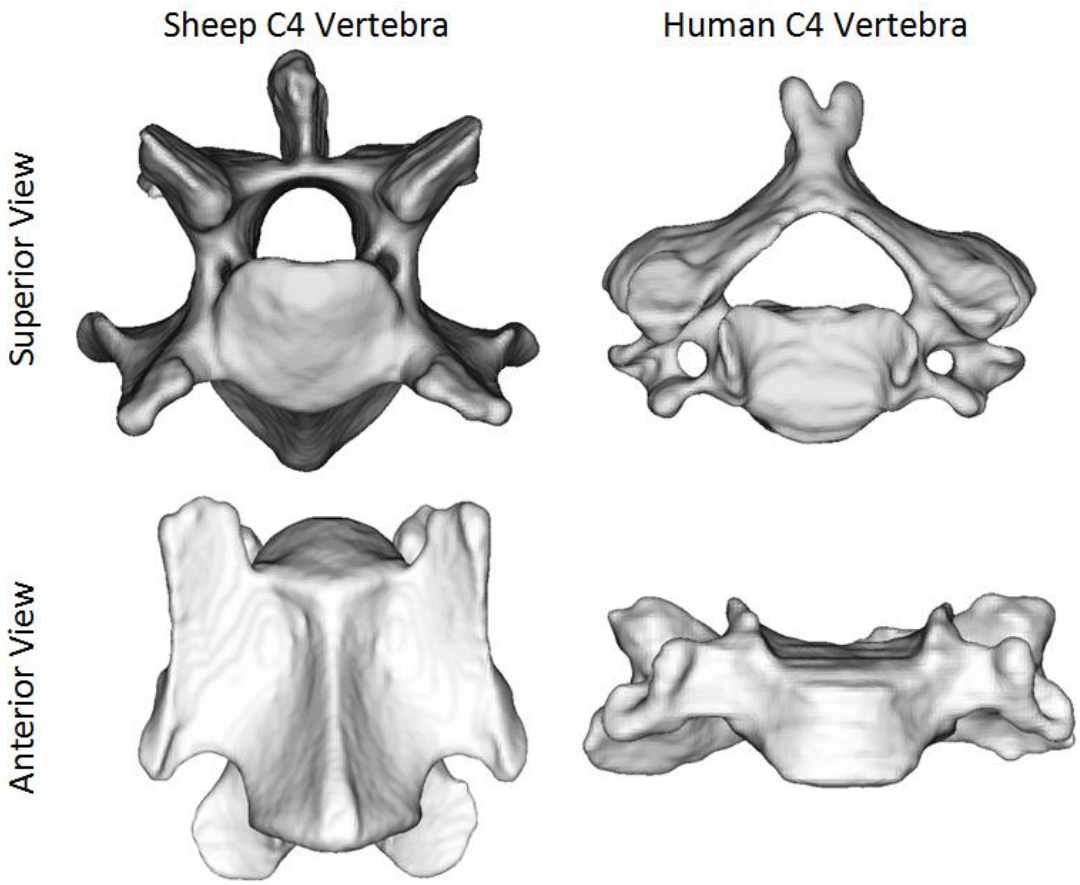

Figure 5 The sheep C4 vertebra and human C4 vertebra.

Previous studies have compared the anatomy of the sheep cervical spine to the human cervical spine [4, 6, 7]. Cain and colleagues [7] studied the similarities and differences of the bony and vascular anatomy, including the spinal cord. They found that sheep have similar vertebral body cross-sectional area, size of the spinal canal and intervertebral discs, and similar structural configuration compared to humans. However, the sheep spine does not have uncovertebral joints like human intervertebral discs have. The uncovertebral joint is an articulation formed by the space between one vertebral body and the unicate processes that project superiorly from the vertebral body immediately below it [25]. Cain and colleagues concluded that the sheep is a suitable anatomical model for spinal trauma and other pathological studies.

Wilke and colleagues [6] studied the cervical, thoracic, and lumbar region of the sheep spine with anatomical comparison to human spines. Sheep vertebral bodies are taller than wide, unlike human vertebral bodies which are wider than tall. Sheep are similar to humans in that the vertebrae are wider than they are deep. They also found that the sheep vertebral body height, width, and depths are greatest in the cervical spine, whereas for humans they are the least. Unlike humans, sheep pedicles are taller than they are wide. But the pedicle widths are similar to humans. The tip to tip transverse process width is similar between the two species. The sheep facets are flat with a dorsolateral orientation whereas human cervical spine facets are laterally oriented. The disc space is approximately two to three mm greater in sheep cervical spine than in humans. Overall they found that the sheep thoracic and lumbar had better correlation to humans than the cervical region. The strongest difference is the vertebral body height, but nonetheless regional trends are similar in most measurements.

Another study conducted by Kandziora et al. [4] focused on a detailed anatomic comparison of the sheep and human cervical spine. They also performed a biomechanical study, which is discussed in Section 2.3. Radiologic measurements were taken in four projections and measured using a digital ruler and goniometer. The bone mineral density was compared utilizing CT scans that were calibrated with a six-point bone mineral density phantom. Measurements were taken at the center of the body and three millimeters from the endplates. They found the bone mineral density was not significantly different between specimens; however there was more variation in the human bone mineral density. The endplate bone mineral density was around 0.4-0.45 g/cm^3 where as the center of the body the density was around 0.3-0.35 g/cm^3 for both human and sheep. Anatomical dimensions taken using a digital ruler found that the sheep vertebral bodies are conical where as human vertebrae are cylindrical. The sheep cervical spine bodies (27-45 mm) are taller than human (14-15 mm). They also found that the sheep pedicles (17-32 mm) are taller than humans (7.4-8.5 mm), but there is no

difference in width (4-7 mm). Based on this study, Kandziora and colleagues deemed sheep cervical spine as an acceptable model for precursor to human models.

2.3 Previous Biomechanical Studies

Although anatomical similarities are important, biomechanical correspondence is imperative for studying the effects of disorders, surgical techniques, and implant designs. Studies by Wilke and colleagues [3], Kandziora et al. [4], and Clarke et al. [16] have focused on experimental biomechanics of the sheep cervical functional spinal units (FSUs). Szotek and colleagues [8] studied the multilevel (C2-C7) sheep spine under axial compression and flexion-extension. The various studies have different loading techniques, rates, and magnitudes which provide a great deal of information but is challenging for comparison purposes.

The study by Wilke and colleagues [3] was a comprehensive study focusing on the entire sheep spine that compared the results to corresponding human spine motion segments. Fourteen four-year-old female Merino sheep specimen were divided into FSUs, providing a minimum of six specimens for each level (C1-C2 to L6-L7). Each FSU was embedded in polymethylmethacrylate. The specimens were tested utilizing a stepper motor spine tester, at a constant rate of 1.7 degrees/second. The cervical FSUs were tested using a non-damaging ±2.5 Nm in flexion, extension, lateral bending, and axial rotation with no preload. At C1-C2, testing was conducted at 1 Nm. Data was gathered on the third cycle to reduce the effects of viscoelastic response. The specimen moved unconstrained in the five uncontrolled degrees of freedom. Motion was measured using a three-dimensional goniometric linkage system. Wilke studied the motion at the maximum moment, the neutral zone, and various stiffness parameters. They found the range of motion (ROM) for the cervical spine is greatest at C1-C2. For C2-C7, the range of motion increases caudally. In general, ROM in extension was greater than in flexion. Lateral bending exhibited the largest motion. Table 1 lists the various ROM for each

loading condition. The neutral zone was 15% to 80% of total motion for all loading modes. The average neutral zone was approximately 60%, 50%, 70%, and 30% of the total motion for flexion, extension, lateral bending, and axial rotation, respectively. They concluded that the ROMs of sheep spine are qualitatively similar in their craniocaudal trends to those motions of human specimens reported in literature. Thus, they can be useful to model disc surgeries, bone healing processes, as well as spinal implants.

Table 1 Biomechanical properties of sheep functional spinal units from C1-C2 to C6-C7 with a pure moment of 2.5 Nm, except at C1-C2 (1 Nm) reported by Wilke and colleagues [3].

FSU	Flexion	Extension	Lateral Bending	Axial Rotation
C1-C2	24.96 ± 6.16	25.36 ± 6.48	17.26 ± 1.67	49.02 ± 5.92
C2-C3	2.75 ± 0.72	3.19 ± 0.52	10.92 ± 1.80	2.88 ± 0.86
C3-C4	5.56 ± 1.81	5.72 ± 1.86	11.55 ± 1.35	3.60 ± 1.40
C4-C5	6.51 ± 1.89	8.05 ± 2.35	11.64 ± 1.31	5.00 ± 1.33
C5-C6	8.40 ± 1.90	9.59 ± 2.46	13.76 ± 1.56	9.45 ± 2.23
C6-C7	11.09 ± 2.30	12.2 ± 1.91	15.86 ± 2.79	8.76 ± 3.54

As mentioned in Section 2.1.2, Kandziora and colleagues [4] conducted a comprehensive study comparing the anatomy and biomechanics of sheep and human cervical spine. They utilized twenty female Merino sheep and twenty fresh human cadaver cervical spines. Each spine was divided into FSUs from C2-C3 to C6-C7. Pure bending moments (flexion-extension, lateral bending, and axial rotation) were applied using a system of cables and pulleys. The study applied a compressive preload of 25N, representing the average weight of the sheep's head. Moments were applied quasi-statically in increments of 1 Nm up to the maximum moment of 6 Nm. Specimens underwent four cycles at a velocity of 1.2 mm/s of the transverse bar, with the fourth

cycle measured. Kandziora and colleagues found that the range of motion was significantly different between the sheep and human, except for flexion-extension at C3-C4 and C5-C6, axial rotation at C2-C3, and lateral bending at C2-C3, C3-C4, and C4-C5. They concluded that the sheep C2-C3 and C3-C4 are the most suitable comparisons to human biomechanics.

Clarke et al. [16] compared the biomechanics of mature and immature spine motion segments in response to dynamic torque applications utilizing sheep specimen. They studied the cervical, thoracic, and lumbar spine. The study used newborn (immature) and 2 year old (mature) merino sheep, using six C3-C4 motion segments for both groups. Flexion-extension, lateral bending, and axial rotation moments (2.5 Nm for mature; 0.25 Nm for immature) were applied at 5°/second for five cycles. Data was gathered on the fifth cycle, focusing on the range of motion, the neutral zone, and stiffness. They found that the torque-deflection curves were significantly different between the mature and immature spine. The range of motion of immature spine segments was greater than the corresponding mature spine segments. Additionally, the neutral zone of immature segments was greater than mature segments. The initial stiffness for the immature segments was much lower than the corresponding mature segments. For the range of motion, neutral zone, and stiffness measures, the magnitude of difference was not the same across segment levels and axes. Based on this study, the authors concluded that under similar loading condition, the pediatric spine would have greater range of motion compared with the adult spine. This may increase the risk of injury due to increased motion or strain of the spinal cord. Finally, they concluded that simple scaling to the torque-deflection properties from the adult spine may not be appropriate for pediatric spine because the variability between the spinal maturity and moment axis and/or motion segment level.

Szotek and colleagues [8] studied the biomechanical response of the sheep cervical spine and porcine lumbar spine. Focusing on the sheep cervical spine, they used

seven 4-year-old sheep to study the C2-C7 biomechanics. The C2 and C7 were fixed in polyester resin casts. Biomechanical testing was performed using a uniaxial material testing machine (MTS 858 Mini Bionix Test System) in both axial compression and flexion-extension. The flexion-extension tests were conducted using a modified loading system where the specimen was placed horizontally with unconstrained motion in the horizontal plane at the C2 (Figure 6). They studied both intact as well as the affects of stabilizing a destabilized spine using an anterior plate and interbody graft in the C4-C5 segment. They found that a maximum compression of 8mm resulted in 450 N and 600 N forces for the intact and stabilized conditions, respectively. At 12 degrees of flexion the intact and stabilized conditions had resulted in 2.7 Nm and 6.7 Nm moments, respectively. For extension to seven degrees, the intact had a 0.1 Nm moment and the stabilized condition had a 0.2 Nm moment. They also compared stiffness along various regions of the nonlinear curves and determined there was no significant difference between the intact and stabilized condition for axial compression. However, there was significant difference for flexion. This study did not give details on how they calculated the angles or moments. Also, the testing apparatus does not provide pure bending moments.

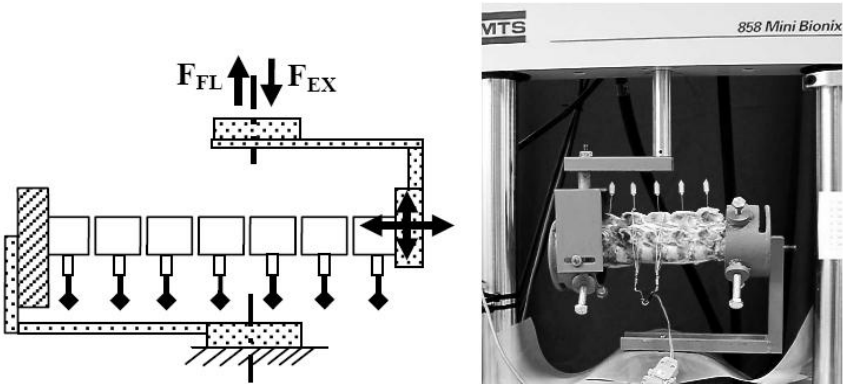

Figure 6 The testing apparatus used by Szotek and colleagues [8] for flexion-extension.

2.4 Finite Element Method

Musculoskeletal finite element (FE) modeling has proven an invaluable tool in orthopaedic-related research, dating back to 1972 [26]. The finite element method was first used to model the human spine in 1973 by Liu and Ray [27]. They focused on the wave propagation in the spine. One of the first attempts to model the intervertebral disc was done by Belytschko et al in 1974 [27, 28]. They developed an axissymetric model incorporating linear material properties. By applying axial loads, they studied the effects of material properties and geometry on the stress-distribution and intradiscal pressure. Since then, there have been several models focusing on the human spine. However, to my knowledge, there has been only one study focusing on the sheep cervical spine, developed by Kiapour and colleagues [17].

2.4.1 Sheep Finite Element Method

Kiapour and colleagues [17] developed a C3-C4 sheep spine model using CT scan data to define the bony geometry. The ligaments (interspinous, intertransverse, posterior longitudinal, capsular, anterior longitudinal and ligamentum flavum) were simulated using two-noded truss elements with "hypoelastic" material properties. Material properties were based on values reported in literature for the human spine. The model was validated through *in vitro* testing, using six fresh cadaveric C3-C4 sheep cervical spine segments. Each segment underwent a bending moment of 2.5 Nm with a 25 N compressive follower load. Additionally, they simulated injury by removing the interspinous, intertransverse, and ligamentum flavum. They report that the finite element model predicted peak motions comparable to the experimental data. However, as shown in Figure 7, the model predicted motions are slightly greater than half of the experimental data. During flexion and lateral bending the motion increased for the injured case, however, there was little difference for extension and axial rotation. They concluded that the sheep spine model showed similar biomechanical behavior to the human spine model.

However, the load sharing of the disc and facets was different between the sheep and human spine. Kiapour and colleagues [29] also modeled the sheep L3-L4 lumbar spine following the same procedure and material properties.

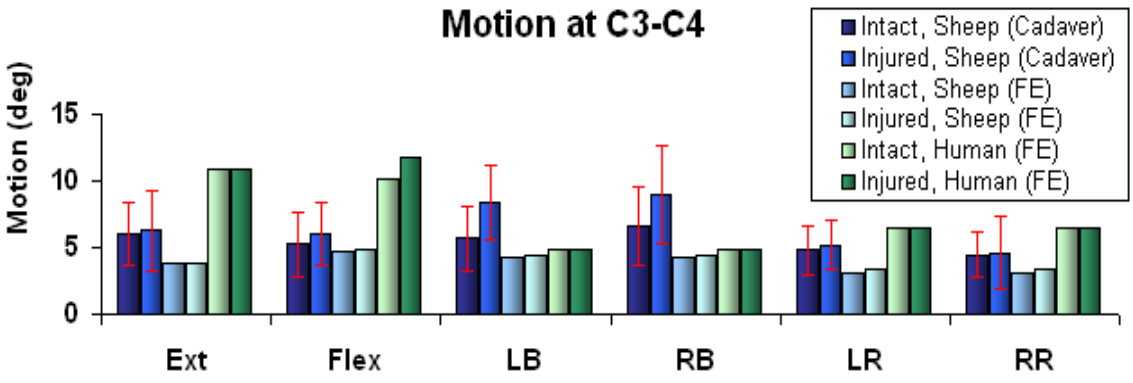

Figure 7 Comparison of motion between the finite element model and cadaver cases for both sheep and human C34 [17].

2.4.2 Human Cervical Spine Finite Element Method

Although the number of sheep finite element models is limited, many researchers have developed human spine models, both lumbar and cervical [30-54]. The concepts are the same between sheep and human spine modeling since both have similar anatomy. Many model geometries are based on image data such as CT images. However, more variability is seen when modeling the soft tissues such as the ligaments, intervertebral discs, and facet cartilage and joints. Therefore, this section will focus on the different techniques used to model the soft tissues.

2.4.2.1 Ligament Definitions

Common methods used to model the ligaments include two-noded truss or cable elements in tension only [30-41], springs [42, 43], and membrane elements [37, 42]. Initial models used linear material properties for the ligaments [32]. Teo et al. [36]

modeled the nonlinearity of the ligaments using linear material properties, but incorporated an initial slackness. To mimic physiologic motion, the ligament material properties are often defined using force-displacement curves [33, 35, 43] or stress-strain curves [30, 31, 37, 40, 41]. Those modeled with stress-strain definition incorporate bi-linear [37] or hypoelastic [31, 40, 41] material properties. Additionally, there have been several lumbar spine models that have incorporated hypoelastic ligament properties [44-47].

2.4.2.2 Intervertebral Disc Definitions

The intervertebral discs are divided into the nucleus pulposus and the annulus fibrosus. The two main methods for modeling the nucleus are using (1) incompressible fluid elements [30, 31, 33, 35, 40, 41, 43] and (2) nearly incompressible solid elements [32, 36, 37, 42, 48, 49, 55]. A majority of the models incorporating solid elements for the nucleus use linear material properties, however del Palomar et al. [37] incorporated hyperelastic (Neo-Hookean) material properties.

The annulus fibrosus has been modeled using various properties and techniques. Yoganandan et al. [48] modeled the annulus by using linear material properties (E=3.4 MPa, v=0.40), where the annular fibers were not included. However, the annulus is often divided into the annular fibers and annulus matrix. This is often captured by modeling the annulus with solid elements (matrix) reinforced with rebar elements (fibers). The fibers are around 20% of the matrix volume and angled at ±25˚. The annulus matrix is often modeled as a linear elastic material [30-33, 35, 36, 40, 41, 49, 55], however a more recent model has included hyperelastic and user defined strain energy functions [37]. The fiber properties are captured with linear [30, 35, 41, 49], hyperelastic [37, 43], or hypoelastic [34, 38-40] material properties.

Wheeldon and colleagues [43] further divided the annulus into anterior, posterior, and lateral regions. Each region and level was defined using specific material properties.

The anterior and posterior grounds were modeled using hyperfoam material properties and the lateral region incorporated linear elastic material properties (1 MPa). For the fibers, the lateral and posterior regions had hyperelastic Marlow material properties and the anterior region was linear elastic (500 MPa). The Poisson's ratio was 0.45 for both the grounds and fibers. Kallemeyn and colleagues [40] also divided the annulus into anterior, posterior, and lateral regions. The annulus grounds were modeled using different linear elastic material properties for each region and level.

In addition to cervical spine models of the intervertebral disc, models of the lumbar intervertebral discs have also incorporated hyperelastic material properties. Noailly et al. [45] modeled the annulus matrix using the Neo-Hookean hyperelastic formulation with hypoelastic fibers. The nucleus was modeled using the hyperelastic Mooney-Rivlin formulation. Schmidt et al. [50] modeled the lumbar disc using the Mooney-Rivlin formulation for the annulus grounds and nucleus; the annular fibers were modeled using unidirectional spring elements. Rohlmann and colleagues [51] modeled the annulus grounds at Neo-Hookean hyperelastic with the fibers incorporated as nonlinear springs. Bowden and colleagues [52] modeled the nucleus using the Mooney-Rivlin formulation with the annulus fibrosus as the Eberlien hyperelastic formulation. Zhong et al. [53] and Chen et al. [54] modeled the lumbar annulus grounds using the hyperelastic Mooney-Rivlin formulation with linear elastic fiber reinforcement. Ayturk and colleagues [56] modeled the lumbar annulus grounds using the hyperelastic Yeoh formulation reinforced with user defined fiber material properties.

2.4.2.3 Facet Joint Definitions

The facet joints have been modeled using gap elements [30, 31] or treating the facets as finite-sliding surface interactions with an exponential pressure-overclosure relationship [36, 38-41]. Recently, detailed models have been developed for the facet. The detailed facet joints are modeled with fluid elements representing the synovial fluid,

membrane elements mimicking the synovial membrane, and solid elements to capture the cartilage definitions [33, 35, 43]. For these models, the elastic modulus is 10.4 MPa for the cartilage and 5.0-12.0 MPa for the membrane. The Poisson's ratio was 0.40 for both the cartilage and the membrane.

2.5 Ligament Testing

For the finite element model to have biomechanical validity, the model requires accurate geometry and material properties. In particular, it is important to understand the material properties and geometries of the ligaments since they play a key role in the stability of the spine. There have been several studies to determined the geometry and material properties of the human cervical spine, however, to date there have not been any studies focusing on the sheep cervical spine. Also note, the studies focusing on human ligament properties have used various loading rates and testing condition making it challenging to compare and determine average material properties.

One of the earlier studies of human cervical spinal ligaments was conducted by Chazal and colleagues [57]. They tested forty-three ligaments from eighteen specimen; a majority of the ligaments from the thoracic and lumbar region. They tested the ALL, PLL, LF, ISL and SSL, and the intertransverse ligaments from both cadaveric and living subjects that were undergoing surgical procedures. Only the ALL and PLL were tested at the cervical level. Ligaments were stretched using an original testing machine with loads measured through electrical strain gauges. The ligaments were not directly clamped, but the bone instead. Cross-sectional area was measured using a palpator; length was measured with a micrometer. The ligaments were stretched at a constant 1 mm/minute. The load-deformation curves were sigmoid shaped, as expected; ligaments experienced hysteresis, most noticeable for the LF during the first portion of the curve. They found that the intertransverse ligaments had the smallest deformation for the highest loads, whereas the ALL had the largest deformations for the smallest loads. They observed a

neutral zone, where small changes in stress resulted in large strains. They determined the LF, intertransverse, and the PLL are the most resistant.

Myklebust and colleagues [58] studied C2-S1 ligaments from 41 fresh human male cadavers. At each level, the disc and all supporting structures except the ligament to be tested was sectioned. They studied the ALL, PLL, CL, ISL, and LF. A minimum of three specimens were tested for each ligament at each level. The CLs were tested as a bilateral unit including the facet joints. The vertebral bodies above and below the ligament were secured in a frame using Steinman pins. Ligaments were aligned to undergo direct axial tension at a rate of 10mm/second using an MTS electrohydraulic system. They found the ALL was the strongest at the high cervical and lower thoracic and lumbar regions. LF was the weakest in the mid-cervical area and strongest in the lower thoracic region. The ISL was the weakest of the ligaments tested. They determined the deflection at failure tended to increase with distance from the center of rotation. Ligament strength increased from cervical to lumbar.

In 1989, Yoganandan et al. [24] studied the effects of loading rate on the human cervical spine ligaments. They used 44 isolated ALL and LFs. The superior and inferior vertebral bodies were fixed in a custom frame using four to six Steinmann pins. Using an electrohydraulic testing machine, the ligaments were loaded at four different constant loading rates (8.89, 25.0, 250.0, and 2500.0 mm/second). The biomechanical response was nonlinear and sigmoidal. With an increase in loading rate, the mean failure forces and energy-absorbing capacity increased nonlinearly for both the ALL and LF.

Yoganandan and colleagues [59] also studied the geometry and mechanical properties of the cervical spine ligaments (ALL, PLL, CL, LF, and ISL) to use as input for a finite element analysis. Eight cadaveric specimens C2-T1 were used to study the ligament geometries; each specimen was scanned in a CT scanner and sectioned using a cryomicrotone at intervals of 20-40 μm. Four specimens were sectioned axially for ligament cross-section measurements and four specimens were dissected sagittally for

length measurements. Ligament lengths were measured as shown in Figure 8. The cross-sectional area of each ligament was projected onto paper and the boundary outline traced; measurements were taken at mid-height approximately for each ligament. Biomechanical properties were determined using 25 cadaveric specimens, C2-T1. The vertebral bodies above and below the ligament of interest were fixed in a custom frame using Steinmann pins and tested using a material testing system. Each specimen was preconditioned under tension at a slow rate of 10mm/second. Displacements were measured using the linear variable differential transformer built into the system. The CL and LF had the highest cross-sectional areas whereas the ALL and PLL have the longest lengths. Biomechanical failure strains were higher for the LF, ISL, and CL than for the ALL and PLL. On the other hand the failure stress was higher for the ALL and PLL, than for the LF, ISL, and CL.

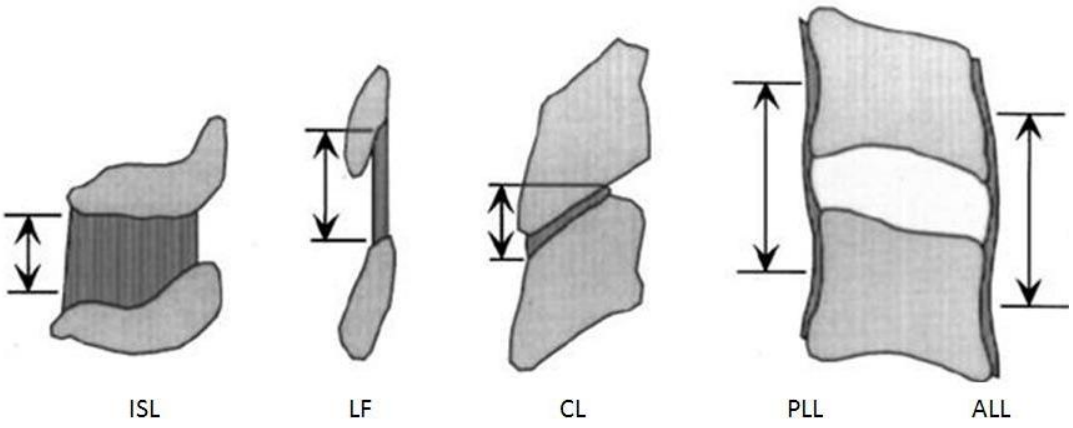

Figure 8 Illustration of the ligament length definitions used by Yoganandan et al. [59].

Ivancic et al. [60] studied the tensile mechanical properties at a fast elongation rate (723 mm/s) for the human cervical ALL, PLL, CL, LF, ISL+SSL, and intervertebral disc. The study used six human cadaveric specimens (C2-T1) divided into FSUs ranging

from C2-C3 to C7-T1. Each FSU was sectioned at the pedicles. The anterior portions were coronally sectioned in thirds to create the ALL, middle-third disc (MTD), and the PLL bone-ligament-bone specimens. The posterior was sectioned to create CL, LF, and ISL+SSL specimens. The bone-ligament-bone specimens were anchored in quick setting polymer resin mounts by using 19-gauge needles inserted through perpendicular drilled holes. Each specimen was placed in an apparatus consisting of a pneumatic cylinder supplied with compressed air. Force was measured with a uni-axial load cell; elongation was measured using a Hall Effect sensor. The ligaments were preloaded with 5N tension to define the zero elongation. Average peak ligament elongation rate was 723 mm/second. In order to compare the elongations to physiological elongations, they created a mathematical model. Physiological elongations were calculated as the difference in ligament lengths at maximum flexion for PLL, CL, LF, and ISL+SLL and at maximum extension for ALL and MTD, relative to neutral posture. The physiological elongations were largest for the ISL+SSL and LF and the MTD had the smallest elongation. The peak ligament elongation was generally greater than the physiological range except for the LF and ISL+SLL. The highest peak forces were in the LF and CL. The highest peak elongation was in the ISL+SLL. The LF is generally the stiffest ligaments and the ISL+SLL is the least stiff. Every attempt was made to elongate the ligaments along the direction of the fibers. Comparing the fast rate results to the previously reported slow rate elongation, they found the average peak force increased whereas the peak elongation and energy-absorbing capacity decreased with increased elongation rate.

Bass et al. [61] also studied the cervical spinal ligaments under a fast strain rate (627mm/s). Eleven cadaveric specimen (6 male, 5 female) divided into FSUs ranging from C3-C4 to C7-T1 were further divided into bone-ligament-bone complexes for the ALL, PLL, and LF. Small wood screws were inserted into the bone on either side of the ligament and the bones were potted with a 2-part urethane casting in aluminum cups.

Each specimen was tested on a universal test machine under uniaxial tension and enclosed in an environmental chamber to maintain physiologic temperature and humidity. Each ligament complex was preloaded to 4N tension where upon the ligament length was measured establishing initial position. The ligaments were preconditioned with a 10% engineering strain sinusoidal input at 2Hz for 20 cycles. The ligament structures were subjected to ramp-hold strains of 25% and 50%, an oscillartory input to 50% strain, ramp-hold input of 75%, 100%, and 300%. Ligament cross-sectional area was assumed to be directly proportional to superior vertebral body endplate width using the cross-sectional area and vertebral body widths published for 50^{th} percentile male. The average deformation rate of the failure tests was 627 mm/s. They found a larger number of male ligaments failed during the 100% strain test whereas the majority of female ligaments failed during the 300% strain test. There were a greater number of transections than any other failure type. There was no significant difference found in true strain for ligament type; however there was a significant difference in force and true stress. The found that the larger moment arm of the LF resulted in lower stress for a similar amount of strain. Comparing these fast loading rates to slower loading rates (10mm/second), the faster rate failure stress was substantially larger, ranging from a factor of two for the LF to five for the PLL.

Additionally, Lucas and colleagues [62] studied the viscoelastic properties of the cervical spine ligaments under fast strain-rate deformation using eleven human cadavers, focusing on the ALL, PLL, and LF. Bone-ligament-bone complexes were generated by dividing the body at midline in the coronal plane (ALL), the pedicles (PLL), and cutting midway between the anterior and posterior aspect of the spinous process (LF). Specimens were potted using wood screws and two-part urethane casting resin. Specimens were tested in tension using a universal test machine with the specimen enclosed in an environmental chamber to maintain physiological temperature and humidity. Zero strain state was defined by applying a 4 N tensile preload with the initial length measured using

digital calipers. The ALL and PLL initial length was measured from endplate to endplate; the LF length was defined as the distance between the adjacent laminas. Each ligament was preconditioned with a 10% sinusoidal input at 2Hz for 120 cycles and then subjected to tensile ramp-hold inputs to strains of 25% and 50%, and an oscillatory sinusoid input to 50% stain. They found that a large amount of the relaxation occurred during the displacement ramp onset. Additionally, there are differences in the ALL, PLL, and LF relaxation functions. However, there was no significant difference in the relaxation function based on gender or among spinal levels for the fast rate and steady-state relaxation. They found the PLL and ALL had larger instantaneous elastic force than the LF, as expected.

Troyer and Puttlitz [63] conducted a study to determine the viscoelastic behavior of cervical spine ligaments under varying levels of applied strain. Six C5-C6 FSUs were transected at the mid-coronal plane of the vertebral body and at the pedicles to obtain bone-ligament-bone structure of the ALL, PLL, and LF. Wood screws were inserted into the endplates for the ALL and PLL structures and the superior and inferior surface of the articulating processes for the LF; each structure was potted using polymethylmethacrylate. Each test was conducted using a material testing machine with the ligaments enclosed in an environmental chamber to keep them hydrated. Specimens were held at 0N for one hour to obtain specimen equilibrium and then compressed to 25N and the displacement was zeroed. Specimens were loaded to 5N tension at 0.05mm/second with the resulting displacement used as the reference point. Ligaments were preconditioned at 10% strain, applied at 1 Hz for 120 cycles, then subsequently subjected to a randomized application of 4, 6, 8, 10, 12, 14, 16, 18, 20, and 25% strain applied at 5mm/second. Strains were held for 100s and then returned to the reference point for 600s, gathering force relaxation data. The data was fitted with a power relationship; this relationship predicted the response well with r^2 averaging 0.983, 0.901, and 0.873 for the ALL, PLL, and LF, respectively. They found there is a strong

correlation between the magnitude of the initial force and the applied level of strain and the relaxation rates were strongly dependent on the applied strain level. All the ligaments showed an increase in relaxation rate as strain increased.

Additionally, Ambrosetti-Giudici and colleagues [64] studied the strain-time dependent relaxation response of the ovine poster spinal ligaments. They studied twenty-four lumber spinal segments from eight sheep focusing on the adjacent spinous process and ISL and/or SSL. Specimens were tested on the hydraulic material testing machine equipped with custom-made clamps used to fix the specimens. A preload of 5N was applied in order to define a uniform reference point for initial length. Preconditioning included three loading (1mm/s) and unloading cycles. Then the specimen was held at a constant length for five minutes to study force relaxation. Specimens were stretched to 5%, 10%, 15%, and 20% with five minute recovery. The force-relaxation response was described with a nonlinear viscoelastic model. They found that the fit functions at lower strains (5% and 10%) had lower correlation coefficients than data at higher strains (15% and 20%). The relaxation rate increased with higher strains for both ligaments. The concluded by applying a 5N preload, the true pre-strain was up to 15%, thus the final total strain was around 35%, which is slightly higher than the physiological strain range for human lumbar posterior ligaments (28-33%) [23].

2.6 Significance

Currently, there is limited knowledge of the biomechanics of the sheep cervical spine. Oftentimes the sheep spine is utilized for preliminary or corresponding studies to the human spine, so it is important to know the biomechanical similarities and differences between the two. For example, it is important to know the differences in soft tissue material properties and the overall range of motion between specimen when comparing the effects of an implant or fusion. Noting the differences and similarities in disc size and shape, as well as material properties and biomechanics between the specimens is critical

for evaluating the effects of disc replacement or fusion techniques. Understanding the role various ligaments have on the range of motion is also something to note. Therefore, having a more detailed comparison between the sheep and human cervical spine is essential.

Previously, studies of the sheep spine have focused on the functional spinal units to study the range of motion and stiffness; however the entire lower cervical spine is often of interest. Many studies of the human cervical spine focus on multilevel specimens/models, so it is important to obtain multilevel sheep spine data as well. Studies [65, 66] have shown differences in the range of motion between a functional spinal unit and the motion of the same level tested in a multilevel segment. Additionally, many research studies look at surgical techniques, implants, or fusions at multiple levels as well as the effects on adjacent levels. Thus, this study focused on the C2-C7 sheep cervical spine to gain knowledge of the multilevel biomechanics of the lower cervical spine.

In addition, this study measured the coupled motions which have not been previously reported for the sheep spine. Coupled motions have been reported for the human cervical spine, especially between axial rotation and lateral bending [40, 67-69]. It is important to study these coupled motions to have a true comparison between the sheep and human spine. Because the facet anatomy between sheep and human cervical spines are different, the coupled motions may be different. Based on previous studies [3], the sheep cervical spine is very flexible and has a large neutral zone, both of which could affect off-axis motions. In order to make a recommendation based on sheep studies looking at an implant or device it is important to know the effects on both the primary motions as well as the off-axis/coupled motions. Therefore, this project also studied the coupled motions seen in the sheep spine and compared the similarities and differences to human cervical spine coupled motions.

Furthermore, this study provides insight into the sheep soft tissue material properties. The soft tissues play a crucial role in stability and flexibility of the spine.

Thus, having a comparison between the sheep material properties and the human material properties will allow for a more accurate understanding of how the sheep studies apply to the human cervical spine. Previous studies have reported the ligament material properties for the human cervical and lumbar spine; however there have not been any studies of the sheep cervical spinal ligaments. This was the first study to analyze the nonlinear properties of the sheep cervical spine ligaments and determine the role of each ligament in spine stability.

Moreover, this presents the first C2-C7 sheep cervical spine finite element model; the model incorporates species-specific material properties. Additionally, the model was validated utilizing the multilevel biomechanical data. This model gives insight into biomechanics that cannot be gathered from basic experimental tests, such as facet forces and contact as well as intervertebral disc pressure. The finite element model provides a more detailed comparison between the sheep and human cervical spine in response to specific loading conditions. The validated model was used to simulate a discectomy and fusion at the C3-C4 providing additional details, such as bone stress and disc pressures, that could not be obtained experimentally. With this validated model, future studies can be conducted to determine the effects of various surgical techniques or what effects changing the material properties of an implant design will have on the bone stresses or disc pressures. A validated sheep cervical spine model allows researchers to perform preliminary testing of various implant designs, which in turn reduces the number of specimen that will need to be experimentally tested.

CHAPTER 3: FINITE ELEMENT MODEL DEVELOPMENT

To date, there has only been one finite element study focusing on the sheep cervical spine [17]; the study was limited to a functional spinal unit (C3-C4). However, it is important to study the multilevel spine in order to have a more detailed comparison between the sheep and human cervical spine. Thus, the focus of this study was to develop an anatomically accurate C2-C7 sheep cervical spine model.

The finite element model of the C2-C7 sheep cervical spine was developed using IA-FEMesh [70] and custom spine modeling software [41]. IA-FEMesh [70] is a user-friendly toolkit for generating hexahedral FE models as well as allowing the user to visualize mesh quality. IA-FEMesh is based on a multiblock approach that uses the benefits of both structured and unstructured meshing. In addition to IA-FEMesh, Kallemeyn and colleagues [41] developed custom meshing tools to generate human cervical spine finite element models. These same techniques were used to define the sheep cervical spine mesh.

3.1 Surface Definitions

The sheep cervical spine surfaces were defined using CT data (Siemens Sensation 64 CT scanner, slice thickness 0.6mm, 0.5mm in-plane resolution). The cervical spine vertebrae were manually segmented to define the regions of interest (ROIs). Surfaces (Figure 9a) were generated from these ROIs using Gaussian image-based smoothing (full width half maximum 0.5 mm; iso-surface level 0.9) and saved in STL format. This follows the technique described by DeVries et al. [71], which has been shown to accurately represent bony geometries. Surfaces were generated for C2 through C7 vertebra. Note, the CT data only captured part of the C2 vertebra, and thus the surface representation is not the entire C2 vertebra.

Due to the complex geometry of the cervical spine vertebra, each surface was divided into the vertebral body (Figure 9b) and posterior region to ease mesh

development. Each bony surface was split using in-house software [72] that allows users to mimic surgical techniques such as cutting bones. The surfaces were cut with either a cutting plane (Figure 10a) or box (Figure 10b); at each cut the surface was patched using Delaunay triangulation to create a closed continuous surface.

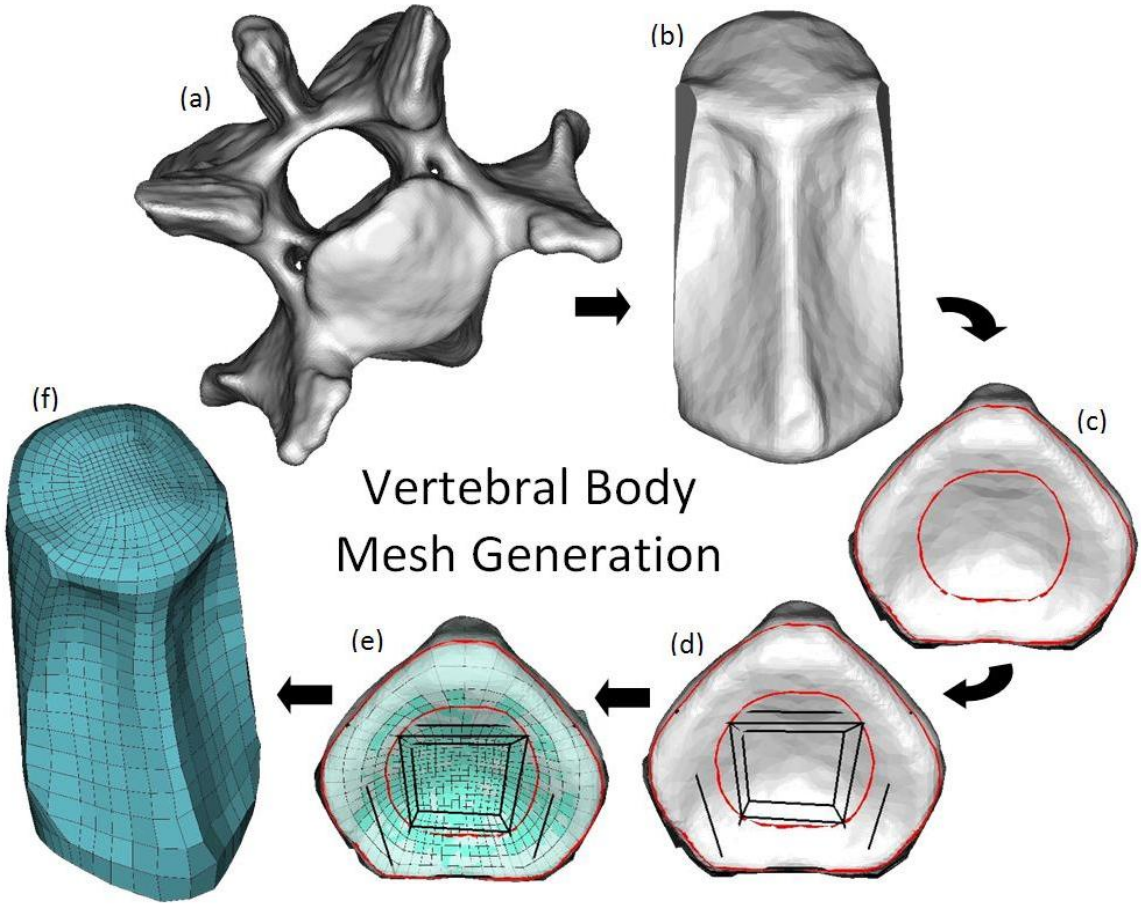

Figure 9 The meshing process for the sheep vertebral body. First (a) the entire vertebra surface is obtained using CT data and (b) the posterior region is clipped off, leaving only the vertebral body. Next, (c) the superior and inferior endplates and periphery of the corresponding nuclei are traced. Based on the surface and traces (d) a butterfly building block is generated. Finally, mesh seeding is assigned and (e) the mesh is projected onto the surface and the interior nodes are interpolated resulting in (f) the final volumetric vertebral body mesh.

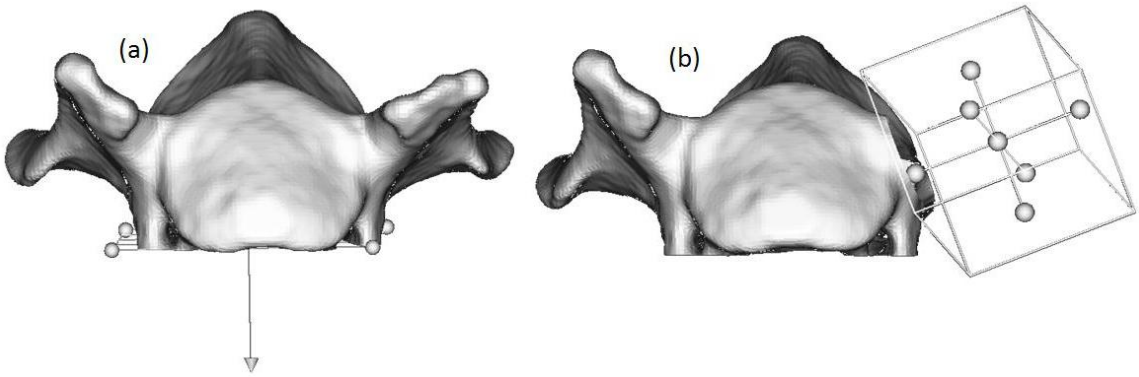

Figure 10 Technique used to remove the posterior region from the body: (a) cutting planes and (b) cutting boxes.

3.2 Building Block Definitions and Mesh Generation

For this study, the vertebral meshes were developed using the building block and mesh generation techniques described by Kallemeyn et al. [41]. The study focused on mesh development of the human cervical spine, focusing on improving the meshing techniques to enable patient-specific models to be generated in a timely fashion. The study described the meshing technique of the vertebral body, posterior region, and intervertebral disc.

3.2.1 The Vertebral Body

Following the techniques described by Kallemeyn and colleagues [41], the first step to generating a mesh of the vertebra was to mesh the vertebral body. The body mesh dictates the mesh of the posterior region and corresponding intervertebral disc meshes. Thus, the body mesh definition is crucial for the remaining mesh definitions.

Using the clipped vertebral body surface, the superior and inferior endplates of the vertebral body, as well as the periphery of the nucleus pulposus were delineated (manually traced) (Figure 9c). This set up the pattern for the intervertebral disc and provides feature edges for the mesh to be projected onto.

The butterfly building block pattern was used to define the building block structure for the sheep cervical spine body (Figure 9d). This pattern allows for easier connectivity and definition of the intervertebral discs. The inner blocks are used to define the nucleus, while the outer ring of blocks defines the annulus layers. The outer-most vertices of the outer blocks are aligned with the endplate delineations. The inner-most vertices of the outer building blocks are aligned with the nucleus periphery tracing.

Mesh seeding was applied to the building block structure, maintaining the same mesh seeding for each vertebral body. It was critical to keep the same mesh seeding along the anterior-posterior and medial-lateral directions for future definition of the intervertebral discs. The corresponding superior and inferior bodies of each intervertebral disc have to consist of the same mesh density in order to maintain mesh continuity. Based on the mesh seeding, a rectilinear mesh is created for the building block structure that is then projected onto the vertebral body, creating a surface mesh (Figure 9e). The mesh projection also takes into account the feature edges earlier delineated at the endplates, capturing the nucleus and endplate definitions. The interior nodes are interpolated between the surface nodes, generating the initial volumetric mesh (Figure 9f).

3.2.2 The Posterior Region

The initial building blocks for the posterior region were created from the vertebral body mesh. Building blocks were defined by picking four nodes where the posterior region attaches to the vertebral body and extruding a given distance (Figure 11a). When choosing the nodes on the vertebral body it is important to consider the building block connectivity, because the mesh seeding from the body mesh will propagate through to corresponding building blocks. Thus, if the building block structure connects the left side to the right side, the same number of elements must be chosen on both sides. From the initial building blocks, additional blocks were added to define the entire posterior region (Figure 11b). Mesh seeding was then applied based on a given distance; however, the

body mesh seeding took precedence over any user defined mesh seeding. Again, the posterior mesh was created by projecting the mesh onto the surface and then interpolating the interior nodes. When creating the posterior mesh, the spine-specific software ensures that the posterior and body nodes match at the interface. This allows the meshes to easily be converged, creating one single mesh instead of separate body and posterior meshes.

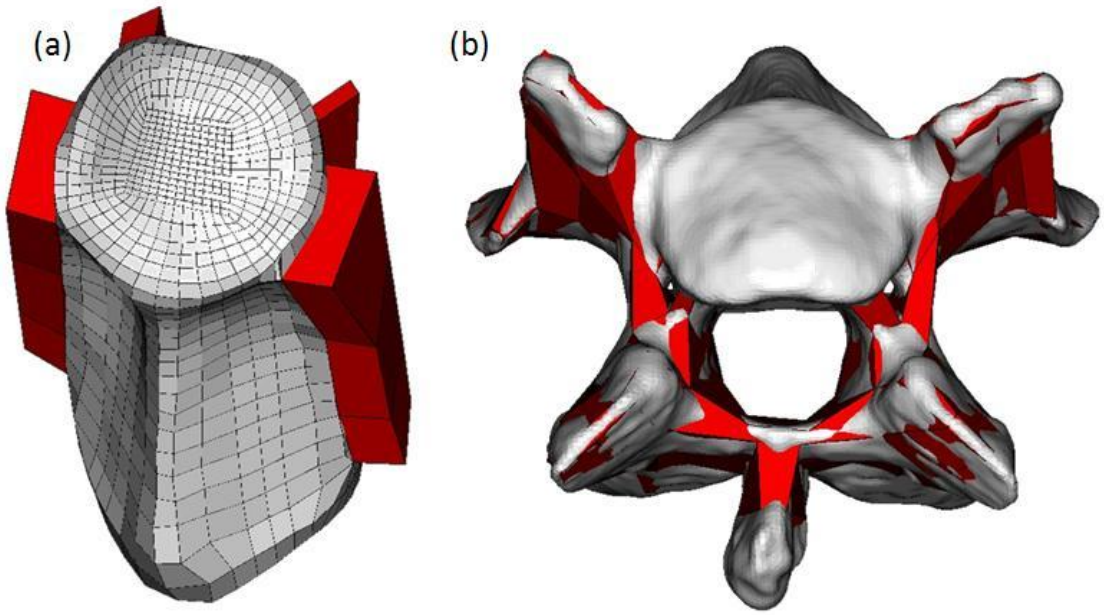

Figure 11 To define the posterior region, (a) initial building blocks were created using the vertebral body mesh and then (b) additional building blocks were added to encompass the entire posterior region.

3.2.3 The Intervertebral Disc

The intervertebral discs were defined using the corresponding vertebral bodies. In the anterior-posterior and lateral directions the intervertebral disc seeding was the same as the vertebral bodies. The number of elements in the axial direction was user defined, assigning the same mesh seeding for each disc. The intervertebral disc meshes were generated by interpolating between the two corresponding vertebral body meshes. The spine code divides the discs into the nucleus and the annulus, which were further divided

into individual rings based on each row of elements. The discs were then subdivided into the anterior, posterior, and lateral regions (Figure 12) for more control over material properties. Additionally, the annulus was reinforced using rebar elements, to mimic the annulus fibers. For the nucleus, a surface mesh was generated to incorporate fluid elements and material properties.

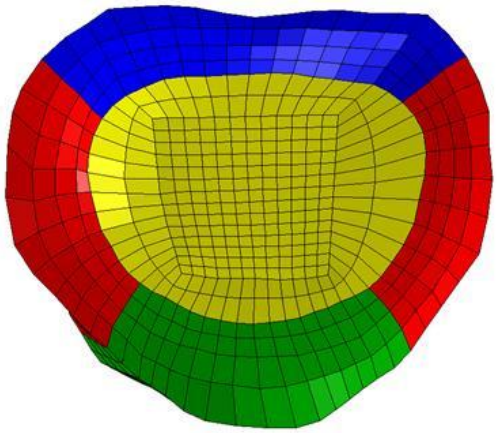

Figure 12 A superior view of the finite element disc definition divided into the anterior (green), posterior (blue), and lateral (red) annulus and nucleus pulposus (yellow).

3.2.4 The Spinal Ligaments

The ligaments of the cervical spine (anterior longitudinal ligament (ALL), posterior longitudinal ligament (PLL), ligamentum flavum (LF), interspinous ligament (ISL), and the capsular ligaments (CL)) were modeled using two-noded truss elements in tension only [30-41]. The ligaments were defined using the in-house code that allowed the user to select the nodes on the mesh. Cross sectional areas for each ligament were based on values reported in literature for the human cervical spinal ligaments. Figure 13a shows an example of the C3-C4 ligamentum flavum defined using five fibers.

3.2.5 The Facet Joints

Due to the small joint space, the cartilage cannot be easily defined at the facet joints. Therefore instead of defining cartilage, the facet joints were modeled as contact over-closures. This technique has been used previously for the human cervical spine [38-41]. This technique incorporates material property definitions at different increments of closure. The material properties increase exponentially as the gap decreases. IA-FEMesh was used to define the surfaces of the facet joints Figure 13b.

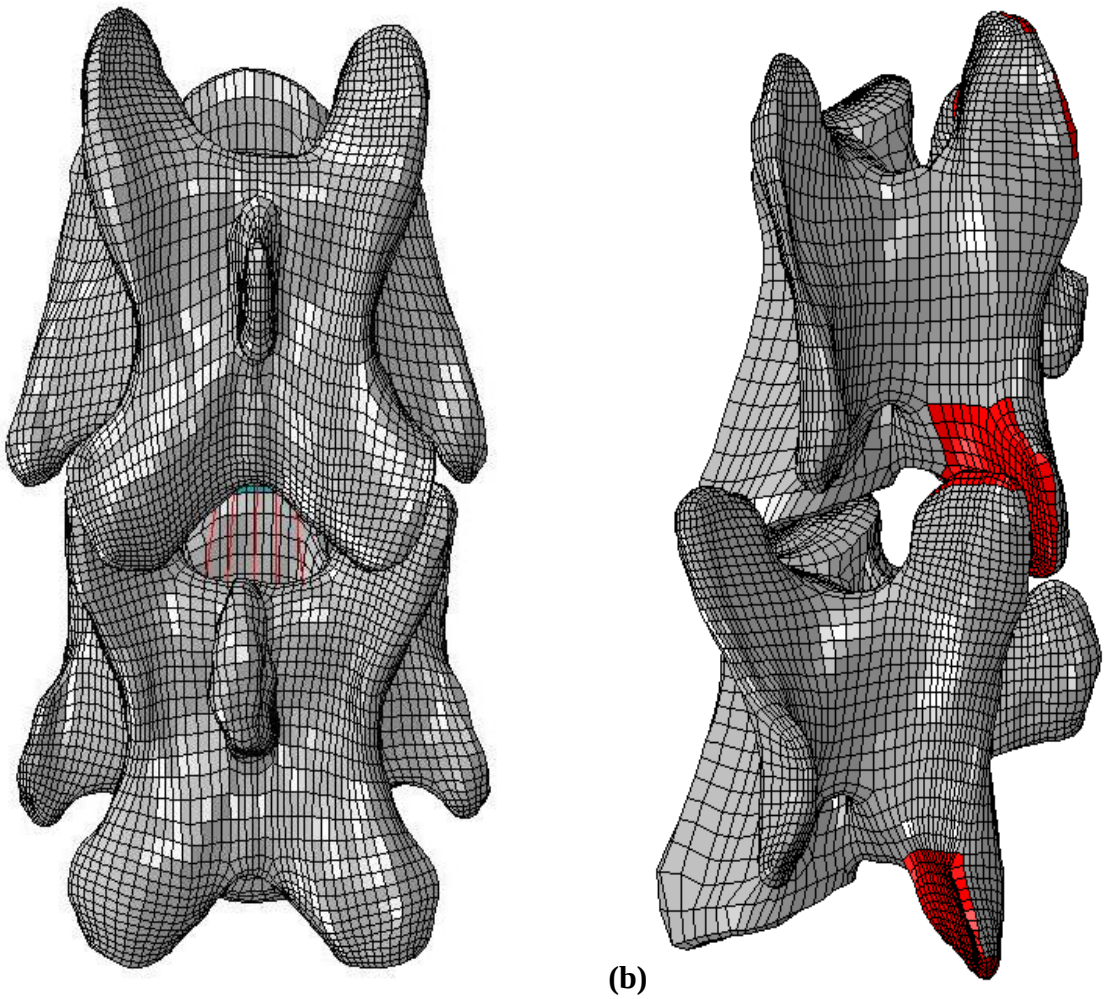

Figure 13 An example of the C34 (a) ligamentum flavum definition (red) and (b) the facet contact area (red) defined using IA-FEMesh.

3.3 Material Properties

For the initial model, material properties were designated based on human material properties reported in literature (Table 2) [40]. Human material properties were utilized because sheep material properties have not been reported in literature. The bony regions (cortical, cancellous, and posterior region) were modeled using linear elastic materials. The nucleus was modeled using fluid elements and the grounds were defined using linear elastic material properties for the various regions of the annulus (anterior, posterior, and lateral). The ligaments and the annulus fibers were defined using hypoelastic material properties

Table 2 The material properties for the initial model; properties were based on human material properties taken from literature [40].

Material	Young's Modulus (MPa)	Poisson's Ratio
Cortical Bone	10000	0.30
Cancellous Bone	450	0.25
Posterior Bone	3500	0.25
Annulus Grounds		
Anterior Region	4.2	0.45
Posterior Region	2.5	0.45
Lateral Region	1.5	0.45
Annulus Fibers	Nonlinear	0.30
Nucleus	Fluid	---
Ligaments	Nonlinear	0.30

3.4 Boundary and Loading Conditions

To mimic physiologic loading and experimental testing, the nodes of the inferior endplate of the C7 were fixed in all directions. A physiologic moment of ±2.5 Nm was applied at the superior surface of C2 using a rigid body surface. Moments were applied in flexion, extension, right and left lateral bending, and right and left axial rotation. At the C2, the model was free to move unconstrained in the five uncontrolled degrees of freedom.

3.5 Comparison to Literature

The initial model was compared to functional spinal unit (FSU) biomechanical data reported by Wilke et al. [3] (Figure 14). At a majority of the levels the predicted motion was underestimated for all directions of loading. One reason for the underestimation may be that the range of motion at each level of the C2-C7 model was compared to the respective FSU ranges of motion reported by Wilke and colleagues [3]. Studies have shown that the specimen length (i.e. multilevel versus FSU) may have an effect on the range of motion at a particular level [65, 66].

Moreover, the lower range of motion predicted by the FE analysis may be attributed to the fact that human soft tissue material properties were used for the initial model. Kiapour and colleagues [17] also incorporated human material properties into their spine finite element model, which underestimated the range of motion. Therefore, it may be that human material properties are too stiff to allow for the range of motion seen for the flexible sheep. Thus, the soft tissue definitions, namely the ligament and disc material properties, as well as the facet contact definitions need to be adjusted accordingly to account for the flexibility of the sheep spine.

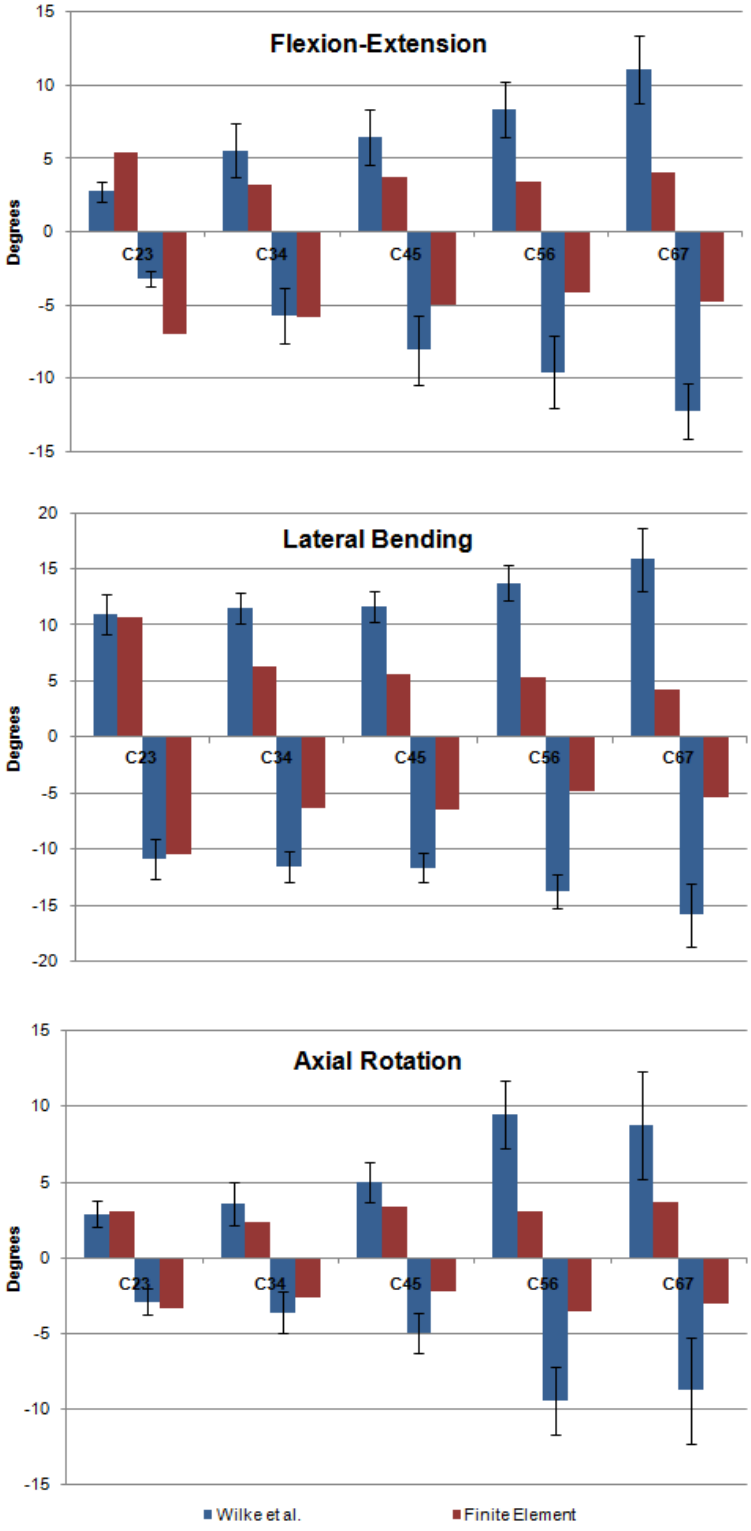

Figure 14 The range of motion predicted by the FE model using human material properties compared to values reported by Wilke et al. [3] for flexion (+) and extension (-), right (+) and left (-) lateral bending, and right (-) and left (+) axial rotation.

CHAPTER 4: BIOMECHANICAL ANALYSIS

Biomechanical correspondence is imperative to understand the effects of disorders, surgical techniques, and implant designs. Studies by Wilke and colleagues [3], Kandziora et al. [4], and Clarke et al. [16] have focused on experimental biomechanics of the sheep cervical functional spinal units (FSUs). In addition to functional spinal unit studies, Szotek and colleagues [8] studied the biomechanics of compression and flexion-extension for the C2-C7 sheep cervical spine. However, to date, there is not a comprehensive study of the sheep spine focusing on all axes of rotation (flexion-extension, lateral bending, and axial rotation) for multilevel specimen.

It is important to study the biomechanics of the entire cervical spine (C2-C7) as opposed to single functional spinal units; studies [65, 66] have shown that the specimen length (i.e. multilevel versus FSU) may have an effect on the measured range of motion at a particular level. Therefore, the purpose of this study was to conduct *in vitro* biomechanics testing (flexion-extension, lateral bending, and axial rotation) of the intact C2-C7 sheep cervical spine. In addition to maximum range of motion, this study focused on the entire loading curve as well as coupled motions. Furthermore, to determine the roles of the ligaments, facets, and intervertebral disc, stepwise destabilization was conducted using functional spinal units. This data will be used to validate the sheep finite element model over the entire loading curve for the multilevel specimen, as opposed to using the maximum range of motion reported in literature.

4.1 Materials and Methods

4.1.1 Intact C2-C7

Ten adult Suffolk sheep cervical (C2-C7) specimens were acquired for biomechanical testing. Computed tomography images were obtained to ensure the specimens were free from abnormal spinal pathologies. Each specimen was stored in two

polypropylene bags and kept frozen at -20˚C until the day of testing. The specimens were thawed to room temperature and denuded of muscle without disruption of the intervertebral discs, ligaments, and joint capsules.

Once the specimens were clean, the inferior surface of the C7 body and the superior surface of the C2 body were potted in a polymer resin (Bondo™, 3M Corporation, St. Paul, MN) using custom designed fixtures. Prior to potting, wood screws were inserted into the endplates to improve interdigitation with the potting material. Each specimen was potted such that the C4-C5 intervertebral disc was parallel to the inferior potting [40].

The specimens were mounted in a biaxial servo-hydraulic materials testing machine (858 Bionix II, MTS Corporation, Eden Prairie, MN) retrofitted with two spine gimbals and a passive XZ table (Figure 15a). The coordinate system was defined as follows: the x-axis points laterally to the left, the y-axis points superiorly, and the z-axis points in the anterior direction. Once fixed in the testing system, each specimen was subjected to nondestructive moments (±2.5 Nm) in flexion-extension, axial rotation, and lateral bending at a rate of 5.0 Nm/min [3] in the absence of a preload. Each test initiated and concluded in the neutral position with zero load. Three loading and unloading cycles were performed with motion data collected on the third cycle (the first two cycles were preconditioning) [73]. The off-axis lateral bending motion during the axial rotation and flexion-extension tests caused instability in several specimens, and therefore could not be tested in pure moment control. Due to this instability, all the specimens underwent flexion-extension and axial rotation loading while lateral bending was held in displacement control (0°) as opposed to moment control (0 Nm). All other channels were in moment/force control.

To establish the moment-rotation relationship for each specimen, motion at each vertebra was monitored using an optoelectronic motion analysis system (Optotrak 3020, NDI, Waterloo, Ontario, Canada), the output of which was synchronized with the MTS

data. Custom-made rigid body markers comprised of three infrared light emitting diodes affixed between two small aluminum plates were placed on each vertebral body and the two gimbals to track the segmental motions (Figure 15b). Motion data was collected at 20 Hz. The relative three-dimensional motion of each vertebra was expressed using Euler angles, with the Euler sequence chosen based on the primary and secondary motions for that particular test. The first rotation in the sequence was the primary motion and the second rotation was assigned to the largest coupled motion. Therefore, XZY, ZYX, and YZX Euler sequences were used for flexion-extension, lateral bending, and axial rotation, respectively.

(a) 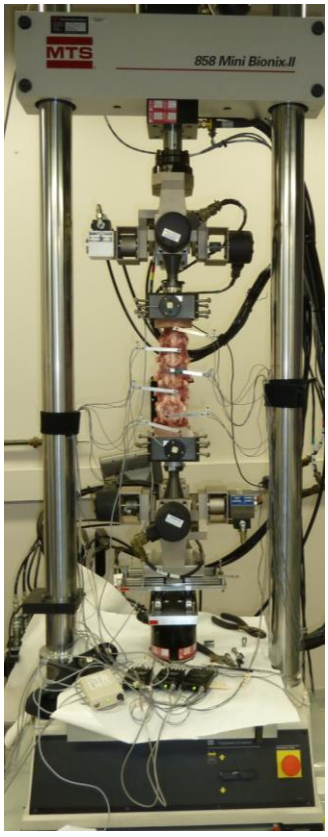

(b) 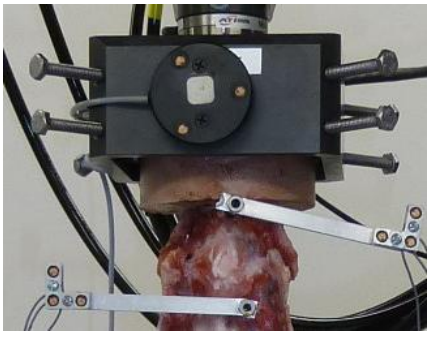

Figure 15 The test setup: (a) a biaxial servo-hydraulic material testing machine including two gimbals and passive XZ table and (b) the rigid body sensors used to track the motions of the vertebral bodies.

An example moment rotation curve is shown in Figure 16. The range of motion can be divided into the neutral zone (NZ) and the elastic zone (EZ). The NZ is the range that the specimen moves free of loading. The EZ is the range of motion from the end of the neutral zone to the point of maximum loading. [73] The neutral position is the mid-point of the neutral zone. Following techniques described by Wilke et al. [73], the neutral position was calculated and the moment-rotation curves were shifted using custom MATLAB software (Version 7.8.0, The MathWorks, Inc., Natick, MA) so the neutral position was at zero degrees.

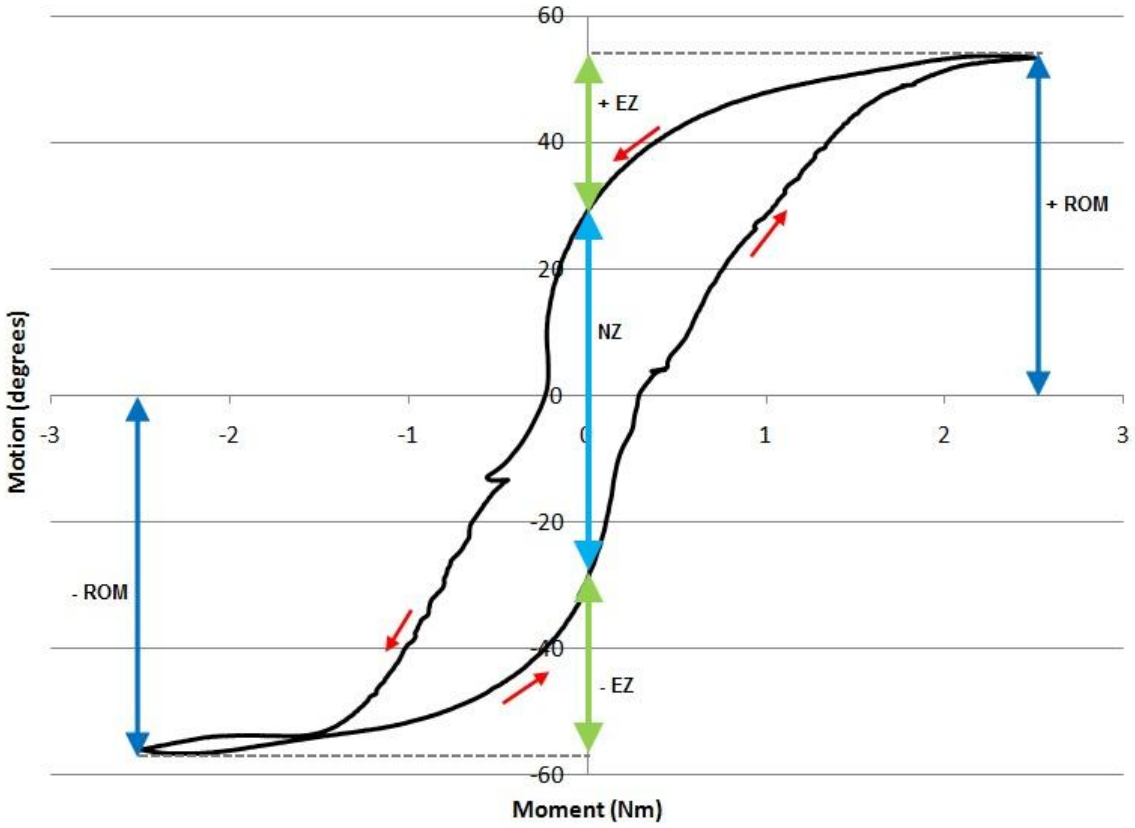

Figure 16 A typical moment-rotation curve defining the neutral zone (NZ), elastic zones (EZ), and range of motion (ROM).

4.1.2 Functional Spinal Unit Destabilization

Two of the ten specimens were subdivided into FSUs (i.e., specimen 1: C2-C3, C4-C5, and C6-C7 and specimen 2: C3-C4 and C5-C6), resulting in a representative specimen for each level. Each FSU was potted with the intervertebral disc parallel to the inferior potting. Each series of tests initiated with the intact FSU followed by the various states of destabilization introduced by sequentially removing the supporting structures in the following order: interspinous ligament, ligamentum flavum, capsular ligaments, facet joints, posterior longitudinal ligament, and anterior longitudinal ligament [40, 74]. After the ligaments and facets were removed, a small slit was cut in the anterior region of the annulus and a large gauge needle was used to damage the nucleus by scraping the nucleus from the endplates and annulus grounds. In an effort to avoid introducing variability by taking the specimen in and out of the gimbals, the FSU destabilizations took place with the specimen fixed in the testing apparatus.

Subsequent to each destabilization, each specimen was tested following the aforementioned protocol. Moreover, each specimen was also subjected to tensile (50 N) and compressive (-250N at C2-C3 and -450 N [8] for C3-C4 to C6-C6) loads at 10N/s after structural destabilization (body-disc-body) and after impairing the nucleus.

Moment-displacement curves were generated for each stage of destabilization. To quantify the change in motion after each level of destabilization, the peak motion at each step of destabilization was normalized to the peak intact motion.

4.2 Results

4.2.1 Intact C2-C7

During pure moment testing eight of the ten specimens were tested for flexion-extension; five of the ten specimens were tested for axial rotation. All ten specimens were tested for lateral bending. The C2-C7 moment-displacement curves are illustrated in Figure 17 for each specimen, as well as the average motion curve. Average moment-

rotation curves for each level are shown in Figure 18. Table 3 summarizes the average range of motion at 2.5 Nm for each level as well as the overall C2-C7 motion for each loading direction. In general, the motions increased from C2-C3 to C6-C7. Figure 19 illustrates the average off-axis motions during pure moment testing. Lateral bending and axial rotation were highly coupled (i.e. during axial rotation moment there was a great deal of off-axis lateral bending motion and vice versa).

Table 3 The average range of motion at 2.5 Nm.

	C2-C3	C3-C4	C4-C5	C5-C6	C6-C7	C2- C7
Flex	2.93 ± 1.84	5.90 ± 2.16	7.32 ± 1.68	10.82 ± 2.46	10.20 ± 1.47	37.17 ± 8.14
Extend	-2.92 ± 0.98	-5.71 ± 1.79	-7.97 ± 1.36	-10.74 ± 1.29	-12.47 ± 1.75	- 39.83 ± 4.08
RLB	10.57 ± 3.16	11.67 ± 2.19	13.46 ± 2.05	14.18 ± 2.17	13.05 ± 2.42	62. 93 ± 9.61
LLB	-10.57 ± 2.99	-12.44 ± 2.31	-13.97 ± 2.17	-15.38 ± 2.09	-14.68 ± 2.54	-67.04 ± 9.76
LAR	1.56 ± 1.20	3.27 ± 2.27	5.70 ± 1.91	11.49 ± 3.12	9.74 ± 2.66	31.76 ± 9.62
RAR	-0.71 ± 0.58	-2.33 ± 1.42	-5.78 ± 1.92	-12.12 ± 4.35	-11.59 ± 2.35	-32.52 ± 8.59

All ten specimens were also tested with lateral bending held in displacement control during axial rotation and flexion-extension tests (Figure 20). It should be noted that although lateral bending was restricted under displacement control, the resulting lateral bending moment was minimal (i.e. on average, approximately 0 Nm, but did not exceed ±0.5 Nm for flexion-extension and ±0.8 Nm for axial rotation). With lateral bending held at zero displacement the flexion-extension motion increased, where as the axial rotation motion decreased compared to the corresponding pure moment tests (Figure 21).

The sheep cervical spine has a large neutral zone, accounting for 63%, 72%, and 52% of the total motion for flexion-extension, lateral bending, and axial rotation, respectively during pure moment testing. With lateral bending held in displacement control, the neutral zone accounts for 73% and 32% of the total motion during flexion-extension and axial rotation, respectively.

4.2.2 Functional Spinal Unit Destabilization

Examples of moment rotation curves for the C4-C5 FSU at the various levels of destabilization are depicted in Figure 22. Table 4 lists the range of motion at each level of destabilization for each FSU. Figure 23 illustrates the normalized motion at each FSU for the various increments of destabilization. In general, the largest changes in motion occurred after removal of the capsular ligaments and the facets. After capsular ligament removal, motions increased 0.85-5.0 fold as compared to intact. With removal of the facets, the motion increased 0.9-10.3 fold as compared to intact. With complete destabilization, there was a large increase in motion at the C2-C3, especially in flexion (1000%), extension (320%), and axial rotation (570%).

During the compression and tension tests, there was not a large change in displacement (less than 10%) between body-disc-body and after nucleus damage except at C2-C3. At C2-C3 the compression displacement increased after nucleus damage by 20% (from 0.196 mm to 0.235 mm) and the tension displacement increased by 120% (from 0.219 mm to 0.478 mm). The largest deformation was at C6-C7, where the body-disc-body displaced 1.513 mm in tension and 0.899 mm in compression. The intact disc displaces more in tension (0.2 mm to 1.5 mm) than in compression (0.2-0.9 mm).

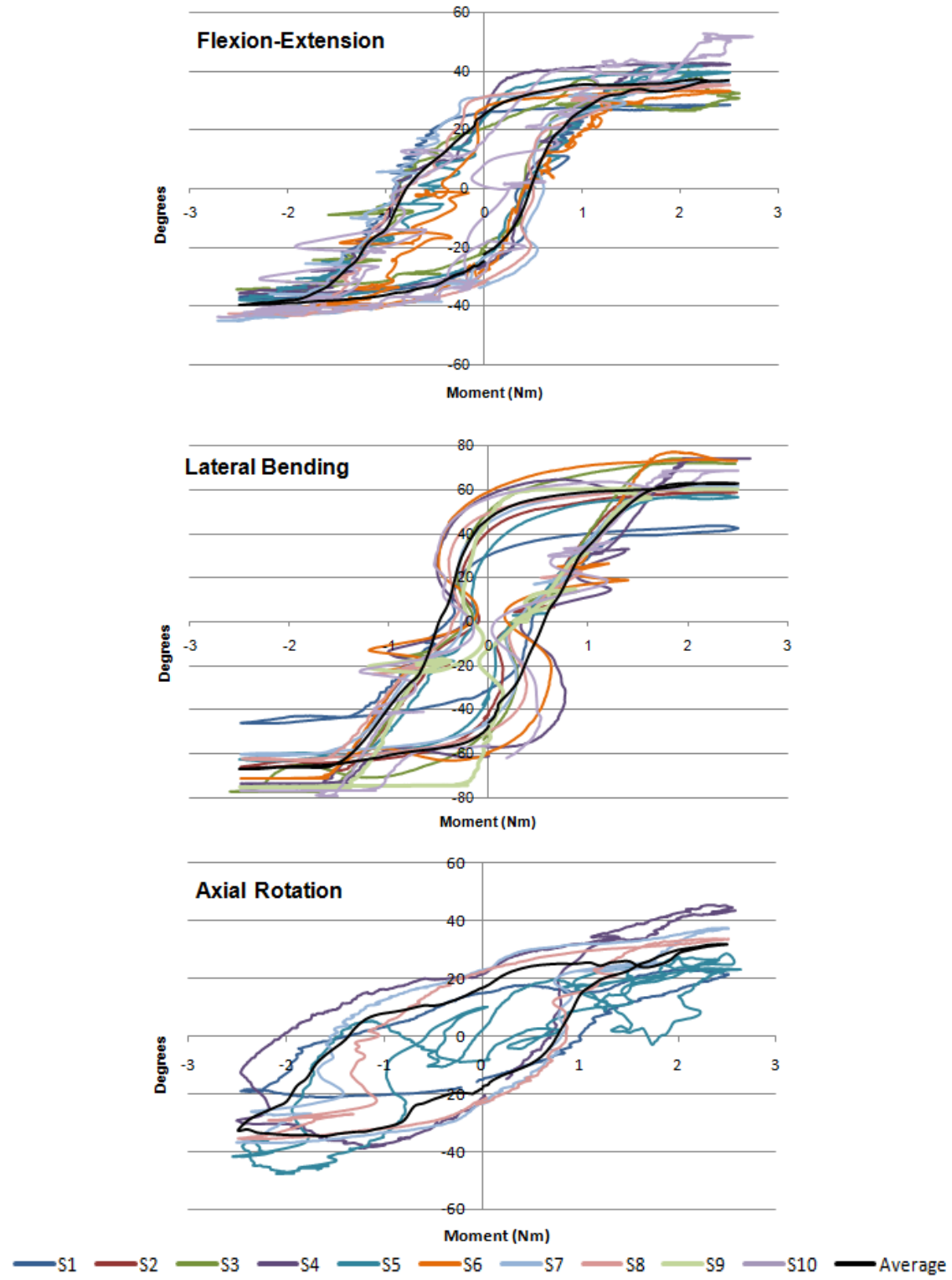

Figure 17 The C2-C7 pure moment-rotation curves for flexion (+) and extension (-), right (+) and left (-) lateral bending, and right (-) and left (+) axial rotation for each specimen.

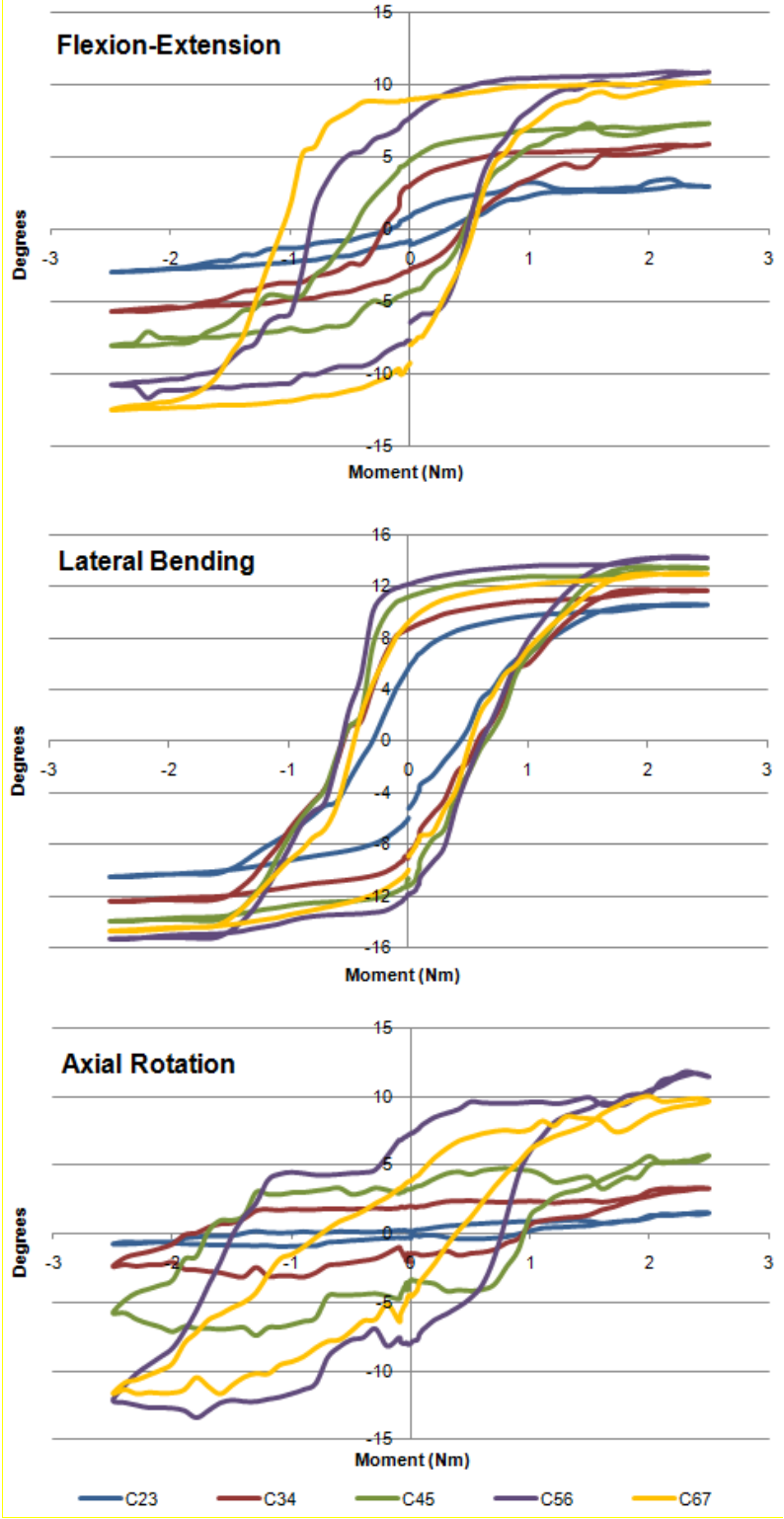

Figure 18 Average moment-rotation curves (pure moments) for flexion (+) and extension (-), right (+) and left (-) lateral bending, and right (-) and left (+) axial rotation at each spinal level.

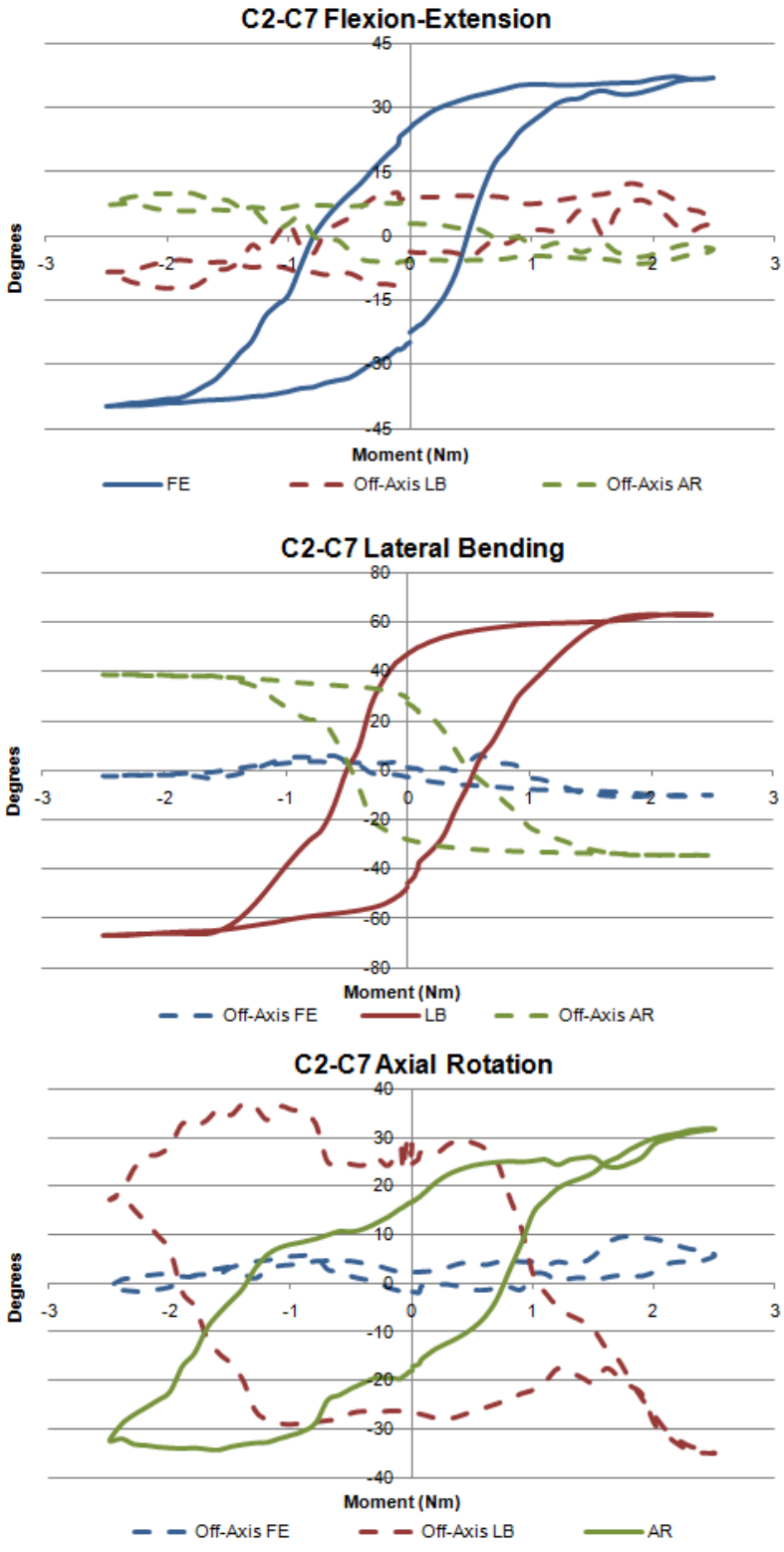

Figure 19 Off-axis (coupled) motions for the C2-C7 for flexion-extension, lateral bending, and axial rotation, while lateral bending is in moment control.

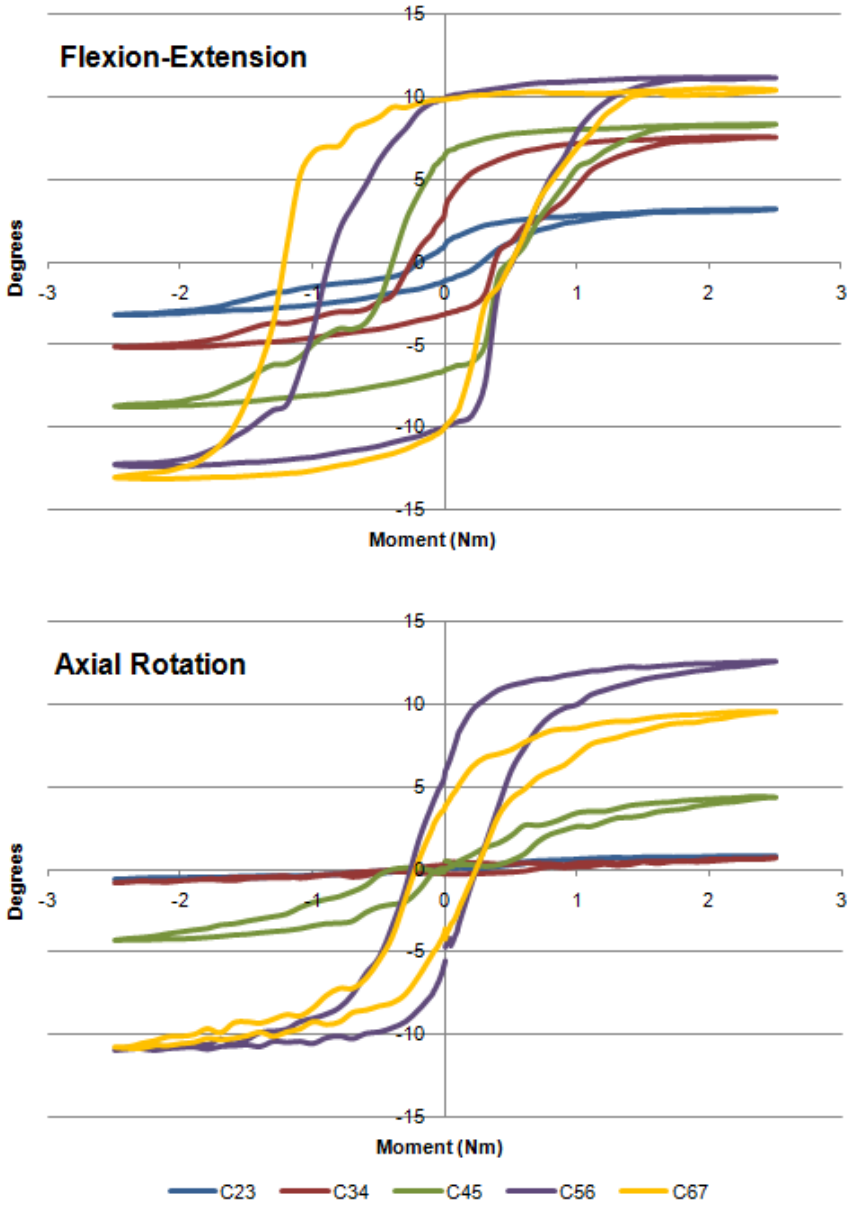

Figure 20 Average moment-rotation curves (lateral bending held in displacement control) for flexion (+) and extension (-) and right (-) and left (+) axial rotation.

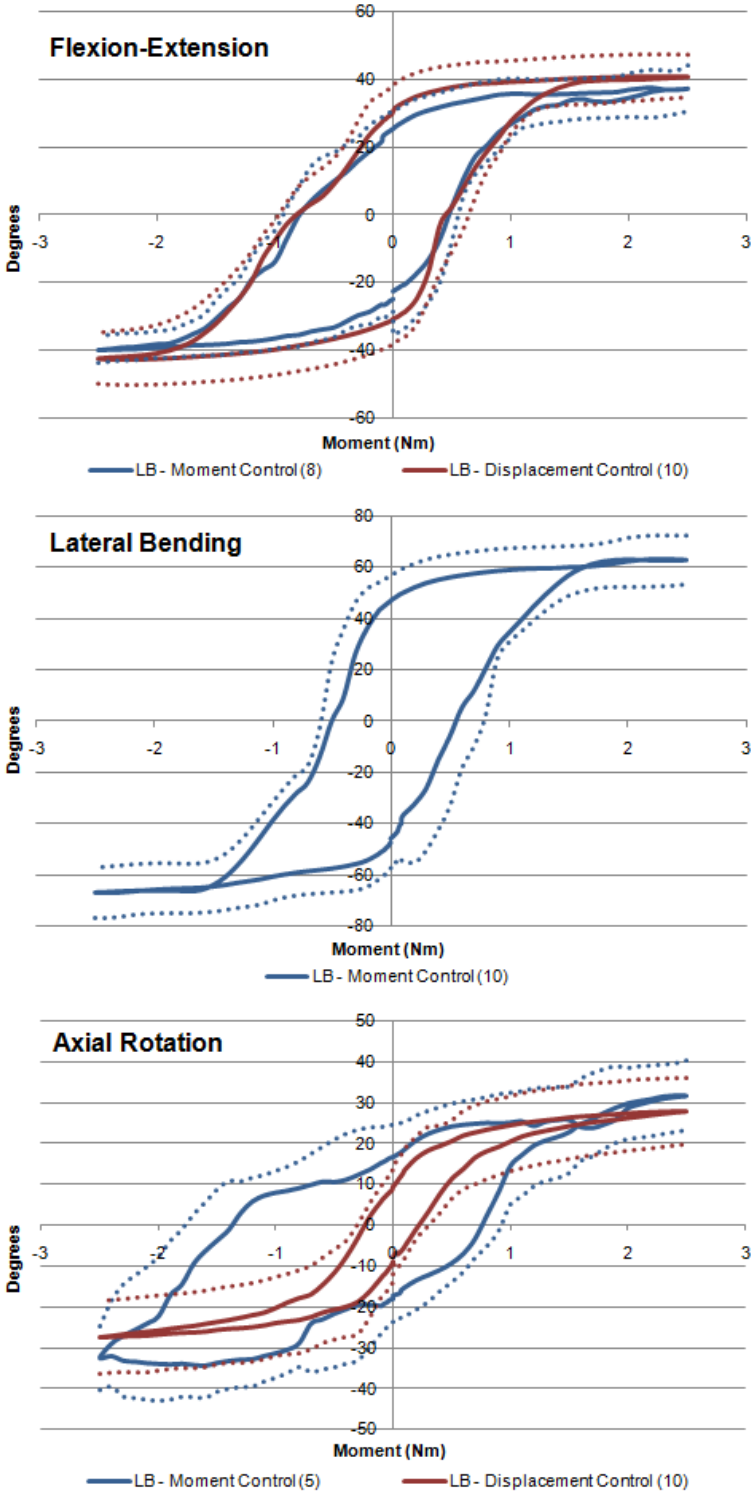

Figure 21 Average C2-C7 moment-rotation curves (solid line) and standard deviation (dashed lines) for both lateral bending in moment control (blue) and displacement control (red) for flexion (+) and extension (-), right (+) and left (-) lateral bending, and right (-) and left (+) axial rotation.

Table 4 The motion at 2.5 Nm for the various levels of destabilization for flexion, extension, right and left lateral bending, and right and left axial rotation.

		Intact	Removed IS	Removed IS, LF	Removed IS, LF, CL	Removed IS, LF, CL, Facets	Removed IS, LF, CL, Facets, PLL	Body-Disc-Body	Damaged Nucleus
Flexion	**C23**	0.54	0.83	1.17	2.68	5.54	5.61	7.67	8.64
	C34	2.92	2.91	3.66	5.20	6.81	6.65	6.96	7.81
	C45	4.24	4.60	4.86	7.83	9.51	10.14	10.17	11.51
	C56	5.76	5.82	5.93	10.54	10.29	10.09	10.43	8.97
	C67	12.10	12.89	13.60	20.06	18.95	16.07	17.77	18.14
Extension	**C23**	-1.84	-1.94	-2.10	-3.82	-5.92	-7.07	-9.19	-10.52
	C34	-5.02	-5.46	-5.68	-6.95	-8.65	-9.94	-9.85	-11.51
	C45	-7.59	-8.40	-8.66	-9.27	-11.85	-12.06	-12.04	-14.01
	C56	-10.49	-11.60	-11.57	-12.30	-12.80	-13.77	-14.13	-17.15
	C67	-14.97	-14.70	-15.02	-13.06	-18.79	-21.58	-20.91	-20.01
RLB	**C23**	8.80	9.35	9.39	9.55	12.23	12.90	12.47	12.54
	C34	10.37	10.86	10.82	10.87	12.99	13.38	12.53	13.00
	C45	13.13	14.33	13.85	15.09	14.98	15.68	15.10	15.96
	C56	17.64	18.98	20.46	22.57	21.69	22.40	23.42	24.48
	C67	13.18	15.05	14.79	17.72	20.57	24.47	23.89	25.12
LLB	**C23**	-7.31	-7.09	-7.60	-8.67	-10.64	-10.34	-11.66	-11.79
	C34	-7.55	-7.34	-7.65	-8.34	-9.26	-9.69	-10.12	-10.54
	C45	-10.35	-9.52	-10.54	-11.37	-13.08	-13.08	-13.85	-14.20
	C56	-12.06	-11.43	-10.41	-11.85	-12.97	-12.53	-13.18	-13.83
	C67	-18.48	-17.70	-17.42	-17.60	-16.91	-14.35	-15.70	-13.48
LAR	**C23**	0.97	1.04	1.15	1.36	5.23	5.28	6.91	6.78
	C34	1.82	1.75	1.99	2.43	4.45	4.96	4.74	5.49
	C45	1.73	1.43	2.24	2.57	6.07	5.93	6.09	6.56
	C56	3.35	4.16	5.55	6.61	8.76	7.53	7.03	8.34
	C67	10.16	9.60	10.38	13.96	15.12	11.16	14.85	14.37
RAR	**C23**	-0.96	-0.93	-1.20	-2.41	-5.84	-5.90	-7.08	-7.24
	C34	-2.90	-2.83	-3.20	-3.46	-5.88	-5.76	-6.06	-6.63
	C45	-4.65	-4.70	-4.51	-5.56	-8.13	-8.10	-8.68	-9.16
	C56	-7.14	-6.43	-6.11	-8.78	-8.46	-9.59	-10.78	-10.62
	C67	-16.82	-15.43	-14.54	-16.03	-16.37	-20.23	-14.29	-16.08

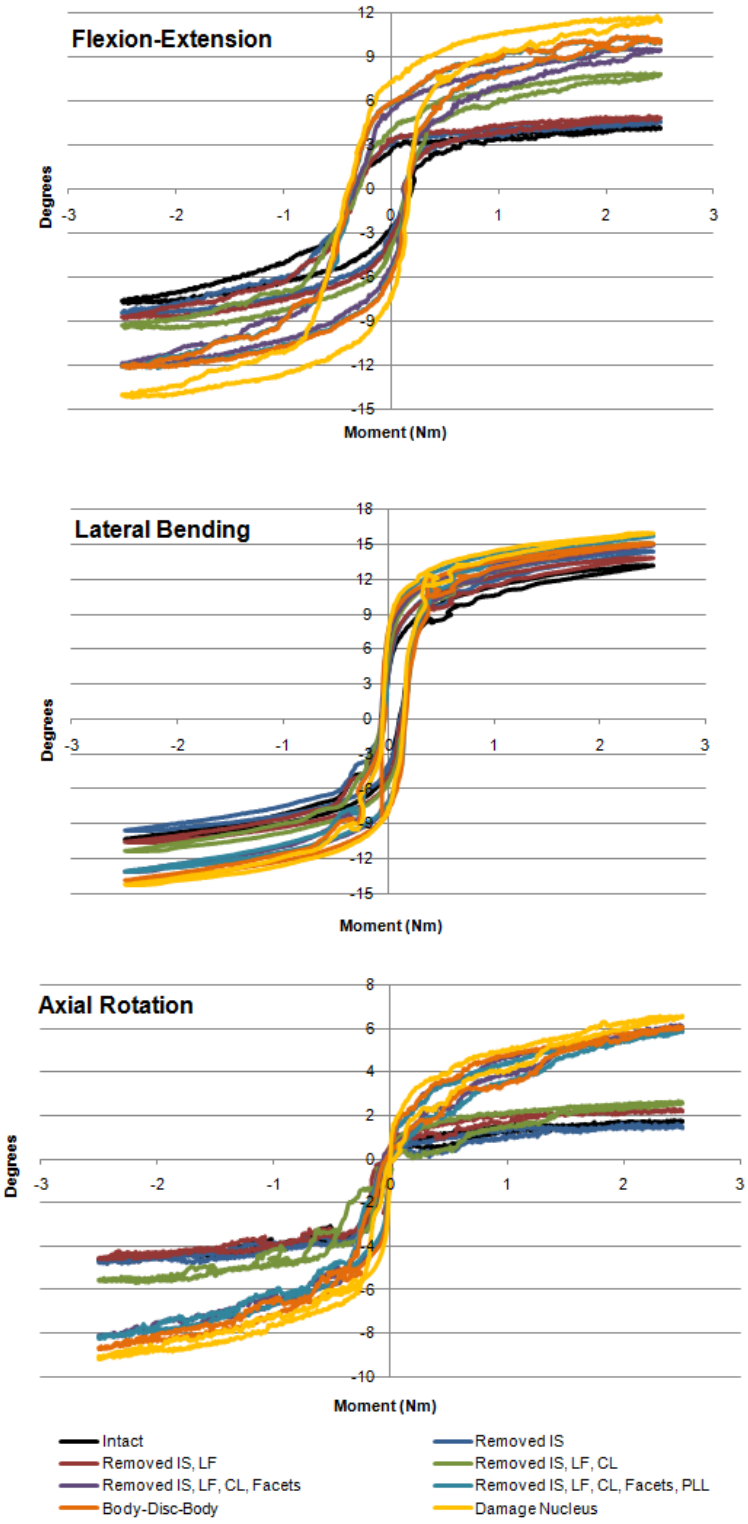

Figure 22 The moment-rotation curves for the C4-C5 FSU at the various stages of destabilization for flexion (+) and extension (-), right (+) and left (-) lateral bending, and right (-) and left (+) axial rotation.

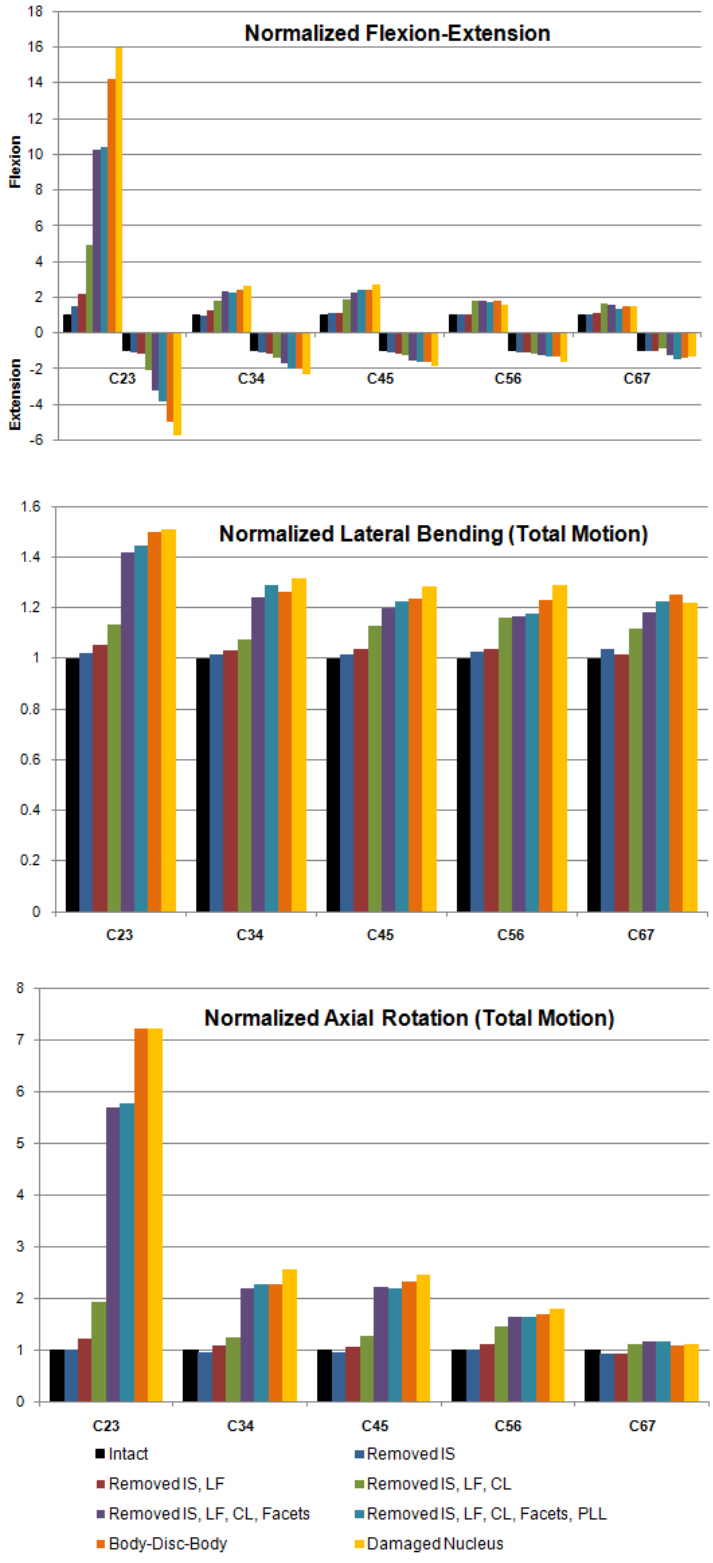

Figure 23 Normalized motion data for each level of destabilization during flexion (+) and extension (-), lateral bending, and axial rotation.

4.3 Discussion

4.3.1 Intact C2-C7

To date, this is the first comprehensive study focusing on the biomechanics of the C2-C7 sheep cervical spine. While the previous study by Szotek and colleagues [8] was limited to axial compression and flexion-extension, the current study addressed flexion-extension, lateral bending, and axial rotation. It is important to understand the biomechanics of the multilevel sheep spine since it is often used as a precursor to human cadaveric and clinical studies [9-13, 75]. This study provides researchers essential biomechanical data for the C2-C7 spine as well as the ranges of motion at the individual levels. Additionally, this is the first study to report the off-axis motions.

Similar to the FSU data reported by Wilke et al. [3], the range of motion increases with caudal progression. The sheep cervical spine exhibits a considerable range of motion in each direction, but especially in lateral bending (±65°). Due to the large range of motion, the two gimbal test setup was needed instead of the traditional one gimbal system. One gimbal is limited to ±50° which the lateral bending motion exceeds. Using two gimbals allows for larger rotations.

Corresponding to high flexibility, the sheep also have a large neutral zone. The size of the neutral zone may contribute to the observed coupled motions. This is similar to the coupling seen in the human cervical spine [40, 67-69]. Panjabi and colleagues [67] reported a large coupling between axial rotation and lateral bending axial rotation tests where the off-axis lateral bending motion was equivalent to the axial rotation motion. Similarly, the sheep cervical spine has equivalent off-axis lateral bending motion during axial rotation during pure moment tests (Figure 19). During lateral bending (±65°), there was ±35° off-axis axial rotation.

The large off-axis lateral bending motion and the limitations of the testing setup may account for the instability during pure moment testing. Only five of the ten

specimens could be tested under pure moments in axial rotation, and eight specimens were tested in flexion-extension. During pure moment testing, the curves for axial rotation do not follow the typical moment-rotation curve due to the large off-axis lateral motions. When lateral bending was held in displacement control, the axial moment-rotation curves resemble typical loading curves (Figure 20). This is because the off-axis lateral bending motion was minimized. Testing specimen with lateral bending in displacement control provided more stability with negligible effect on the maximum C2-C7 motion.

Averaging the data consequently smoothed the moment-rotation curves, as shown in Figure 17. However, averaging the data eased analysis among the specimens. Additionally, a majority of the spikes or "noise" shown in the loading and unloading curves is due to the large flexibility coupled with the limitations of the test setup. Since the specimen was tested using moment control, there is a considerable amount of motion in a short time, corresponding to the large neutral zone. Due to friction and the passive nature of the XZ table, the test set-up cannot keep up with the fast translation movements, thus creating peaks in the force/moment. Although the average data does not capture the spikes in the moment curve, it still accurately captures the neutral zone and elastic zones, which is critical to understanding the overall biomechanics of the cervical spine.

4.3.2 Functional Spinal Unit Destabilization

The ligaments provided the most stabilization during flexion, which was expected based on the posterior location of the majority of the ligaments. The ligaments and facets play a large role in stabilizing the C2-C3 during flexion, extension, and axial rotation. Overall, the facets provide the most stability, especially during axial rotation, extension, and flexion. The capsular ligaments also play a stabilizing role during flexion, extension, and axial rotation. There was little change in motion at the various levels of destabilization for lateral bending. This suggests that the ligaments and facets do little to

stabilize or limit the motion during lateral bending as compared to the other axes of motion. The largest change in displacement during compressive-tensile tests also occurred at C2-C3.

In general, there was little change in motion from the body-disc-body state to the damaged nucleus state for all testing conditions. The largest difference was seen during flexion-extension, which corresponds to the anterior slit of the annulus fibrosus. The minimal change in motion may be due to the limitations of the technique used to damage the nucleus. It was difficult to damage the nucleus without disrupting the annulus fibrosus as well. Therefore, the nucleus may not have been damaged to a high degree, thus having similar motion as seen for the body-disc-body. Additionally, the nucleus damage may have a larger biological effect over time, which cannot be accounted for during cadaveric studies.

It appears that some of the motions decreased with destabilization which is counter-intuitive. However, looking at the total range of motion for lateral bending and axial rotation, there is a general increase with destabilization. What appears to be a decrease in motion may be because the neutral position changes with the different levels of destabilization. The neutral position is used to shift the loading curve, defining the positive (Flexion, RLB, LAR) and negative (Extension, LLB, RAR) rotation curves. The neutral position may have shifted because the passive XZ shifted slightly while the ligaments and facets were transected. Thus, it is important to look at the total motion, especially for lateral bending and axial rotation.

Although this study provided insight into the roles of the ligaments and facets, the FSU destabilization method was limited to one specimen per level. Additional specimens should be tested to strengthen these results. Additionally, removing the posterior and anterior longitudinal ligaments was challenging due to the attachment to the intervertebral disc. During the removal of the longitudinal ligaments, some of the disc grounds and fibers may have been unintentionally cut as well. Therefore the increases in

motion after removal of the PLL and ALL may be in part due to disc damage and not just ligament destabilization.

In conclusion, this study provides invaluable *in vitro* biomechanical data for the mulitlevel sheep cervical spine as well as insight into the roles of stabilizing structures. It is important to understand the biomechanics of the intact sheep spine in order to design sound *in vivo* and *in vitro* sheep cervical spine studies focusing on surgical techniques such as discectomies and fusions. The large flexibility and neutral zone of the sheep spine should be accounted for when designing future studies and interpreting results. Additionally, understanding the roles of the ligaments and facets is important when planning surgical techniques. Future work should focus on testing additional specimen at the various levels of destabilization to gain a better understanding of the stabilizing structures. Additionally, this study data will be utilized to validate the comprehensive finite element model of the sheep cervical spine (Chapter 6).

CHAPTER 5: LIGAMENT TENSILE TESTING

For the finite element model to have biomechanical validity, the model requires accurate anatomical and biomechanical data of bone and soft tissues [59]. Bony anatomy can be captured using computed tomography imaging, providing the anatomical geometry needed for modeling. The detailed biomechanical study provided the range of motion over the entire loading curve for the multilevel sheep cervical spine. However to my knowledge, there are no previous studies focusing on the sheep cervical spine soft tissues, specifically the ligaments.

The initial sheep cervical spine finite element model incorporated human spine ligament properties. However, these material properties did not provide the flexibility seen in sheep experimental motion studies. Therefore the purpose of this study was to determine the geometric and mechanical material properties of the sheep cervical spine ligaments to be used as input for finite element models.

5.1 Materials and Methods

Seven adult Suffolk sheep cervical (C2-C7) specimens were acquired and sectioned into bone-ligament-bone complexes. To obtain ligament complexes at each level (C2-C3, C3-C4, C4-C5, C5-C6, and C6-C7), the vertebra was cut along the midline in the axial plane, thus dividing the vertebra in half (Figure 24a). Each level was further divided along the midline in the coronal plane (Figure 24b) using a diamond band saw, separating the anterior longitudinal ligament (ALL) complex from the posterior complex. Thereafter, the posterior complex was sectioned at the pedicles using a high speed burr, resulting with a posterior longitudinal ligament (PLL) complex as well as the ligaments corresponding to the posterior region (Figure 24c) [60, 63]. The ALL and PLL were isolated by carefully removing all nonosteoligamentous soft tissue, including the intervertebral disc. For the posterior region, the capsular ligaments (CL), ligamentum flavum (LF), or interspinous ligament (IS) were isolated by carefully removing all

nonosteoligamentous soft tissue, including the other ligaments not of interest. Note, to preserve the capsular ligament the posterior complex was not divided at the pedicles. Therefore, the PLL was not isolated at that level. For each FSU, there were either two bone-ligament-bone specimens (ALL and CL) or three bone-ligament-bone specimens (ALL, PLL, and IS or LF). Specimens were kept hydrated throughout ligament isolation with saline solution.

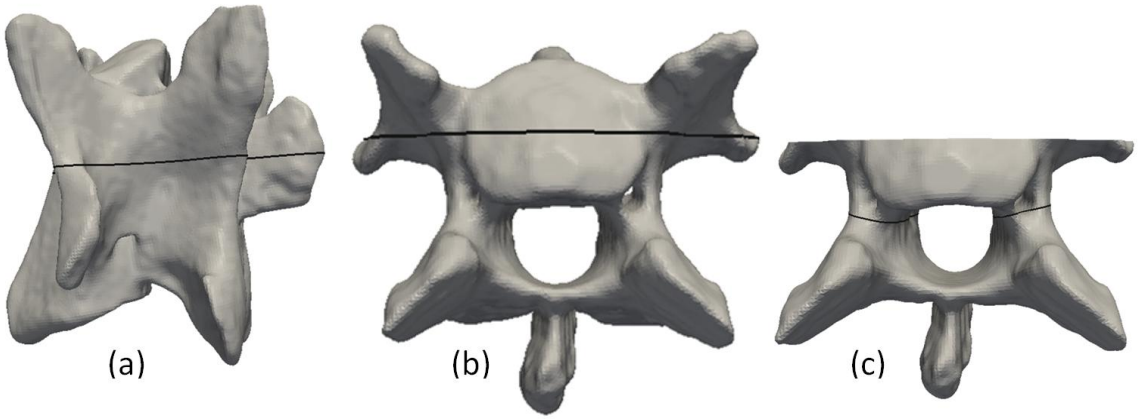

Figure 24 To obtain three ligaments for each functions spinal unit, the bodies were cut (a) mid height in the axial plane, (b) and mid body in the coronal plane, and (c) then at the pedicles as depicted by the black lines.

For each specimen, wood screws were used to improve interdigitation with the potting material [61]. The specimens were potted in a polymer resin (Bondo™, 3M Corporation, St. Paul, MN) utilizing custom designed fixtures, maintaining axial ligament alignment. The specimens were wrapped in saline soaked gauze and stored in sealed polypropylene bags until time of testing.

The ligament lengths were measured using digital calipers. The lengths of the longitudinal ligaments were defined as the distance between the adjacent endplates [61]. The length of the ligamentum flavum and interspinous ligament were defined as the

distance between the adjacent lamina and adjacent spinous processes, respectively [59]. The capsular ligament length was measured at the origin and insertion along the fiber axis of the facet capsule. The cross-sectional area for each ligament was calculated by measuring the width and thickness using a digital caliper and assuming an elliptical cross-section [64]. The cross-section of the CL was approximated by considering the capsular joint as a circle, and thus the ligament having a ring-like shape. It should be noted that the anatomy of the CL prohibited measurement of the thickness until the specimens had been tested and the ligament could be dissected. All other measurements were taken before the specimens were placed in the testing apparatus. Each ligament was measured three times and averaged to determine the initial length and cross-sectional area.

Specimens were tested using a biaxial servo-hydraulic materials testing machine (858 Bionix II, MTS Corporation, Eden Prairie, MN). Specimens were affixed to the testing machine using a custom fixture (Figure 25). Each ligament was loaded to 5 N to define a uniform reference point for the initial position and to ensure there was no slack in the ligament [60, 63, 64]; specimens were preconditioned at 10% strain for twenty loading and unloading cycles [61] at 0.25 Hz. After preconditioning, each specimen was held at zero displacement for 30 seconds and then underwent tensile loading at 3% strain/s [76, 77] until failure. The force and displacement data were recorded at 100 Hz, where the ligament displacement corresponded to the displacement of the actuator. This assumed there was no slipping between the specimen and the potting or between the potting and the testing fixture.

Failure was defined as the point in which force did not increase with increase in displacement. Nominal stress and strain values were calculated based on the ratios of the force to initial cross-sectional area and displacement to initial length, respectively. The Young's modulus was determined by calculating the slope of the stress-strain curve. Data was normalized with respect to the corresponding failure force and failure displacement

magnitudes. Average force-displacement and stress-strain curves for each ligament type and level were created by multiplying the abscissa and ordinate of the normalized loading curve with the mean failure displacement/strain and average failure force/stress, respectively [59].

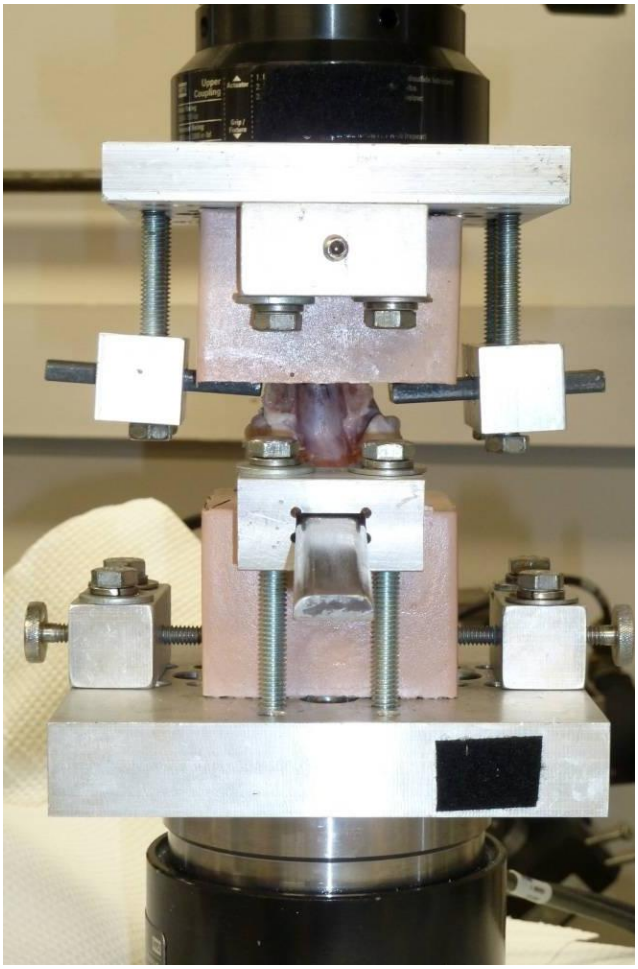

Figure 25 The ligament testing fixture, with the ligamentum flavum specimen fixed in the apparatus.

5.2 Results

Figure 26 shows the average force-displacement curves for each of the ligaments at each spinal level; Figure 27 shows the corresponding average stress-strain relationship.

Figure 28 and Figure 29 illustrate the overall average force-displacement curves and stress-strain curves, respectively, for the five major ligaments. Note, eleven specimens (12%) were not included in the results; two of the CL specimen failed at the potting and nine longitudinal ligaments were damaged during ligament isolation.

Table 5 and Table 6 summarize the geometrical and biomechanical properties, respectively, of the five major ligaments at each spinal level; there were notable differences between the ligaments. The CL had the largest cross-sectional area (59.6-122.7 mm^2) and the PLL had the smallest (2.4-11.7 mm^2). The IS had the longest initial length (15.1-25.1 mm) whereas the PLL was the shortest (3.8-12.4 mm). Focusing on failure biomechanics, the posterior complex ligaments had the largest failure forces (CL: 563-2128 N; IS: 77-705 N; LF: 79-710 N) and the longitudinal ligaments had the lowest (ALL: 32-294 N; PLL: 14-226 N). There was less variation in failure stress among ligament types. The ALL had the lowest average failure stress (~8 MPa) and the LF had the largest (~20 MPa). The failure displacement for all the ligaments ranged from 1.3 mm to 21.6 mm; on average the CL had the longest failure displacement (8.5 mm) and the PLL had the shortest (5.3 mm). The longitudinal ligaments had the largest average failure strains (ALL: 0.32-1.63; PLL: 0.16-1.69); they had the most variation as well The IS and LF had the smallest averages failure strain (0.43).

5.3 Discussion

Animal models are often used to study the effects of different surgical procedures and spinal disorders [9-13, 75]. The sheep cervical spine is often used due to the similar vertebral geometry and lordosis [8]. To date, there is limited knowledge of the sheep cervical ligamentous structures. To my knowledge, this is the first study focusing on the geometry and biomechanics of the sheep cervical spine ligaments

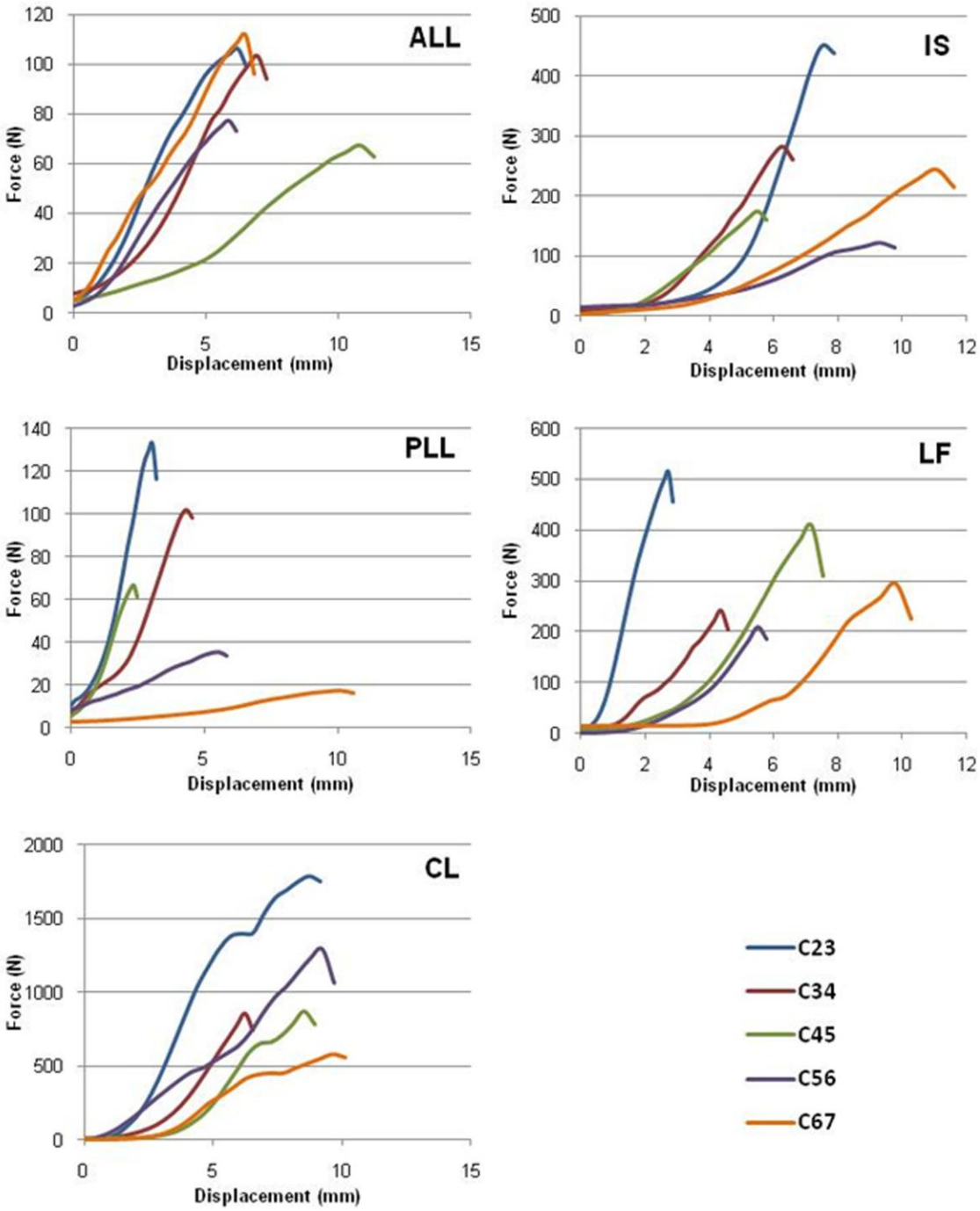

Figure 26 The average force-displacement curves for the anterior longitudinal ligament (ALL), posterior longitudinal ligament (PLL), capsular ligament (CL), interspinous ligament (IS), and ligamentum flavum (LF) for each spinal level.

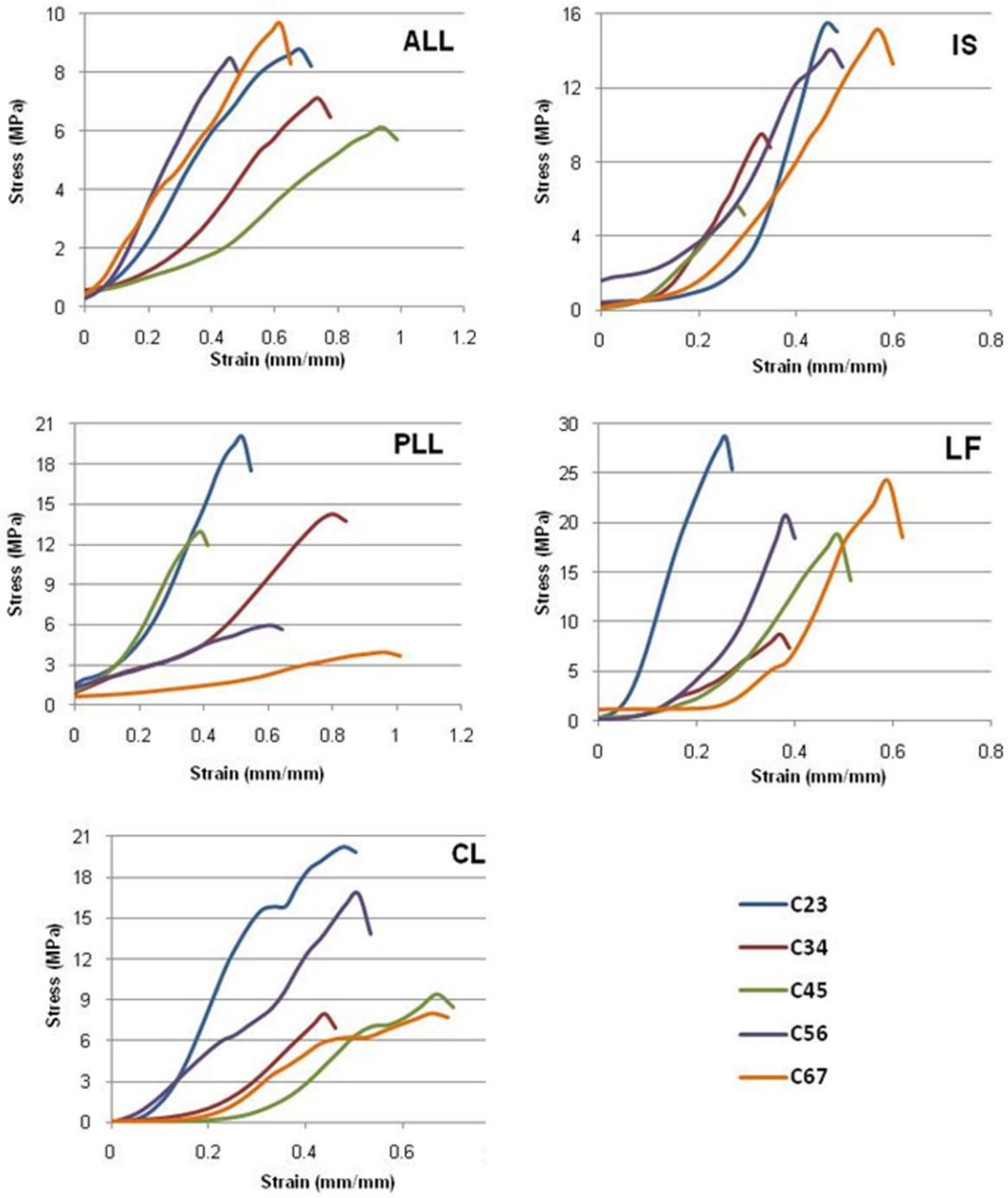

Figure 27 The average stress-strain curves for the anterior longitudinal ligament (ALL), posterior longitudinal ligament (PLL), capsular ligament (CL), interspinous ligament (IS), and ligamentum flavum (LF) for each spinal level.

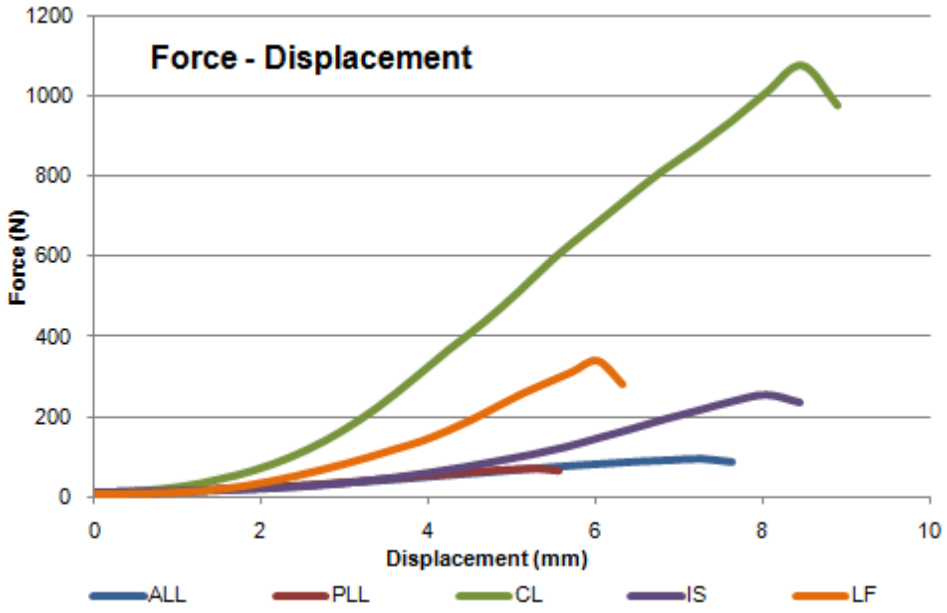

Figure 28 The overall average force-displacement curve for each ligament: anterior longitudinal ligament (ALL), posterior longitudinal ligament (PLL), capsular ligament (CL), interspinous ligament (IS), and ligamentum flavum (LF).

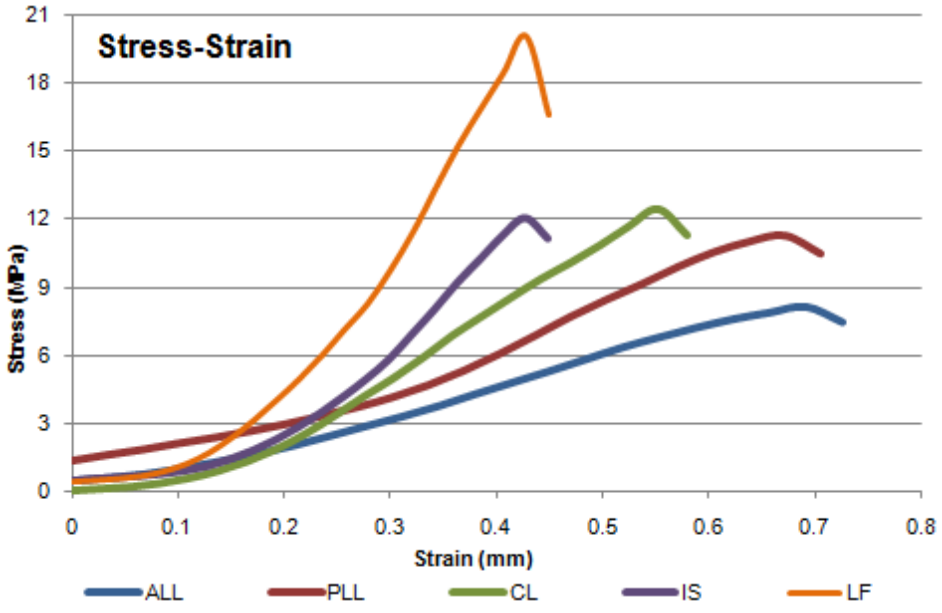

Figure 29 The overall average stress-strain curve for each ligament: anterior longitudinal ligament (ALL), posterior longitudinal ligament (PLL), capsular ligament (CL), interspinous ligament (IS), and ligamentum flavum (LF).

Table 5 The average geometrical properties for the anterior longitudinal ligament (ALL), posterior longitudinal ligament (PLL), capsular ligament (CL), interspinous ligament (IS), and ligamentum flavum (LF).

	Level	Sample Size	Initial Length (mm)	Initial Width (mm)	Initial Thickness (mm)	Initial Cross-sectional Area (mm^2)
	C2-C3	6	9.39 ± 1.38	15.09 ± 3.28	1.020 ± 0.49	12.78 ± 7.95
	C3-C4	5	10.18 ± 2.14	16.73 ± 3.41	1.14 ± 0.35	14.42 ± 4.00
ALL	C4-C5	6	10.99 ± 2.36	15.05 ± 3.92	1.02 ± 0.38	12.49 ± 7.10
	C5-C6	5	12.75 ± 1.72	14.92 ± 4.09	0.74 ± 0.23	9.19 ± 4.68
	C6-C7	7	10.73 ± 3.57	13.44 ± 1.37	1.11 ± 0.27	11.61 ± 2.49
	C2-C3	4	5.80 ± 0.59	15.73 ± 4.13	0.53 ± .15	6.92 ± 3.60
	C3-C4	4	5.57 ± 1.31	13.88 ± 1.10	0.69 ± 0.16	7.46 ± 1.60
PLL	C4-C5	4	6.57 ± 1.26	14.40 ± 3.40	0.53 ± 0.28	5.67 ± 2.55
	C5-C6	3	8.96 ± 1.80	11.26 ± 4.45	0.62 ± 0.20	5.86 ± 3.95
	C6-C7	5	10.71 ± 1.24	13.80 ± 2.01	0.41 ± 0.09	4.48 ± 1.09
	C2-C3	2	17.92 ± 1.52	18.48 ± 2.62	0.77 ± 0.15	91.37 ± 14.91
	C3-C4	2	14.18 ± 1.24	17.53 ± 2.15	1.05 ± 0.05	109.06 ± 19.35
CL	C4-C5	2	12.70 ± 0.79	19.03 ± 4.08	0.83 ± 0.19	92.55 ± 0.11
	C5-C6	2	18.22 ± 0.35	19.99 ± 0.82	0.64 ± 0.23	83.35 ± 33.63
	C6-C7	2	14.63 ± 1.96	15.88 ± 205	0.77 ± 0.06	72.73 ± 4.84
	C2-C3	2	15.95 ± 1.23	14.41 ± 3.98	2.61 ± 2.03	32.74 ± 31.11
	C3-C4	3	19.99 ± 4.44	13.70 ± 2.33	2.88 ± 2.14	28.98 ± 17.09
IS	C4-C5	2	19.62 ± 0.27	12.25 ± 3.00	3.40 ± 2.82	23.86 ± 26.97
	C5-C6	2	19.53 ± 0.41	13.41 ± 4.20	1.29 ± 0.91	15.08 ± 13.84
	C6-C7	3	19.52 ± 1.82	18.90 ± 2.06	1.10 ± 0.28	16.53 ± 5.62
	C2-C3	2	10.30 ± 0.32	12.82 ± 4.81	1.74 ± 0.14	17.22 ± 5.19
	C3-C4	2	11.88 ± 0.18	15.30 ± 4.53	1.90 ± 0.73	24.15 ± 15.52
LF	C4-C5	3	14.60 ± 1.56	17.80 ± 0.71	1.64 ± 0.54	22.76 ± 6.79
	C5-C6	2	14.11 ± 1.47	13.07 ± 1.87	0.99 ± 0.29	9.95 ± 1.55
	C6-C7	2	17.02 ± 4.61	15.93 ± 1.26	1.11 ± 0.62	14.13 ± 8.91

Table 6 The average biomechanical properties for the anterior longitudinal ligament (ALL), posterior longitudinal ligament (PLL), capsular ligament (CL), interspinous ligament (IS), and ligamentum flavum (LF). The Young's Modulus was calculated for the linear region of the average stress-strain curve for each ligament at each level.

	Level	Sample Size	Failure Force (N)	Failure Displacement (mm)	Failure Stress (MPa)	Failure Strain (mm/mm)	Young's Modulus (MPa)
	C2-C3	6	108.45 ± 83.00	6.18 ± 2.91	8.94 ± 5.43	0.68 ± 0.34	14.90
	C3-C4	5	104.74 ± 50.50	6.93 ± 2.79	7.22 ± 2.95	0.74 ± 0.47	12.60
ALL	C4-C5	6	69.09 ± 24.27	10.79 ± 6.03	6.27 ± 2.42	0.94 ± 0.37	8.78
	C5-C6	5	79.06 ± 48.65	5.84 ± 1.51	8.67 ± 2.44	0.46 ± 0.11	21.32
	C6-C7	7	113.32 ± 82.35	6.49 ± 2.47	9.80 ± 6.32	0.62 ± 0.15	15.72
	C2-C3	4	136.48 ± 66.45	3.05 ± 1.12	20.51 ± 4.48	0.52 ± 0.14	53.77
	C3-C4	4	105.04 ± 64.62	4.34 ± 0.76	14.73 ± 9.33	0.80 ± 0.15	26.83
PLL	C4-C5	4	68.79 ± 40.72	2.37 ± 1.02	13.38 ± 10.24	0.39 ± 0.27	42.02
	C5-C6	3	37.43 ± 27.34	5.57 ± 4.08	6.22 ± 0.37	0.61 ± 0.38	7.99
	C6-C7	5	18.58 ± 5.17	10.09 ± 4.12	4.30 ± 1.34	0.96 ± 0.46	7.45
	C2-C3	2	1788.19 ± 480.11	8.73 ± 3.11	20.27 ± 8.56	0.48 ± 0.13	78.57
	C3-C4	2	861.65 ± 35.71	6.25 ± 1.87	8.00 ± 1.09	0.44 ± 0.09	30.98
CL	C4-C5	2	872.05 ± 154.59	8.52 ± 0.38	9.42 ± 1.66	0.67 ± 0.01	33.37
	C5-C6	2	1288.36 ± 19.84	9.22 ± 4.01	16.77 ± 6.53	0.51 ± 0.23	48.39
	C6-C7	2	579.55 ± 22.31	9.64 ± 1.82	7.98 ± 0.22	0.66 ± 0.04	24.70
	C2-C3	2	449.47 ± 361.64	7.52 ± 4.43	15.46 ± 3.65	0.46 ± 0.24	86.97
	C3-C4	3	283.15 ± 228.06	6.29 ± 0.99	9.52 ± 3.74	0.33 ± 0.11	46.49
IS	C4-C5	2	174.56 ± 138.26	5.48 ± 1.19	5.59 ± 1.07	0.28 ± 0.06	26.97
	C5-C6	2	121.11 ± 3.85	9.30 ± 4.59	14.06 ± 13.15	0.47 ± 0.23	52.20
	C6-C7	3	243.75 ± 126.89	11.06 ± 6.52	15.16 ± 8.40	0.57 ± 0.33	37.88
	C2-C3	2	513.71 ± 276.94	2.73 ± 0.61	28.71 ± 7.43	0.26 ± 0.05	143.68
	C3-C4	2	242.53 ± 231.44	4.37 ± 1.22	8.78 ± 3.94	0.37 ± 0.11	27.83
LF	C4-C5	3	409.96 ± 130.18	7.17 ± 1.87	18.71 ± 5.59	0.49 ± 0.14	69.30
	C5-C6	2	209.29 ± 72.34	5.51 ± 2.24	20.72 ± 4.05	0.38 ± 0.12	122.18
	C6-C7	2	295.09 ± 67.64	9.80 ± 0.94	24.18 ± 10.45	0.59 ± 0.11	95.85

This study determined the posterior ligaments (CL, IS, LF) had large failure forces. The average capsular ligament failure force was 3 to14 times larger than that of the other ligaments. There were two specimens that failed at the potting-bone interface due to the high forces required for failure. This large force corresponds to the large cross-sectional area. Both capsular joints were tested as one specimen accounting for the large cross-sectional area. The capsular joints were tested as one specimen to provide more bone to securely affix the specimen. Overall, the largest failure forces and stresses occurred at the C2-C3 level suggesting the C2-C3 can withstand large loads. This corresponds well with the destabilization study (Section 4.2.2) showing that the ligaments play a key role in stabilizing the C2-C3. The largest failure displacements and strains occurred at the C6-C7 level, which corresponds to the high range of motion reported for the C6-C7 (Section 4.2.1).

The sheep ALL had the lowest average failure stress, while the ALL and PLL demonstrated the largest average failure strain. On the contrary, the human longitudinal ligaments exhibit the largest failure stresses and lowest failure strains as compared to the other ligaments [59]. The variation in failure strain may be due to the definition of the initial ligament length. Yoganandan and colleagues [59] defined the longitudinal ligaments to span from mid-body to adjacent mid-body. However, for the current study, the longitudinal ligament lengths were defined to span between adjacent endplates.

There was considerable variation in the biomechanical data for the same ligament type at the same level. This may be due in part to the small sample size as well as the limitations of the test setup. The posterior ligaments (CL, LF, and IS) were limited to two to three specimens for each level. Another limitation of this study was the accuracy of the load cell (±5 N). This may have resulted with the ligaments starting pre-strained (decreased toe region) or with slack introduced (increased toe region). The toe region is defined by a period of low stiffness. Consequently, the failure displacement and strain may have been affected as well. However, there should have been little effect on the

failure force and stress as well as the Young's modulus of the elastic region. Future studies should include additional specimens to obtain a better understanding of the ligaments at each level as well as incorporate a more precise load cell to better capture the initial phase of the force-displacement curve.

Furthermore, isolating the ligaments proved challenging due to the surrounding anatomy. The longitudinal ligaments were difficult to isolate due to the close attachment to the intervertebral discs; in addition the longitudinal ligaments are very thin (thickness 0.29-1.79 mm) which resulted in several specimen tearing during the isolation process. Also, there were challenges isolating the posterior complex ligaments. Both the capsular ligament and interspinous ligaments were near tendon attachments making it difficult to remove the tendons without damaging the ligaments. Additionally, the posterior ligaments are in close proximity to each other, thus making it challenging to isolate each. Bony anatomical boundaries assisted in determining the ligament boundaries in addition to ligament orientation. Similar challenges were reported during ligament isolation for the human cervical spine [59, 78]. Yoganandan and colleagues [59] reported approximately 40% of the sample size could not be tested due to difficulties during isolation; recall that less than 12% of the ligaments were discarded for the current study.

This study was the first step towards determining the geometric and biomechanical properties of the sheep spinal ligaments. Geometric properties were measured using digital calipers, similar to previous human ligament studies [61, 62, 64]. This allowed each specimen to be used for both geometric and biomechanical data. Other studies have used cryomicrotome [59, 79] to measure initial length and cross-sectional area. However, cryomicrotome sections the specimen into small slices, and thus the same specimens cannot be used for anatomical measurements and biomechanical analysis. Another option is magnetic resonance imaging, but this is limited to image resolution. Note, the average thickness of the longitudinal ligaments is fractions of a millimeter, making it challenging to accurately capture using medical imaging. Additionally,

magnetic resonance imaging is time and cost intensive as compared to physically measuring the ligament length and cross-section.

In conclusion, this study offers valuable insight on the geometry and biomechanics of the sheep spinal ligaments. It is the first study to focus on the sheep cervical spine soft tissue material properties. Since there is a large variation in material properties amongst ligaments, future studies should include additional specimen to gain a larger sample size, especially for the CL, IS, LF. Additional specimen would allow for statistical analysis to be conducted, thereby establishing whether significant differences exist between the different levels or ligament types. This study will be used to define the material properties of the spinal ligaments for the multilevel sheep cervical spine (C2-C7) finite element model (Section 6.1.1).

CHAPTER 6: FINITE ELEMENT MODEL VALIDATION

To ensure a finite element model is providing useful information, it is important to validate the model. Traditionally, models are compared to values reported in literature or to complimentary experimental studies for validation. Similarly, to validate the C2-C7 sheep spine model, the ranges of motion were compared to the corresponding experimental study (Chapter 4). Both the overall range of motion and the motion at each level were compared over the entire loading curve, ensuring the model matches throughout, not just at the peak moment. This is particularly important for the sheep spine because it is highly nonlinear.

The initial sheep spine model incorporated human material properties. However, the human material properties did not provide the flexibility seen in the sheep cervical spine (Section 3.5). Thus, to better capture the flexibility of the spine, the sheep-specific ligament material properties determined in Chapter 5 were incorporated. Additionally, the intervertebral discs were adjusted to better capture the nonlinear nature of the sheep cervical spine.

6.1 Methods

Starting with the initial model (incorporating human material properties), the material properties were systematically changed in an effort to calibrate the model over the entire loading curve, including the neutral zone. As described earlier, the neutral zone is a region in which the specimen moves free of loading. For the sheep cervical spine, this is 50%-75% of the total motion.

6.1.1 Intervertebral Disc Material Properties

The first step to calibrate the model was to determine the intervertebral disc material properties to better capture the neutral zone. The disc material properties were determined using single level body-disc-body models and comparing the predicted results

to those of the experimental body-disc-body motions (Section 4.2.2). As discussed in Section 3.5, linear elastic material properties for the annulus grounds did no account for the flexibility seen in the sheep cervical spine. Therefore, different hyperelastic functions were studied.

Recent finite element studies of the human lumbar spine have incorporated hyperelastic material properties to capture the nonlinear behavior. Several studies [45, 51, 52] have modeled the annulus grounds using the Neo-Hookean hyperelastic function. Others [50, 54] have incorporated the Mooney-Rivlin hyperelastic function. Ayturk and colleagues [56] used the Yeoh hyperelastic model to depict the nonlinearity of the lumbar annulus. For the sheep FE model, the Mooney-Rivlin and Neo-Hookean functions could not capture the nonlinearity of the neutral zone. Thus, the Yeoh hyperelastic model was used to capture the large neutral zone seen in the sheep cervical spine. The Yeoh model defines the strain energy function by:

$$U=C_{10}(\bar{I}_1 - 3) + C_{20}(\bar{I}_1 - 3)^2 + C_{30}(\bar{I}_1 - 3)^3 + (1/D_1) (J^{el} - 1)^2,$$

where C_{10}, C_{20}, C_{30}, and D_1 are material coefficients, $\bar{I}_1$ is the first invariant of deviatroic component of the Cauchy-Green strain tensor, and J^{el} is the elastic volume ratio. The elastic volume ratio accounts for the compressibility of the material and is determined based on the Poisson's ratio. [80]

Similar to the study by Auturk et al. [56], the material coefficients were determined from the stress-strain curve reported by Fujita and colleagues [81]. For this study, the stress-strain curve was altered to determine stiffer and more flexible material properties. For example, for stiffer properties the strain was lowered given the same stress; for more flexible material properties the strain was increased given the same stress (Figure 30). Yeoh coefficients for the various curves were determined using Abaqus CAE (SIMULIA, Dassault Systèmes, Providence, RI); the Poisson's ratio was assumed to be

0.45 [36, 40, 43, 49]. The finite element model incorporates region and level dependent material properties for the annulus in an effort to capture the range of motion at each level. Recall, motion increased with caudal progression, thus more flexible properties were incorporated for C5-C6 and C6-C7. Table 7 shows the Yeoh coefficients for the various regions and levels as well as the relative flexibility compared to the original stress-strain curve by Fujita and colleagues [81].

The annulus fibers were modeled using the rebar function in Abaqus (Simulia, Rhode Island, USA). The rebar were modeled at ±25° from the vertical axis as four alternating layers per element, mimicking the alternating fiber angles through the annulus. The rebar were assigned hypoelastic material properties similar to the techniques used to define the fibers in the human intervertebral disc [34, 38-40].

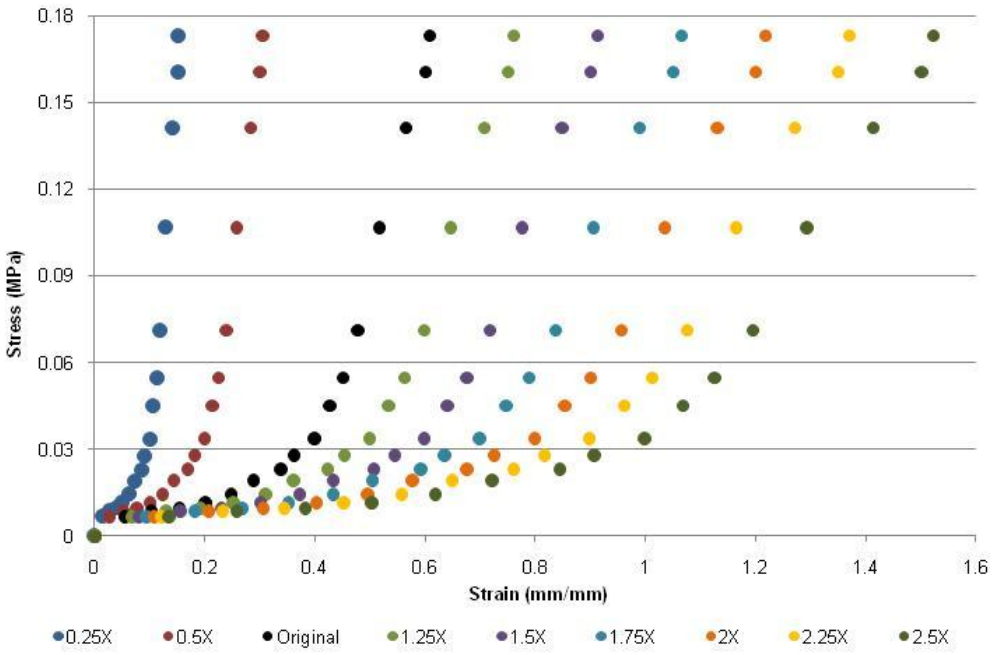

Note: The "X" in the legend stands for times. For example, 2X stands for a material properties that is two times as flexible as the original stress-strain curve.

Figure 30 The stress-strain curve derived from the study by Fujita et al [81] (original) and curves corresponding to the levels of flexibility.

Table 7 The material coefficients for the disc material properties at each level.

Disc Region	Level	Yeoh Coefficients C10	C20	C30	D1	Relative Flexibility
Anterior and Posterior	C23	5.508E-2	-8.880E-1	24.804	1.878	0.25
	C34	2.911E-2	-1.351E-1	1.014	3.554	0.5
	C45	1.318E-2	-1.271E-2	1.822E-2	7.849	1.25
	C56	8.978E-3	-3.877E-3	2.483E-3	11.523	2.0
	C67	9.997E-3	-5.437E-3	4.364E-3	10.348	1.75
Lateral	C23	2.911E-2	-1.351E-1	1.014	3.554	0.5
	C34	1.134E-2	-8.020E-3	8.384E-3	9.124	1.5
	C45	8.978E-3	-3.879E-3	2.483E-3	11.523	2.0
	C56	7.513E-3	-2.198E-3	9.681E-4	13.770	2.5
	C67	8.170E-3	-2.876E-3	1.510E-3	12.662	2.25

6.1.2 Ligament Material Properties

In addition to the disc, the species-specific ligament material properties were incorporated. The ligaments were modeled as a hypoelastic material similar to previous human spine finite element studies [31, 40, 41]. The ligament properties were based on the average stress-strain curves determined experimentally (Section 5.2), incorporating level specific material properties. For several of the ligaments, a larger toe region was introduced than was determined experimentally to help capture the large neutral zone and flexibility of the sheep spine.

6.1.3 Facet Joints

As described in Chapter 3, the facet joints were modeled using finite-sliding surface interactions with an exponential pressure-overclosure relationship. The initial model incorporated a 0.5mm gap at every facet. However, the gaps were changed based on the varying stiffness for each level. Additionally, the material properties were adjusted at different facets in effort to capture the relative flexibility at each level.

6.2 Results

Figure 31 shows the calibrated model range of motion as compared to the experimental C2-C7 range of motion for all specimens for each loading direction. The C2-C7 model-predicted motion matched the experimental motions well for a majority of the loading curves. The model over predicts extension and slightly under predicts lateral bending. However, lateral bending has the largest range of motion and the largest neutral zone, making it challenging to capture the nonlinearity. For axial rotation and flexion, the motion matches the experimental results well, including at the ends of the loading curve.

Figure 32, Figure 33, and Figure 34 compare the finite element predicted motions to the average experimental motion at each level for flexion-extension, lateral bending, and axial rotation, respectively. Comparing level by level, the model over predicts extension at C2-C3 and C4-C5; however it matches the C6-C7 motion throughout the loading curve The model matches the flexion moment-rotation curve well at all levels except C4-C5. For lateral bending, the model matches well at C3-C4 and C4-C5. The motion is slightly under predicted at C5-C6 and C6-C7; however the motion is greatest at these levels as well. For axial rotation, the model over predicts the rotation at C2-C3 and matches well at the other levels. Overall, the predicted motion is within one standard deviation of the experimental motion for a majority if the loading curves.

Table 8 compares the percentage of coupled motion during lateral bending and axial rotation predicted by the model to the experimental coupled motions. The percent of coupled motion is the fraction of off-axis motion to primary motion. In general, the model captured the coupling, especially for the off-axis axial rotation during lateral bending.

The von Mises stress distributions for flexion and extension, lateral bending, and axial rotation are illustrated in Figure 35, Figure 36, and Figure 37, respectively. The peak von Mises stresses occurred at the capsular ligament attachment sites; however this

is related to the point loading of the ligaments. Overall the stresses are largest in the cortical shell, corresponding to the higher Young's modulus.

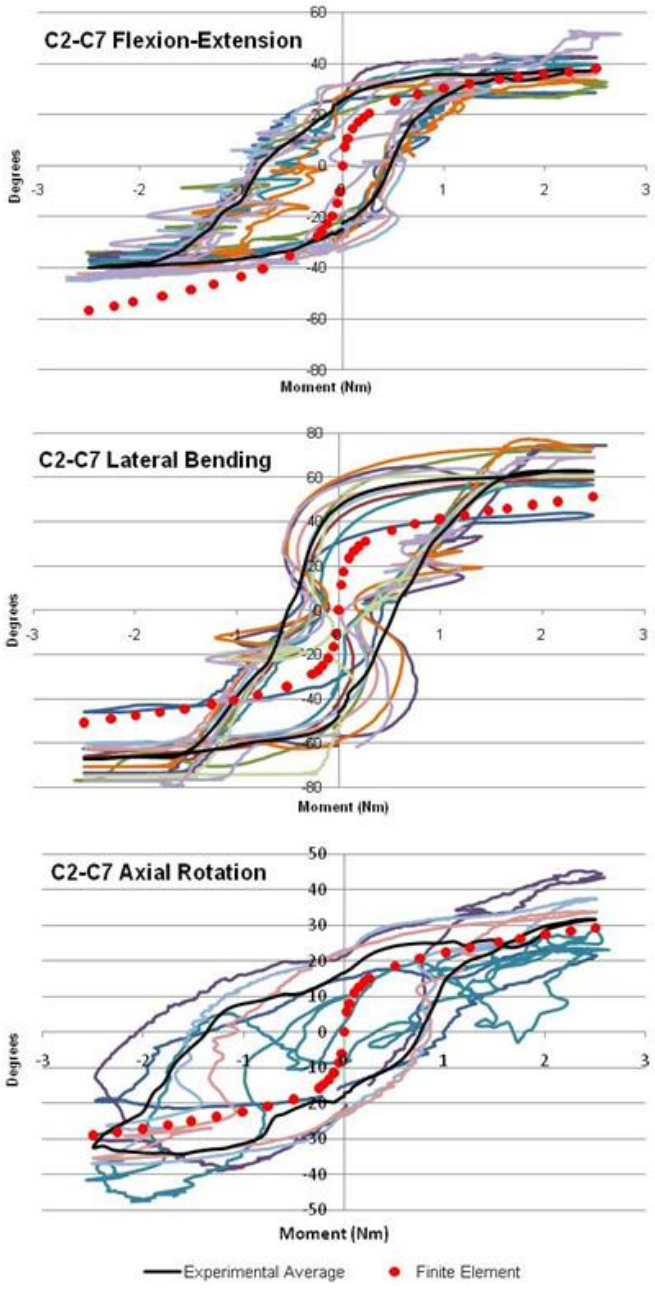

Figure 31 The C2-C7 finite element predicted motion compared to the experimental motion-rotation curves for flexion-extension, lateral bending, and axial rotation.

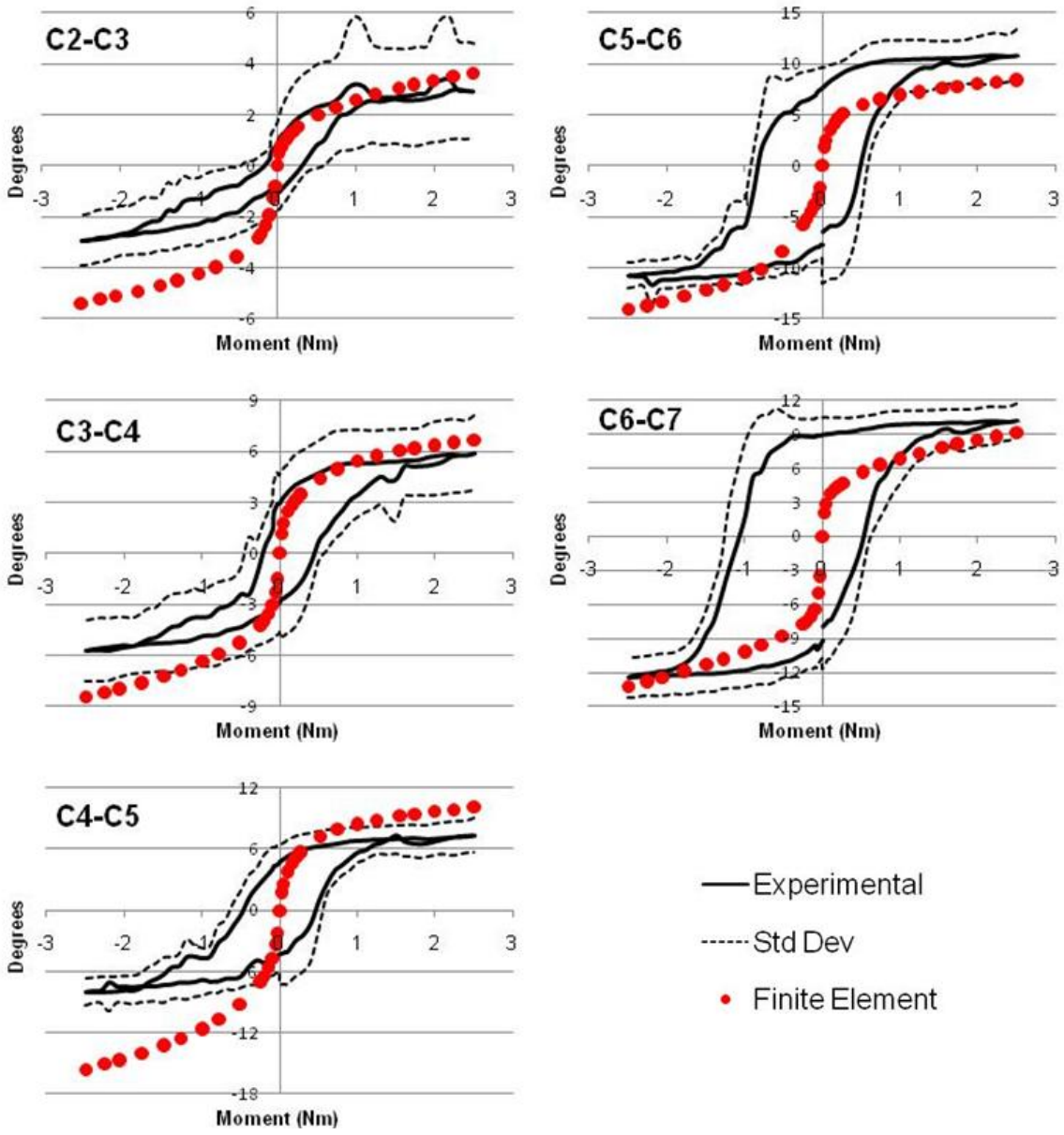

Figure 32 Finite element flexion-extension results compared to the average experimental moment-rotation curves for each level.

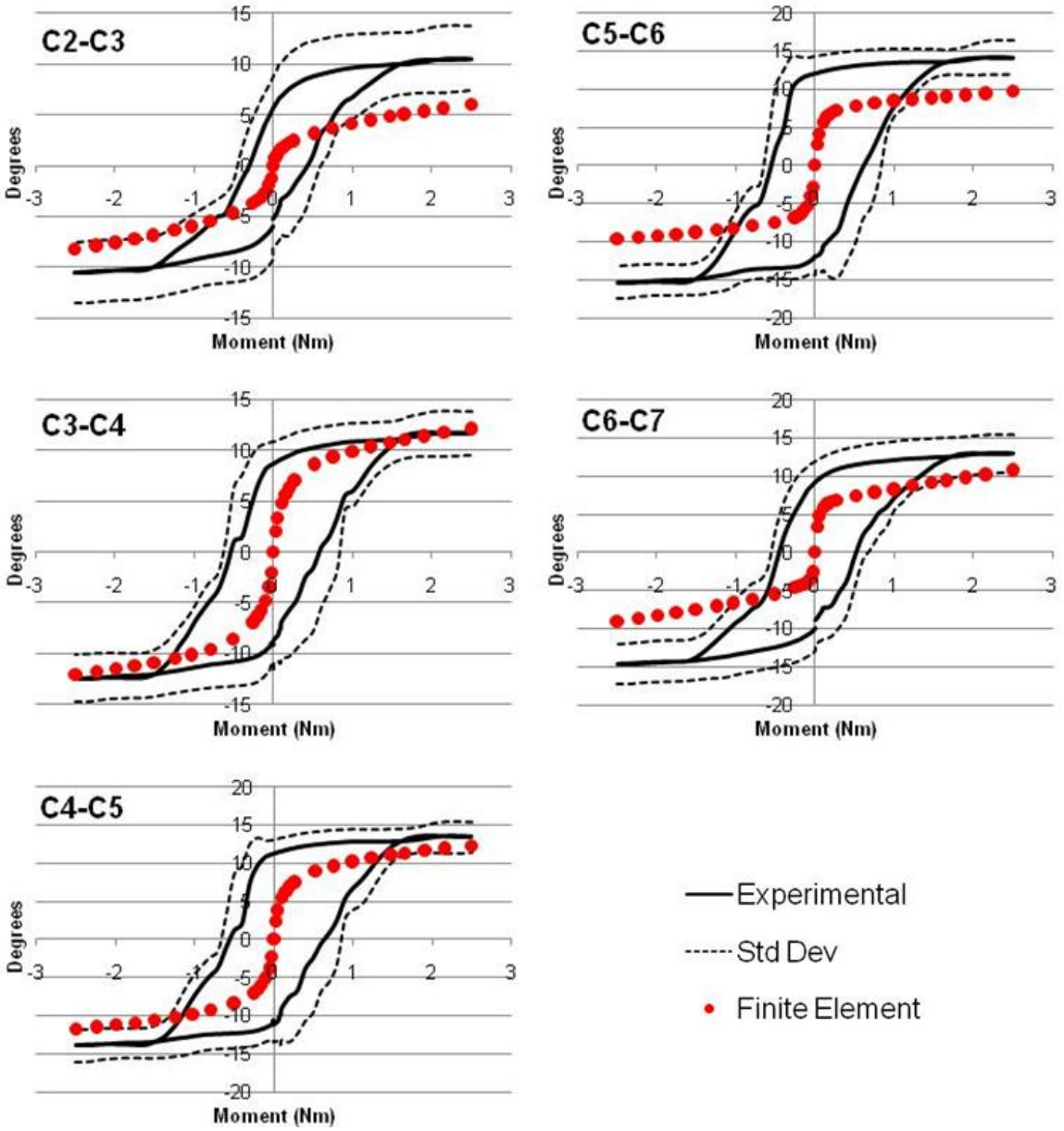

Figure 33 Finite element lateral bending results compared to the average experimental moment-rotation curves for each level.

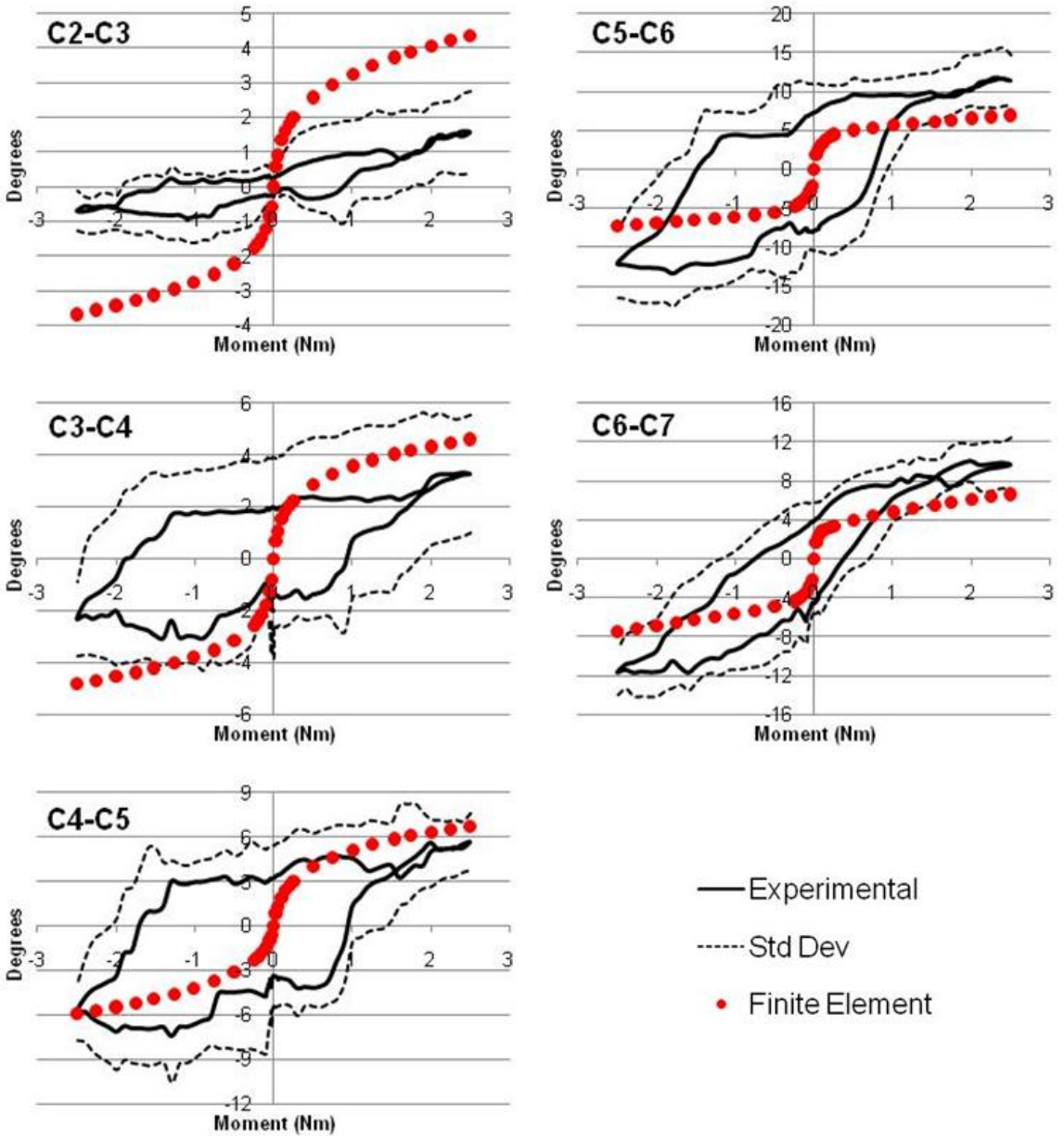

Figure 34 Finite element axial rotation results compared to the average experimental moment-rotation curves for each level.

Table 8 The percentage of coupled motion between axial rotation and lateral bending at 2.5 Nm.

		Percent of Primary Motion	
Primary Motion	**Coupled Motion**	**Experimental**	**Finite Element**
RLB	**RAR**	54.7%	43.1%
LLB	**LAR**	57.5%	43.8%
LAR	**LLB**	110.1%	74.4%
RAR	**RLB**	53.2%	64.1%

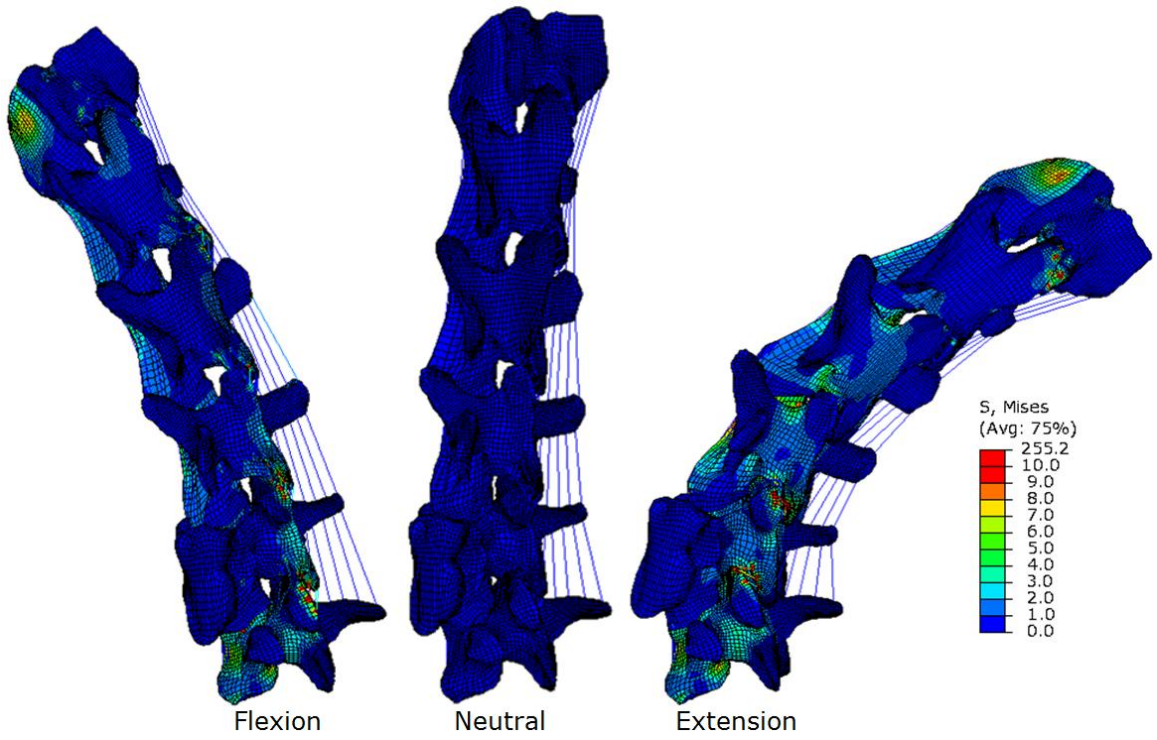

Figure 35 The von Mises stress distribution at 2.5 Nm for flexion and extension.

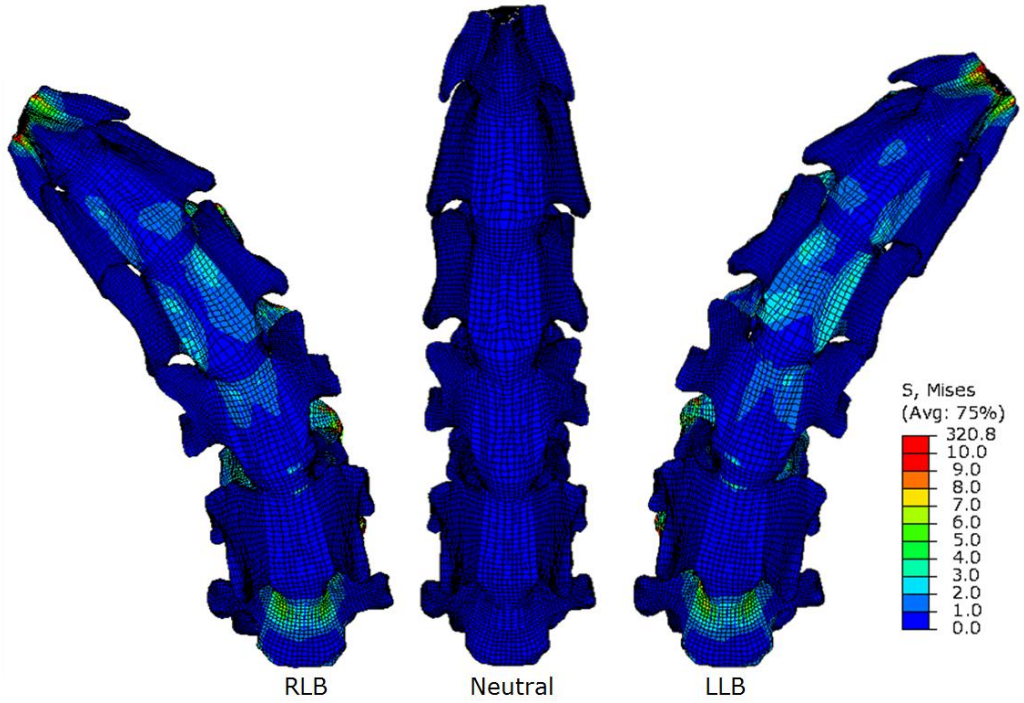

Figure 36 The von Mises stress distribution at 2.5 Nm for right and left lateral bending.

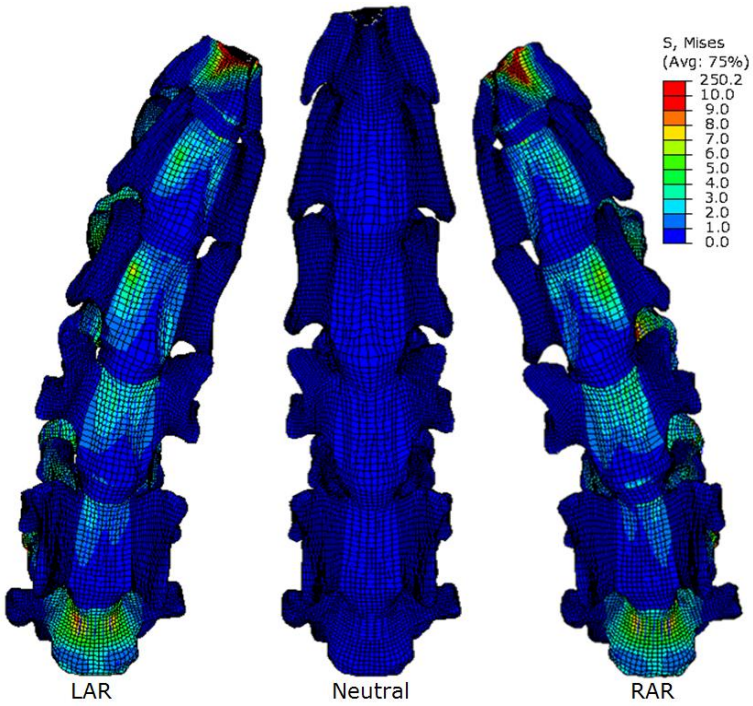

Figure 37 The von Mises stress distribution at 2.5 Nm for left and right axial rotation.

6.3 Discussion

To better understand spinal biomechanics, finite element (FE) analyses are often performed. FE models afford the ability to study internal biomechanics in response to a given external stimulus. Several studies have focused on the human cervical spine [37, 40, 43, 82], however to my knowledge there has only been one study [17]that has employed an FE analysis to study the sheep cervical spine focusing on the C3-C4 FSU only. Since the sheep is often used for in vivo studies [11, 75, 83], it is important to have a comprehensive understanding of both external (i.e. motion) and internal biomechanics (i.e., bone stress and strains, disc pressures, facet contact, etc.) of the sheep. This is the first multilevel model of the sheep cervical spine and to include species-specific material properties.

Overall, this model corresponds well with experimental data. The model does over predict extension and under predict lateral bending, however it is more accurate than the initial model that incorporated human material properties. Due to the large neutral zone it is difficult to determine material properties that can account for the high flexibility and neutral zone while still capturing the elastic zone as well.

The model compared favorably for the off-axis motions in lateral bending and axial rotation as well. The computational off-axis axial rotation during lateral bending was similar to the experimental results. The model was not as accurate at capturing the off-axis lateral bending during axial rotation. However, the experimental axial rotation test was the least stable (only five of the ten specimens could be tested) so the large off-axis lateral bending motion may be due to the instability of the specimen.

As mentioned in the Section 6.1, the model incorporated larger ligament toe regions than were found experimentally. The toe region was minimal during experimental studies because the ligaments were preloaded to 5 N to define a uniform reference starting point. However, in some cases this introduced a pre-strain, as described by Ambrosetti-Giudici et al. [64], and thus reduced the physiological toe region. Therefore,

the introduction of the toe region in the finite element model accounts for the experimental pre-strain.

To more accurately predict all motions, future studies should focus on determining the intervertebral disc material properties at the level and regional basis. The annulus properties of the current model were based on variations of the stress-strain curve for the human lumbar spine [81]. Although this curve was adjusted to capture the more flexible nature of the sheep cervical spine, experimental testing of the sheep intervertebral disc would provide species-specific properties to better define the annulus grounds and fibers. Corresponding to this, determining the fiber orientation and material properties on a regional basis would be beneficial. Currently, the model incorporates the same fiber angle throughout the entire annulus. Previous studies [50, 54]for the human lumbar spine have reported that the fiber orientation and material properties vary between annular layers (inner versus outer) as well as annulus regions (posterior versus anterior). This may be true for the sheep intervertebral disc as well. The regional differences were taken into consideration with the region dependent annulus ground, but in the future this should be extended to the annular fibers as well.

Another future effort to more accurately define the intervertebral disc would be to incorporate user-defined material properties. The current model incorporates hyperelastic (annulus grounds) and hypoelastic (annulus fibers) material property functions provided by Abaqus (Simulia, Rhode Island, USA). However, more recently user-defined material properties are being incorporated to better capture the human intervertebral disc [37, 56]. Similar techniques should be explored to capture the high nonlinearity observed in the sheep spine and to correlate the annulus matrix deformation with the annulus fiber strain. However, there are also challenges and limitations to user-defined material properties as well. They are time consuming to develop and are highly dependent on experimental input. It is also important to check the stability and validity of the user defined materials because many hyperelastic models become unstable at different strain rates and

magnitudes. If a predefined hyperelastic function captures the nonlinearity of the intervertebral disc, then that function should be incorporated since it has been validated for accuracy in formulation.

Beyond the intervertebral disc, future work should also focus on the facet joint. Currently, the facet cartilage is modeled assuming a uniform layer which is not anatomically accurate. This is a valid assumption if the facets are not the focus of the study. Since it is difficult to determine the anatomical cartilage layer from medical imaging, other studies [38-40] have made the assumption of a uniform cartilage layer. However, if the facet contact pressure and area are of particular interest, it would be beneficial to incorporate an anatomically accurate cartilage layer to capture the contact pattern and forces more accurately. The utilization of high resolution magnetic resonance imaging could assist in capturing the facet cartilage. These images could be registered with corresponding computed tomography images to obtain accurate definitions of both bone and soft tissues.

Although this study has limitations it still provides insight into the sheep biomechanics such as stress distribution and intervertebral disc stress. The model predicts the large change in motion at the neutral zone and captures the high flexibility of the sheep cervical spine. Also, the model captured the coupling between axial rotation and lateral bending. The model affords additional biomechanical insight into the intact sheep cervical spine that cannot be easily determined experimentally. The model illustrates the stress distributions for the given loading conditions and can be used to predict regions of high stress concentration in the bone, facets, and intervertebral discs. This validated model can be used to study disc pressures, facet contact, and bone stresses under given loading conditions. Additionally, the validated model can be used to study various surgical techniques and material properties of new implant and fixation devices.

CHAPTER 7: FINITE ELEMENT MODEL APPLICATION

To demonstrate an application of the finite element model, the effects of a discectomy and fusion at the C3-C4 were studied since this procedure has been of interest in previous experimental studies [9-11]. The finite element model can provide more insight into the effects of the fusion that cannot be obtained experimentally, such as bone stresses, facet contact, and disc pressures at adjacent levels.

7.1 Methods

To mimic the discectomy and fusion, the C3-C4 annulus grounds and nucleus were modeled as linear elastic, with cancellous bone material properties. Cancellous bone material properties were used to depict an iliac crest bone graft that has completely fused with the adjacent vertebral bodies.

In an effort to see how the cervical spine compensates for lack of motion at one level due to fusion, the fused model was rotated to the maximum range of primary motion of the corresponding intact model for all loading conditions. To do so, the C7 was held in displacement control in all direction while the C2 was rotated about primary axis. The model was unconstrained in all other directions. The resultant moment and changes in adjacent level motion were observed.

Additionally, the von Mises stresses at each intervertebral disc were compared for the intact and fused model for the given loading conditions. The stresses in the discs were compared at a subset of the interior elements of the different regions. The stresses were monitored in the anterior region for flexion, posterior region for extension, left lateral region for left axial rotation and lateral bending, and the right lateral region for right axial rotation and lateral bending.

7.2 Results

To obtain the same range of motion as the intact model, the resultant moment increased to over 3.5 Nm for extension and axial rotation and over 5 Nm for flexion and lateral bending after fusion. The motion at the fused level C3-C4 was reduced to less than one degree (0.23˚ to 0.71˚). To obtain the same peak range of motion, the motion at the unaltered levels increased (Figure 38). The largest compensation in motion was at the C6-C7 with an average increase of 27%.

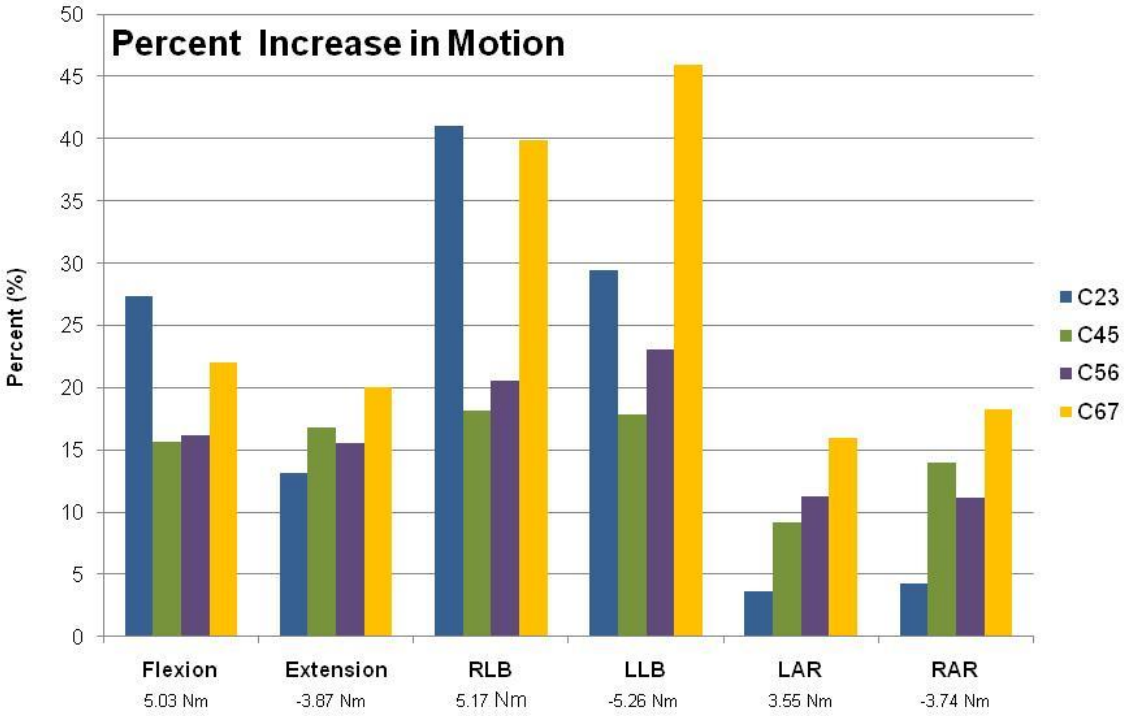

Figure 38 The percent increase in motion at each level after fusion at the C3-C4 level.

With the increase in resultant moment, the von Mises stresses also increased. Figure 39, Figure 40, and Figure 41 show the von Mises stress distribution after fusion for flexion and extension, lateral bending, and axial rotation, respectively. Figure 42

illustrates the percent change in the intervertebral disc stress between the fused model and the intact model for the various loading conditions. The stress increased for each level and loading condition with the largest change in stresses occurring during flexion. On average the stresses increased 100-200% for the various loading conditions. Additionally, the largest changes in stress occurred at the C6-C7 level, corresponding with the large increase in motion.

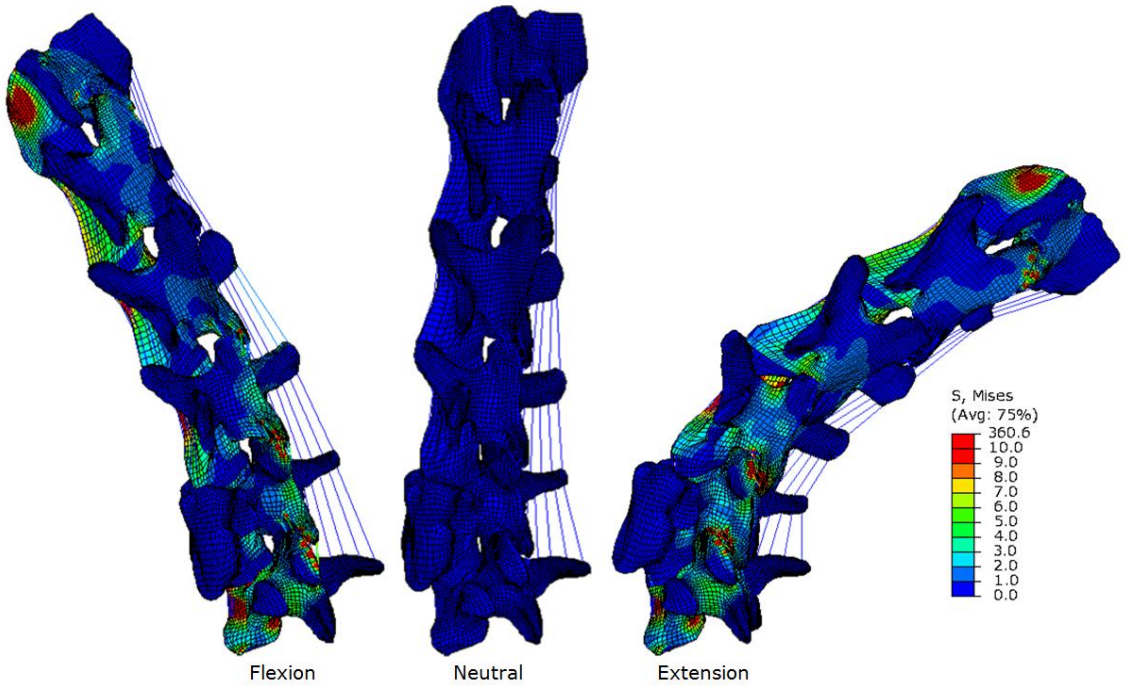

Figure 39 The von Mises stress distribution after C3-C4 fusion for flexion and extension.

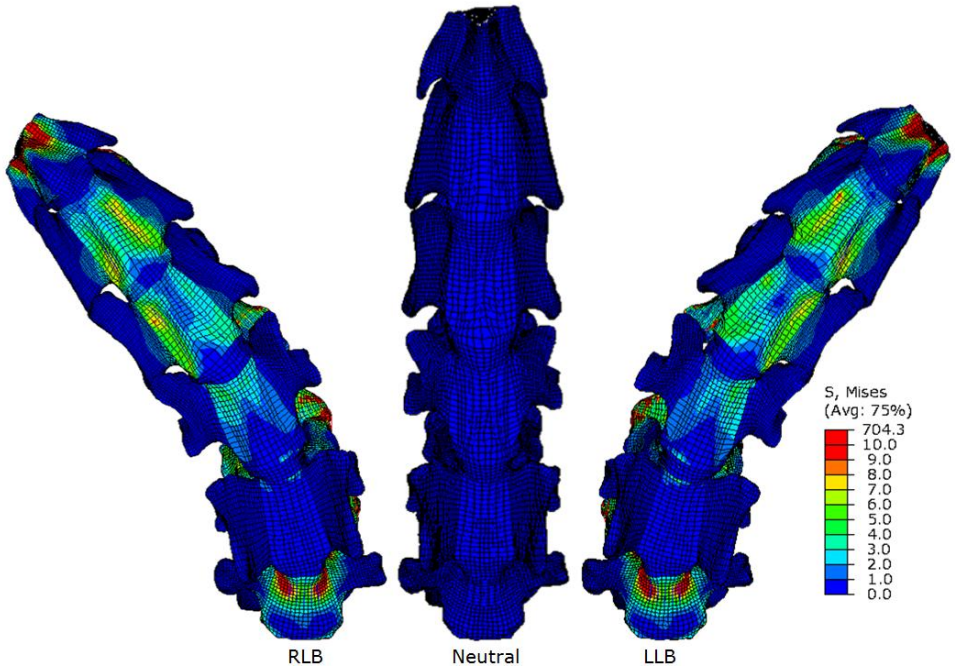

Figure 40 The von Mises stress distribution after C3-C4 fusion for right and left lateral bending.

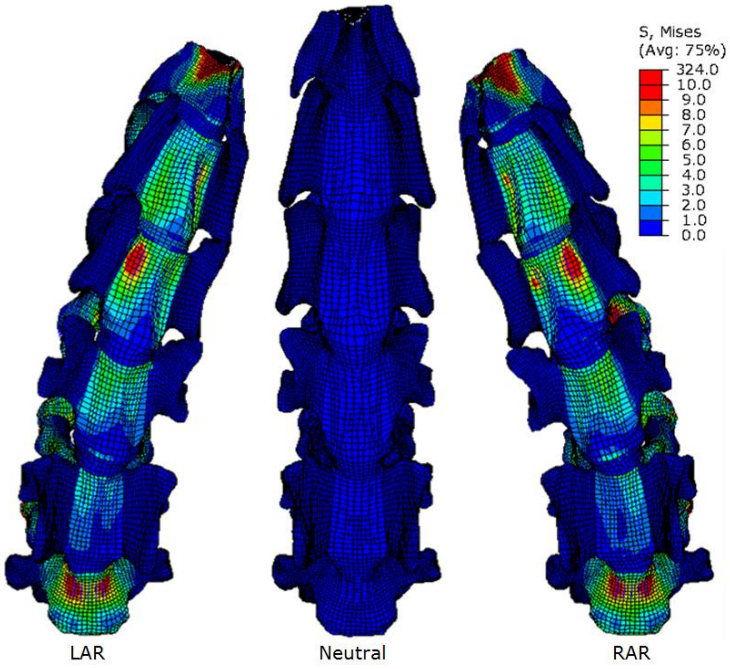

Figure 41 The von Mises stress distribution after C3-C4 fusion for left and right axial rotation.

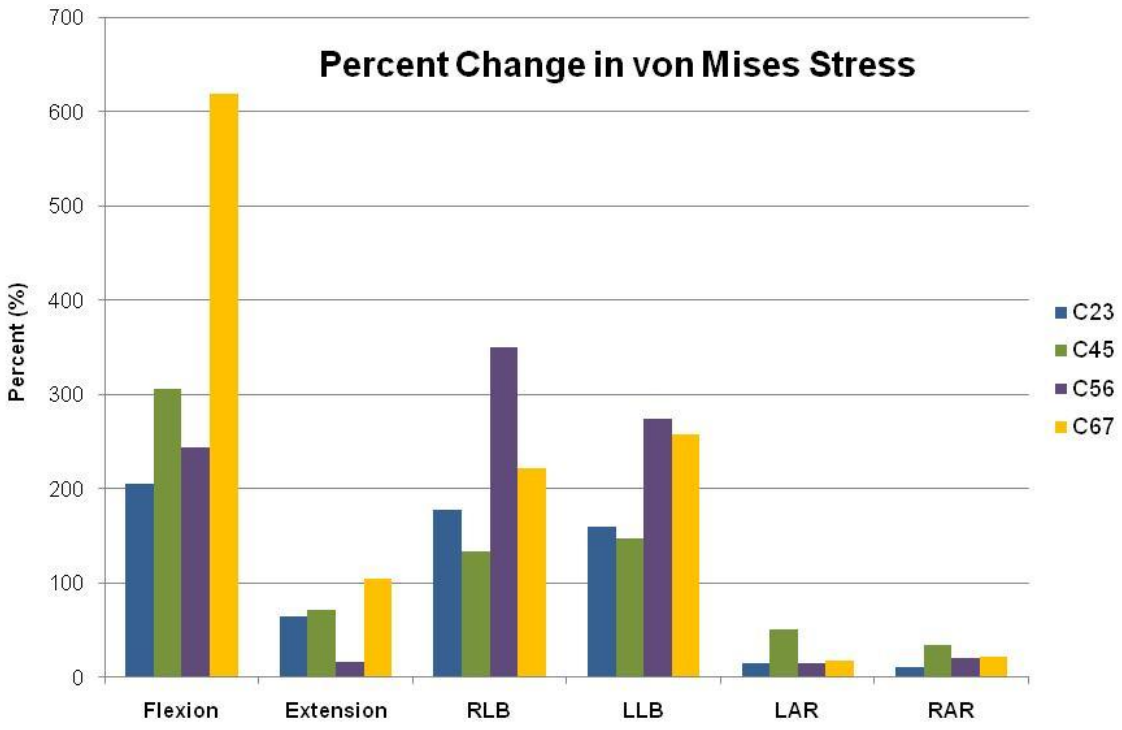

Figure 42 The percent change in von Mises pressure after fusion at level C3-C4.

7.3 Discussion

The finite element model was used to simulate a single level fusion at the C3-C4 level. As described in literature [9-11], the intervertebral disc is removed and replaced with a bone graft. It was assumed the bone graft had fused completely with the adjacent bodies. No cages or plates were used for the fusion.

The fused model was rotated to the motion at 2.5 Nm of the corresponding intact model. This resulted in an increase in motion at adjacent levels following a fusion, which was expected. Similarly, the disc stress also increased after fusion, corresponding to an increase in motion. The largest increase in motion and stress occurred at the C6-C7 disc followed by C2-C3 disc. The increase in stress and motion could lead to damage at the adjacent levels over time. The effect of the increased motion and stresses is difficult to

determine theoretically, however coupled with *in vivo* studies, it could provide insight into the long term effects of fusion.

This study is just one example of how the finite element model can be used to gain insight into different surgical techniques and procedures. It provides researchers with additional biomechanical parameters to consider when designing relevant *in vivo* and *in vitro* studies. The changes in stress distribution and magnitude can gives insight into problematic or beneficial results for a given change. In conclusion, the finite element model is a great tool for researchers to study the biomechanics of the sheep spine and is a great complement to experimental studies.

CHAPTER 8: CONCLUSIONS

The sheep is often used as a precursor to human cadaveric and clinical trials; however there is limited knowledge of the flexibility and material properties. It is important to understand the biomechanics of the intact sheep spine in order to design sound *in vivo* and *in vitro* sheep cervical spine studies focusing on surgical techniques such as discectomies and fusions. Therefore, this study provides insight into the multilevel biomechanics of the sheep cervical spine as well as the ligament properties.

This study presents *in vitro* biomechanical data for the mulitlevel sheep cervical spine as well as insight into the roles of stabilizing structures. The sheep cervical spine is highly flexible, with motion increasing with caudal progression. Additionally, there is a large neutral zone, accounting for 50% to 75% of the total motion. The large flexibility and neutral zone of the sheep spine should be accounted for when designing future studies and interpreting results.

Additionally, understanding the roles of the ligaments and facets is important when planning surgical techniques. This study found the capsular ligaments and facets provide stability during flexion, extension, and axial rotation. The ligaments and facets do not provide a great deal of stability in lateral bending however. Also, the ligaments play a key role in stabilizing the C2-C3 level. Future work should focus on testing additional specimen at the various levels of destabilization to gain a better understanding of the stabilizing structures.

In addition to destabilization, ligament tensile testing was conducted to determine the material properties of each ligament. The capsular ligament has the highest failure force whereas the ligamentum flavum has the largest failure stress. The longitudinal ligaments had the largest failure strain. Due to the small sample size and limitations in the test setup, there was a great deal of variation in the material properties for the same type of ligaments. Thus, future studies should include additional specimen so statistical

analysis can be conducted, thereby establishing whether significant differences exist between the different levels and ligament types.

Moreover, the finite element model was validated against the experimental flexibility data. A majority of the model predicted motions were within one standard deviation of the experimental motion. The model was used to study the effects of fusion at C3-C4. The motion at the fused level decreased to nearly zero degrees for all loading conditions. To compensate for the loss of motion, the non-fused level motion increased 15- 27% with the largest increase at C6-C7. Also, to obtain the same range of motion as the intact case, the resultant moment increased to over 5Nm for a flexion and lateral bending over 3.5Nm for extension and axial rotation.

Overall, this study provides valuable insight into the sheep cervical spine multilevel biomechanics. The high flexibility and neutral zone should be considered when designing studies for comparison to the human cervical spine. Additionally, the finite element model can provide important biomechanical data that is difficult to determine experimentally. The model can be used to study the effects of different surgical procedures such as fusion.

BIBLIOGRAPHY

[1] Singh, K., Masuda, K., and An, H., (2005), Animal Models for Human Disc Degeneration, The Spine Journal, 5 pp. 267S-279S.

[2] Sheng, S., Wang, X., et al., (2010), Anatomy of Large Animal Spines and its Comparison to the Human Spine: A Systematic Review, European Spine Journal, 19 pp. 46-56.

[3] Wilke, H., Kettler, A., and Claes, L., (1997), Are Sheep Spines a Valid Biomechanical Model for Human Spines? Spine, 22:(20) pp. 2365-2374.

[4] Kandziora, F., Pflugmacher, R., et al., (2001), Comparison between Sheep and Human Cervical Spines, Spine, 26:(9) pp. 1028-1037.

[5] Smit, T., (2002), The use of a Quadruped as an in Vivo Model for the Study of the Spine - Biomechanical Considerations, European Spine Journal, 11 pp. 137-144.

[6] Wilke, H., Kettler, A., et al., (1997), Anatomy of the Sheep Spine and its Comparison to the Human Spine, The Anatomical Record, 247 pp. 542-555.

[7] Cain, C., and Fraser, R., (1995), Bony and Vascular Anatomy of the Normal Cervical Spine in the Sheep, Spine, 20:(7) pp. 759-765.

[8] Szotek, S., Szust, A., et al., (2004), Animal Models in Biomechanical Spine Investigations, Bulletin of the Veterinary Institute in Pulawy, 48 pp. 163-168.

[9] Kandziora, F., Schollmeier, G., et al., (2002), Influence of Cage Design on Interbody Fusion in a Sheep Cervical Spine Model, Journal of Neurosurgery: Spine, 96 pp. 321-332.

[10] Pflugmacher, R., Schleicher, P., et al., (2004), Biomechanical Comparison of Bioabsorbable Cervical Spine Interbody Fusion Cages, Spine, 29:(16) pp. 1717-1722.

[11] Kandziora, F., Pflugmacher, R., et al., (2004), Bioabsorbable Interbody Cages in a Sheep Cervical Spine Fusion Model, Spine, 29:(17) pp. 1845-1855.

[12] Thomas, K., Toth, J., et al., (2008), Bioresorbable Polylactide Interbody Implants in an Ovine Anterior Cervical Discectomy and Fusion Model: Three Year Results, Spine, 33:(7) pp. 734-742.

[13] Kadoya, K., Kotani, Y., et al., (2001), Biomechanical and Morphologic Evaluation of a Three-Dimensional Fabric Sheep Artificial Intervertebral Disc: In Vitro and in Vivo Analysis, Spine, 26:(14) pp. 1562-1569.

[14] Kotani, Y., Cunningham, B., et al., (1998), The Effects of Spinal Fixation and Destabilization on the Biomechanical and Histologic Properties of Spinal Ligaments: An in Vivo Study, Spine, 23:(6) pp. 672-682.

[15] Oda, I., Cuuningham, B., et al., (1999), Does Spinal Kyphotic Deformity Influence the Biomechanical Characteristics of the Adjacent Motion Segments? an in Vivo Animal Model, SPINE, 24:(20) pp. 2139-2146.

[16] Clarke, E., Appleyard, R., and Bilston, L., (2007), Immature Sheep Spines are More Flexible than Mature Spines: An in Vitro Biomechanical Study, Spine, 32:(26) pp. 2970-2979.

[17] Kiapour, A., Khere, A., et al., (2008), Biomechanics of C3-C4 Sheep Cervical Spine Compared to Human: An Experimentally Validated FE Study, Orthopaedic Research Society, San Francisco, CA, March 2-5.

[18] Gray, H., (1918), Anatomy of the Human Body. Philadelphia:, Lea & Febiger, Philadelphia, pp. 1396.

[19] Pooni, J., Hukins, D., et al., (1986), Comparison of the Structure of Human Intervertebral Discs in the Cervical, Thoracic and Lumbar Regions of the Spine, Surgical and Radiologic Anatomy, 8:(3) pp. 175-182.

[20] Filler, A., The Complete Spine, http://www.backpain-guide.com/Chapter_Fig_folders/Ch05_Anatomy_Folder/4OverallSpine.html.

[21] Hochman, M. and Tuli, S., Cervical Spondylotic Myelopathy: A Review, http://www.ispub.com/ostia/index.php?xmlFilePath=journals/ijn/vol4n1/cervical.xml.

[22] Trammell, TR., What Makes Up A Healthy Spine? http://www.indyspinemd.com/Normal/index.asp.

[23] White, A., and Panjabi, M., (1990), Clinical biomechanics of the spine, J. B. Lippincott, Philadelphia, pp. 722.

[24] Yoganandan, N., Pintar, F., et al., (1989), Dynamic Response of Human Cervical Spine Ligaments, Spine, 14:(10) pp. 1102-1110.

[25] Medcyclopaedia. Uncovertebral Joint, http://www.medcyclopaedia.com/library/topics/volume_iii_1/u/uncovertebral_joint.aspx.

[26] Brekelmans, W., Poort, H., and Sloof, T., (1972), A New Method to Analyse the Mechanical Behaviour of Skeletal Parts, Acta Orthopaedica, 43:(5) pp. 301-317.

[27] Kurtz, S., and Edidin, A., (2006), Spine Technology Handbook, Elsevier Academic Press, Burlington, MA, pp. 535.

[28] Belytschko, T., Kulak, R., and Schultz, A., (1974), Finite Element Stress Analysis of an Intervertebral Disc, Journal of Biomechanics, 7:(3) pp. 277-285.

[29] Kiapour, A., Khere, A., et al., (2008), Biomechanics of L3-L4 Sheep Lumbar Spine Compared to Human: An Experimentally Validated FE Study, Orthopaedic Research Society, San Francisco, CA, March 2-5.

[30] Clausen, J., Goel, V., et al., (1997), Uncinate Processes and Luschka Joints Influence the Biomechanics of the Cervical Spine: Quantification using a Finite Element Model of the C5-C6 Segment, Journal of Orthopaedic Research, 15 pp. 342-347.

[31] Goel, V., and Clausen, J., (1998), Prediction of Load Sharing among Spinal Components of a C5-C6 Motion Segment using the Finite Element Approach, Spine, 23:(6) pp. 684-691.

[32] Kumaresan, S., Yoganandan, N., and Pintar, F., (1999), Finite Element Analysis of the Cervical Spine: A Material Property Sensitive Study, Clinical Biomechanics, 14 pp. 41-53.

[33] Kumaresan, S., Yoganandan, N., et al., (1999), Finite Element Modeling of the Cervical Spine: Role if Intervertebral Disc Under Axial and Eccentric Loads, Medical Engineering & Physics, 21 pp. 689-700.

[34] Puttlitz, C., Goel, V., et al., (2000), Biomechanical Rationale for the Pathology of Rheumatoid Arthritis in the Craniovertebral Joint, SPINE, 25:(13) pp. 1607-1616.

[35] Kumaresan, S., Yoganandan, N., et al., (2001), Contribution of Disc Degeneration to Osteophyte Formation in the Cervical Spine: A Biomechanical Investigation, Journal of Orthopaedic Research, 19 pp. 977-984.

[36] Teo, E., Yang, K., et al., (2004), Effects of Cervical Cages on Load Distribution of Cancellous Core: A Finite Element Analysis, Journal of Spinal Disorders & Techniques, 17:(3) pp. 226-231.

[37] del Palomar, A., Calvo, B., and Doblare, M., (2008), An Accurate Finite Element Model of the Cervical Spine Under Quasi-Static Loading, Journal of Biomechanics, 41 pp. 523-531.

[38] Sasa, T., Yoshizumi, Y., et al., (2009), Cervical Spondylolysis in a Judo Player: A Case Report and Biomechanical Analysis, Archives of Orthopaedic and Trauma Surgery, 129:(4) pp. 559-567.

[39] Faizan, A., Goel, V., et al., (2009), Do Design Variations in the Artificial Disc Influence Cervical Spine Biomechanics? A Finite Element Investigation, European Spine Journal, .

[40] Kallemeyn, N., Gandhi, A., et al., (2010), Validation of a C2-C7 Cervical Spine Finite Element Model using Specimen-Specific Flexibility Data, Medical Engineering & Physics, 32:(5) pp. 482-489.

[41] Kallemeyn, N., Tadepalli, S., et al., (2009), An Interactive Multiblock Approach to Meshing the Spine, Computer Methods and Programs in Biomedicine, 95 pp. 227-235.

[42] Brolin, K., and Halldin, P., (2004), Development of a Finite Element Model of the Upper Cervical Spine and a Parameter Study of Ligament Characteristics, Spine, 29:(4) pp. 376-385.

[43] Wheeldon, J., Stemper, B., et al., (2008), Validation of a Finite Element Model of the Young Normal Lower Cervical Spine, Annals of Biomedical Engineering, 36:(9) pp. 1458-1469.

[44] Goel, V., Konz, R., et al., (2001), Hinged-Dynamic Posterior Device Permits Greater Loads on the Graft and Similar Stability as Compared with its Equivalent Rigid Device: A Three-Dimensional Finite Element Assessment, Journal of Prosthetics and Orthotics, 13:(1) pp. 17-20.

[45] Noailly, J., Lacroix, D., and Planell, J., (2005), Finite Element Study of a Novel Intervertebral Disc Substitute, SPINE, 30:(20) pp. 2257-2264.

[46] Goel, V., Grauer, J., et al., (2005), Effects of Charite Artificial Disc on the Implanted and Adjacent Spinal Segments Mechanics using a Hybrid Testing Protocol, SPINE, 30:(24) pp. 2755-2764.

[47] Sairyo, K., Goel, V., et al., (2006), Biomechanical Comparison of Lumbar Spine with Or without Spina Bifida Occulta. A Finite Element Analysis, Spinal Cord, 44 pp. 440-444.

[48] Yoganandan, N., Kumaresan, S., et al., (1996), Finite Element Modeling of the C4-C6 Cervical Spine Unit, Medical Engineering & Physics, 18:(7) pp. 569-574.

[49] Ha, S., (2006), Finite Element Modeling of Multi-Level Cervical Spinal Segments (C3-C6) and Biomechanical Analysis of an Elastomer-Type Prosthetic Disc, Medical Engineering & Physics, 28 pp. 534-541.

[50] Schmidt, H., Heuer, F., et al., (2006), Application of a New Calibration Method for a Three-Dimensional Finite Element Model of a Human Lumbar Annulus Fibrosus, Clinical Biomechanics, 21 pp. 337-344.

[51] Rohlmann, A., Burra, N., et al., (2007), Comparison of the Effects of Bilateral Posterior Dynamic and Rigid Fixation Devices on the Loads in the Lumbar Spine: A Finite Element Analysis, European Spine Journal, 16 pp. 1223-1231.

[52] Bowden, A., Guerin, H., et al., (2008), Quality of Motion Considerations in Numerical Analysis of Motion Restoring Implants of the Spine, Clinical Biomechanics, 23 pp. 536-544.

[53] Zhong, Z., Chen, S., and Hung, C., (2009), Load- and Displacement-Controlled Finite Element Analyses on Fusion and Non-Fusion Spinal Implants, Journal of Engineering in Medicine, 223 pp. 143-157.

[54] Chen, S., Zhong, Z., et al., (2009), Biomechanical Comparison between Lumbar Disc Arthroplasty and Fusion, Medical Engineering & Physics, 31 pp. 244-253.

[55] Ng, H., and Teo, E., (2001), Nonlinear Finite-Element Analysis of the Lower Cervical Spine (C4-C6) Under Axial Loading, Journal of Spinal Disorders, 14:(3) pp. 201-210.

[56] Ayturk, U., Garcia, J., and Puttlitz, C., (2010), The Micromechanical Role of the Annulus Fibrosus Components Under Physiological Loading of the Lumbar Spine, Journal of Biomechanical Engineering, 132:(8) pp. 61007-1.

[57] Chazal, J., Tanguy, A., et al., (1985), Biomechanical Properties of Spinal Ligaments and a Histological Study of the Supraspinal Ligament in Traction, Journal of Biomechanics, 18:(3) pp. 167-176.

[58] Myklebust, J., Pintar, F., et al., (1988), Tensile Strength of Spinal Ligaments, Spine, 13:(5) pp. 526-531.

[59] Yoganandan, N., Kumaresan, S., and Pintar, F., (2000), Geometric and Mechanical Properties of Human Cervical Spine Ligaments, Journal of Biomechanical Engineering, 122 pp. 623-629.

[60] Ivancic, P., Coe, M., et al., (2007), Dynamic Mechanical Properties of Intact Human Cervical Spine Ligaments, The Spinal Journal, 7:(6) pp. 659-665.

[61] Bass, C., Lucas, S., et al., (2007), Failure Properties of Cervical Spine Ligaments Under Fast Strain Rate Deformations, Spine, 32:(1) pp. E7-E13.

[62] Lucas, S., Bass, C., et al., (2008), Viscoelastic Properties of the Cervical Spinal Ligaments Under Fast Strain-Rate Deformations, Acta Biomaterialia, 4:(1) pp. 117-125.

[63] Troyer, K., and Puttlitz, C., (2010), Nonlinear Viscoelastic Behavior of Human Cervical Spine Ligaments, 56th Annual Meeting of the Orthopaedic Research Society, New Orleans, LA, .

[64] Ambrosetti-Giudici, S., Gedet, P., et al., (2010), Viscoelastic Properties of the Ovine Posterior Spinal Ligaments are Strain Dependent, Clinical Biomechanics, 25 pp. 97-102.

[65] Dickey, J., and Kerr, D., (2003), Effect of Specimen Length: Are the Mechanics of Individual Motion Segments Comparable in Functional Spinal Units and Multisegment Specimens? Medical Engineering & Physics, 25 pp. 221-227.

[66] Kettler, A., Wilke, H., et al., (2000), Effects of Specimen Length on the Monosegmental Motion Behavior of the Lumbar Spine, Spine, 25:(5) pp. 543-550.

[67] Panjabi, M., Crisco, J., et al., (2001), Mechanical Properties of the Human Cervical Spine as shown by Three-Dimensional Load-Displacement Curves, Spine, 26:(24) pp. 2692-2700.

[68] Yoganandan, N., Pintar, F., et al., (2007), Level-Dependent Coronal and Axial Moment-Rotation Corridors of Degeneration-Free Cervical Spines in Lateral Flexion, Journal of Bone and Joint Surgery, 89:(5) pp. 1066-1074.

[69] Yoganandan, N., Stemper, B., et al., (2008), Normative Segment-Specific Axial and Coronal Angulation Corridors of Subaxial Cervical Column in Axial Rotation, Spine, 33:(5) pp. 490-496.

[70] Grosland, N., Shivanna, K., et al., (2009), IA-FEMesh: An Open-Source, Interactive, Multiblock Approach to Anatomic Finite Element Model Development, Computer Methods and Programs in Biomedicine, 94:(1) pp. 96-107.

[71] DeVries, N., Gassman, E., et al., (2008), Validation of Phalanx Bone Three-Dimensional Surface Segmentation from Computed Tomography Images using Laser Scanning, Skeletal Radiology, 37:(1) pp. 35-42.

[72] Tadepalli, S., Shivanna, K., et al., (2010), Toward the Development of Virtual Surgical Tools to Aid Orthopaedic FE Analyses, EURASIP Journal on Advances in Signal Processing, 2010 pp. 1-7.

[73] Wilke, H., Wenger, K., and Claes, L., (1998), Testing Criteria for Spinal Implants: Recommendations for the Standardization of in Vitro Stability Testing of Spinal Implants, European Spine Journal, 7 pp. 148-154.

[74] Heuer, F., Schmidt, H., et al., (2007), Stepwise Reduction of Functional Spinal Structures Increase Range of Motion and Change Lordosis Angle, Journal of Biomechanics, 40 pp. 271-280.

[75] Slivka, M., Spenciner, D., et al., (2006), High Rate of Fusion in Sheep Cervical Spines Following Anterior Interbody Surgery with Absorbable and Nonabsorbable Implant Devices, Spine, 31:(24) pp. 2772-2777.

[76] Sikoryn, T., and Hukin, D., (1988), Failure of the Longitudinal Ligaments of the Spine, Journal of Materials Science Letters, 7 pp. 1345-1349.

[77] Waters, R., and Morris, J., (1973), An in Vitro Study of Normal and Scoliotic Interspinous Ligaments, Journal of Biomechanics, 6 pp. 343-348.

[78] Panjabi, M., Oxland, T., and Parks, E., (1991), Quantitative Anatomy of Cervical Spine Ligaments. Part II - Middle and Lower Cervical Spine, Journal of Spinal Disorders, 4:(3) pp. 277-285.

[79] Pintar, F., Yoganandan, N., et al., (1992), Biomechanical Properties of Human Lumbar Spine Ligaments, Journal of Biomechanics, 25:(11) pp. 1351-1356.

[80] Abaqus Version 6.5, 2004, , Chap. 10.5.1.

[81] Fujita, Y., Duncan, N., and Lotz, J., (1997), Radial Tensile Properties of the Lumbar Annulus Fibrosus are Site and Degeneration Dependent, Journal of Orthopaedic Research, 15:(6) pp. 814-819.

[82] Yoganandan, N., Kumaresan, S., and Pintar, F., (2001), Biomechanics of the Cervical Spine Part 2. Cervical Spine Soft Tissue Responses and Biomechanical Modeling, Clinical Biomechanics, 16 pp. 1-27.

[83] Thompson, R., Barker, T., and Pearcy, M., (2003), Defining the Neutral Zone of Sheep Intervertebral Joints during Dynamic Motions: An in Vitro Study, Clinical Biomechanics, 18 pp. 89-98.